

Title	Research on hyperfast growth in de Sitter complexity
Author(s)	姉川, 尊徳
Citation	大阪大学, 2024, 博士論文
Version Type	VoR
URL	https://doi.org/10.18910/96381
rights	
Note	

Osaka University Knowledge Archive : OUKA

<https://ir.library.osaka-u.ac.jp/>

Osaka University

Doctoral thesis

Research on hyperfast growth in de Sitter complexity

Takanori Anegawa

Department of Physics, Osaka University, Toyonaka, Osaka 560-0043, JAPAN

E-mail: takanegawa@gmail.com

ABSTRACT: This thesis is based on [1, 2] and investigates the hyperfast growth in de Sitter (dS) spacetime complexity, inspired by the conjecture of a new dS spacetime holographic principle [3]. Complexity is defined in quantum theory as the “effort” to create a certain state or operator. Complexity is considered as the volume or on-shell action of a certain codimension region in bulk side. There are several proposals (CV, CA, CV2.0) for this. The main results are: 1. considering dS spacetime in 2D JT gravity theory, CV is “bad”. 2. considering the response by shockwave in 3D Einstein gravity theory, it causes the delay of hyperfast growth.

Contents

1	Introduction	2
2	de Sitter/ DSSYK dual	8
2.1	(Anti-)de Sitter spacetime	8
2.2	DSSYK	11
2.3	Review of AdS/CFT	15
2.4	dS/DSSYK conjecture	30
3	Holographic Complexity	34
3.1	Basics of Complexity	34
3.2	Holographic Complexity in AdS	37
3.3	Holographic Complexity in dS	39
4	CA in JT gravity	39
4.1	Setup	40
4.2	Action manual and dimensional reduction	41
4.3	Action evaluation	46
5	Geodesics, Volume and Weyl dependence	51
5.1	Volume complexity in dS ₂	51
5.2	Weyl field redefinition	51
5.3	Refined volume for complexity	56
6	BTZ/dS spacetime with shock waves	57
6.1	BTZ spacetime	58
6.1.1	Single shock wave	59
6.1.2	Double shock waves	63
6.2	de Sitter spacetime	65
6.2.1	Single shock wave	66
6.2.2	Double shock waves	69
7	Delay of Hyperfast	72
7.1	BTZ case	72
7.2	de Sitter case	77
7.3	CV calculation	82
8	Summary	86

1 Introduction

The AdS/CFT correspondence [4] plays an extremely important role since it gives a nonperturbative definition of quantum gravity in terms of dual field theory. Through this, we can deepen our understanding of the emergent anti-de Sitter (AdS) spacetime bulk physics. Similarly, we are naturally motivated to establish the holographic framework for de Sitter (dS) spacetime. This is because the holographic principle has originally developed independently of the concrete structure or solution of spacetime [5, 6]. dS spacetime is a good model of our current universe and describes well the features of the accelerating expansion of the universe. Therefore understanding de Sitter’s holographic principle will lead to a better understanding of the structure of quantum theory in our universe.

However, the holographic principle in dS spacetime is not as clearly understood as in AdS. Since AdS and dS spacetime are connected by an analytic connection, it seems that the dual field theories are connected by a similar analytic connection [7–9]. In this case, the holographic screen on which the field theory is considered would be the spacelike surface. However the field theory on the space-like surface has an imaginary central charge and has no time, thus its physical meaning is not much clear. Another proposal was made by Susskind [3], where the claim is that the two-dimensional dS spacetime reproduced in the framework of Jackiw-Teitelboim(JT) gravity is equivalent to the double-scaled Sachdev-Ye-Kitaev (SYK) model with $q \sim \sqrt{N}$, where q specifies the size of the interaction terms in the Hamiltonian schematically as $H \sim \psi^q$ and N is the number of flavors of fermions in the high temperature [10, 11]. Using the static patch holography [12], the holographic screen is placed on the stretched horizon which is close to the dS horizon. Some results on this model can be found in [13–17]. Before discussing Susskind’s argument, we will briefly comment on two important quantities developed recently: out-of-time ordered correlator (OTOC) and complexity.

OTOC is one of the good indicators to show whether a theory is chaotic or not and is a correlation function that is not aligned in time order. It is related to the commutator of operators and describes how much the influence of one operator is likely to affect distant operators. In particular, in the holographic setting, this corresponds to considering a black hole geometry with a small energy inserted as a perturbation from the boundary, which induces a shock wave geometry due to the exponential blue shift near the horizon. This shock wave destroys the entanglement structure of the thermo-field double state and shows the characteristic behavior of chaos [18]. In this way, a black hole exhibits a very large chaotic nature [19], which turns out to satisfy the so-called MSS bound [20]. This in turn implies that a field theory that has gravitational dual must show the similar maximally chaotic nature of a black hole. For example, the SYK model reproduces this MSS bound in its

low temperature limit [21, 22]. This is one of the reasons why the SYK model is extremely useful for understanding two-dimensional gravity.

Complexity for a state $|\psi\rangle$ on the field theory side is originally the minimum number of gates required to achieve that state $|\psi\rangle$ from a reference state [23]. A geometric definition of complexity as the length of shortest geodesics on the (Riemann) manifold of unitary operators has been introduced in [24] for quantum systems with a finite number of degrees of freedom. In the holographic setting, it reflects the geometrical structure of the bulk spacetime, especially it captures the feature of the late time t -linear growth of the Einstein-Rosen bridge wormholes [25, 26].

There are various proposal for holographic complexity, called complexity = action (CA) [27, 28], CV2.0 [29], complexity = volume (CV) [30] respectively. These correspond to the full gravitational action of the Wheeler-DeWitt (WdW) patch (CA), the spacetime volume of the WdW patch (CV2.0), or the volume of codimension-one extremal surfaces (CV). Qualitative nature of all these proposals at late time match in many situations¹, and recently, it has been pointed out in [40, 41] that an infinite class of such observables can exist which might correspond to some arbitrariness of the choice of gates in the field theory complexity definition.

Holographic complexity for AdS in JT gravity and in two-dimensional dilaton-gravity theories has been investigated in [33–38, 42]. Semi-classical corrections give a volume that saturates at late times [43–45]. In recent years, holographic complexity calculations have also been performed in hybrid spacetimes interpolating between AdS and dS [39, 46], for general-dimensional dS spacetime in Einstein gravity [47], and for two-dimensional dS spacetime in JT gravity [39]. See [26, 48, 49] as good reviews. Applications of the geometric approach to free quantum field theories have been studied in [50–53]. Extensions of complexity to CFTs have been addressed in [54–61].

Now let us return Susskind’s hyperfast conjecture [3]. This claim consists mainly of the following two conjectures. First, if we consider the stretched horizon as a holographic screen, then the behavior of OTOC, *i.e.*, scrambling, should be hyperfast in the sense that there is no $\log S$ factor for scrambling time². Second, the growth rates of complexity must also exhibit a hyperfast behavior. This is naturally understood from the fact that dS spacetime well reflects the properties of the expanding universe. In [3, 47], as we approach a critical time $\tau = \tau_\infty$ on the stretched horizon clock, the

¹Jackiw-Teitelboim (JT) gravity [31, 32] is one of the exception where CV and CA can behave differently [33–38] due to dilaton. This is because the JT vacuum is characterized by both the dilaton and metric and the dilaton gives the difference. See for recent works on JT gravity complexity on dS [1, 39].

²If the position at which the operator is inserted is just above the stretched horizon which is very close to the cosmological horizon, the behavior of the OTOC is very different from the one of the chaotic system due to the disappearance of warping factor. Clearly, the behavior of the OTOC depends on where one inserts the operator in dS.

complexity of dS spacetime behaves as follows,

$$\lim_{\tau \rightarrow \tau_\infty} \mathcal{C}_V \rightarrow \infty, \quad \lim_{\tau \rightarrow \tau_\infty} \frac{d\mathcal{C}_V}{d\tau} \rightarrow \infty. \quad (1.1)$$

Thus, the divergence of complexity itself as well as its growth rate can be seen as an evidence of the hyperfast property of dS complexity.

On the other hand, two-dimensional JT gravity [31, 32] has been actively studied in recent years. JT gravity in AdS background, which is an effective low-energy theory for near-extremal Reissner-Nordström black holes in four dimensions, has deep connections with the SYK [21, 62] and the random matrix theory [63]. The reason for our interest in JT gravity arises from its simplicity and analytic tractability, as well as from the hope that it may be regarded as a solvable toy model for higher-dimensional quantum gravity. Given this, it is quite natural to investigate JT gravity in the dS background too.

In this thesis, we focus on holographic complexity for dS spacetime. Then, first of all, the hyperfast property, as Susskind says, is formulated properly on the bulk side. This is also the work of [47]. Then, in the case of the two-dimensional de Sitter spacetime in JT gravity specifically focused by Susskind, we give a good definition of complexity. This is the author’s work [1].

As far as we are aware of, complexity computations in JT dS₂ have been done only using the CV conjecture. One surprising fact in this regard is that holographic volume complexity in dS₂ has been found to be upper-bounded by an $\mathcal{O}(1)$ value at early times [39, 47], prior to a sudden infinite jump at a critical time [47]. However, at first sight, this result might cause confusion from the following perspective. Contrary to the late time linear growth of the wormhole volume behind the event horizon of an AdS black hole [25, 26], the dS space beyond the cosmological horizon of the static patch increases exponentially in time [3]. This exponential expansion of dS is one of the reasons why Susskind originally conjectured the growth of holographic complexity in dS to be “hyperfast” [3]. In light of this, one might ask why holographic complexity for dS₂ does not keep growing as for AdS black holes.

One simple answer to this question is that in two dimensions there is only one spacelike direction and no “volume”. For instance, in four-dimensional gravity, the black hole horizon is a two-sphere S^2 , whereas in two dimensions it is just a point. The lack of spatial dimensions prevents the metric from reading the characteristics of the expanding dS space. Does this mean that the features of the expanding universe disappear in two dimensions? No, because there is a dilaton.

To gain a better grasp on this point, recall that in the original CA papers [27, 28] for AdS spacetime in Einstein gravity

$$S = \frac{1}{16\pi G} \int \sqrt{-g} (R - 2\Lambda), \quad (1.2)$$

it is pointed out that CA is related to CV as

$$C \sim \frac{V}{G\ell} \sim \frac{W}{G\ell^2}, \quad (1.3)$$

where ℓ is the curvature radius of the background spacetime, G is Newton’s constant and V, W is the space and spacetime volume of the WDW patch, respectively. Schematically, these are related by

$$W \sim \ell V. \quad (1.4)$$

In JT gravity, there is a crucial difference due to the dilaton. In this case, one can never get the action in the so-called “Einstein-frame”, rather one always has the “string-frame” form of the action:

$$S = \frac{1}{16\pi G} \int \sqrt{-g} \phi (R - 2\Lambda) + \dots, \quad (1.5)$$

where ϕ is the dilaton. Even after Weyl transformation-like field redefinition

$$g_{\mu\nu} \rightarrow \Omega(\phi)g_{\mu\nu}, \quad (1.6)$$

one can never get rid of ϕ in front of the Ricci scalar in the action. Therefore, in JT gravity the relation between action complexity and volume complexity is not given by eq. (1.3), but it is rather corrected by the presence of the dilaton as

$$C \sim \frac{\phi_b W}{G\ell^2}, \quad (1.7)$$

where ϕ_b is the boundary value of the dilaton. This is reminiscent of the proposal in [33], where the effective Newton’s constant is employed for volume complexity in AdS to manifest the expected late-time linear growth. The dilaton dependence is more significant in dS spacetime. Indeed, since the dilaton diverges at the spacelike future infinity behind the cosmological horizon, it renders action complexity divergent as well. On the other hand, in AdS spacetime the dilaton remains finite but the volume grows linearly in time. The point is that both ϕ_b and W matter in JT gravity.

This is consistent with dimensional reduction. In two-dimensional dS, volume complexity is upper bounded at early times, but in higher dimensions, it diverges due to the large expansion of the sphere in the transverse spatial directions. However, after compactification, the growing radius of this transverse spatial sphere reduces to the dilaton in JT gravity. The dilaton is crucial to properly capture the increase in holographic complexity.

Another subtle issue with volume complexity is that in two-dimensional gravity there is no preferred “frame”, as we have discussed. We should emphasize that physics must be invariant under the field-redefinition of eq. (1.6) because fields are

not directly observable. Despite the on-shell action being invariant under field-redefinition, the solution apparently changes. Since in JT gravity, both the dilaton and the metric characterize the solution, it is strange that complexity is defined by the volume, which picks up only the information contained in the metric. In this regard, it is natural to take action complexity as a starting point to understand the effect of the dilaton in JT gravity.

Next, we digress a little and treat in this thesis the de Sitter spacetime complexity for the higher dimensional case. One quantity of high interest in complexity is the response to perturbations. In particular, the switchback effect in the AdS/CFT case is a good example. Therefore, we will focus on the hyperfast nature of dS complexity, and we study how the small perturbation influences this. In dS bulk, a shock wave is induced by a small and early perturbation. Our goal is to investigate how the property of the hyperfast nature is affected by the shock waves. This is the author's work [2]. See also a very good work done with the same interest as ours [64].

Specifically, we estimate the critical time, at which complexity diverges, based on both the WdW patch and CV proposal. Our WdW patch calculations are for dS_3 , but CV calculations are in dS_{d+1} . Regarding dS_3 WdW patch, since the critical times in both CA and CV2.0 are when the WdW patch reaches the point which has infinite radius (See figure 20) [47], studying the effect of shock waves on WdW patch enables us to evaluate the critical time shift by shock waves in both CA and CV2.0 holographic complexity. We also study the critical time shift in CV conjecture, and we confirm that both WdW patch and CV calculation give exactly the same answer³.

Regarding the WdW patch of dS, the main contribution of the divergence at the critical time $\tau \rightarrow \tau_\infty$ is the volume divergence at the radius r which becomes large. In both CV2.0 and CA, this means that we only need to examine the depth to which the most future tip of the WdW patch is reached. Interestingly, we find that for dS_3 complexity, the critical time τ_∞ delays, *i.e.*, τ_∞ becomes always greater after the insertion of the shock waves, which satisfies averaged null energy condition. However, the result is opposite in the case of AdS, where critical time⁴ becomes faster, *i.e.*, τ_∞ becomes lesser after that shock wave perturbation. In the AdS case, this is reflected in the fact that shock waves make the wormholes longer [18]. In some sense, in the dS case, the effects of shock waves are opposite compared with the AdS case, therefore traveling between the north pole to the south pole becomes

³Because qualitative behavior near the critical time $\tau \rightarrow \tau_\infty$ in all CA, CV2.0, CV conjecture are very similar in general dimensions [47], and furthermore, in both CA and CV2.0, the critical times are when the WdW patch touches the $r = \infty$, we expect our conclusion should hold in general dimensions.

⁴Although AdS complexity does not exhibit hyperfast growth, nevertheless we can still define the ‘critical time’ as when the ‘tip’ of WdW patch reaches $r = 0$ of the black hole. See figure 18 and 19.

easier. This can be regarded as “time advance” [65].

The reader might think it a little bit strange that hyperfast is delayed by perturbation in de Sitter spacetime since generically complexity grows under a perturbation. However, in the bulk dS viewpoint, this is very natural. dS spacetime is a spacetime where cosmological constant dominates. However, shock wave makes the universe “radiation/matter dominance”, instead of cosmological constant dominance. The universe no more exponentially expands if the cosmological constant does not dominate, and thus, the nature of hyperfast can be destroyed by inserting a small perturbation in the past. This is essentially the reason why the critical time τ_∞ becomes greater in the dS case. Before we go on, we comment on the related literature. The effects of shock waves were studied in relation to quantum information. Especially on the BTZ black hole background, it was studied in [18, 30, 66–68]. On dS background, it was studied in [69–71]. Especially in [69], the effect of a single shock wave in dS spacetime and OTOC was studied, which stimulated us.

Organization of this thesis

Section 2 reviews the basics of de Sitter spacetime, which is the setting for the discussion in this thesis. We also consider its relation to the Double Scaled SYK(DSSYK) proposed by Susskind in [3]. This DSSYK argument is not so important for this thesis, but it is important as a background, so we will consider it here. In addition, a rudimentary review of AdS/CFT is provided as a supplement.

In Section 3, we define complexity and review the basics of its conjecture about bulk dual, volume of / (action value in) codimension region. In particular, we will consider the basics in the case of AdS spacetime.

In Section 4, we consider the complexity of de Sitter spacetime in two-dimensional JT gravity theory. First, by adopting CA (Complexity = Action) and computing the on-shell values of action in WdW (Wheeler-de Witt) patch, we show that the de Sitter spacetime exhibits the behavior called “hyperfast”. In this section, we derive the two-dimensional JT gravity theory as a dimensional reduction from the three-dimensional Einstein gravity theory and calculate the action complexity.

In Section 5, based on the results of Section 4, we discuss the volume complexity in the two-dimensional JT gravity theory. In particular, we point out that, in the case of two-dimensional JT gravity, the conventional volume complexity is not a well-defined quantity due to the Weyl invariance of action, and consider redefining the volume complexity in the two-dimensional JT gravity theory.

In Sections 6 and 7 we will look at the response of hyperfast property of de Sitter spacetime to shockwave. In particular, this corresponds, in holography, to a perturbation to the corresponding quantum theory, a situation which is in the context of the switchback effect. Finally, as a consequence of the perturbation we see a delay of hyperfast.

Finally, a light summary concludes this thesis.

2 de Sitter/ DSSYK dual

2.1 (Anti-)de Sitter spacetime

de Sitter (dS) spacetime is the maximally symmetric solution of the Einstein equation with a positive cosmological constant. The dS spacetime in $(d + 1)$ dimensions has the following positive cosmological constant

$$\Lambda = \frac{d(d-1)}{2L_{\text{dS}}^2}. \quad (2.1)$$

where L_{dS} is cosmological length. A more advanced approach to the definition for de Sitter spacetime is to view it as a hyperboloid

$$-(X^0)^2 + (X^1)^2 + \dots + (X^{d+1})^2 = L_{\text{dS}}^2 \quad (2.2)$$

embedded in a one-dimensional higher Minkowski spacetime $\mathbb{R}^{1,d+1}$

$$ds^2 = -(dX^0)^2 + (dX^1)^2 + \dots + (dX^{d+1})^2 \quad (2.3)$$

We consider many coordinates satisfy the above equation. A good example is **global coordinates** (τ, z_i) where we set the following.

$$X^0 = L_{\text{dS}} \sinh(\tau/L_{\text{dS}}), \quad X^i = L_{\text{dS}} z_i \cosh(\tau/L_{\text{dS}}) \quad (2.4)$$

z_i are coordinates constrained on the unit sphere, $\sum_i z_i^2 = 1$. Then we have

$$ds_{d+1}^2 = -d\tau^2 + L_{\text{dS}}^2 \cosh^2(\tau/L_{\text{dS}}) d\Omega_d^2 \quad (2.5)$$

Now τ is proper time and this metric shows that the radius of \mathbb{S}^d increases as τ increases. There is another good coordinate, **static patch** (t, r, z_i) defined as

$$X^0 = \sqrt{L_{\text{dS}}^2 - r^2} \sinh(t/L_{\text{dS}}), \quad (2.6)$$

$$X^1 = \sqrt{L_{\text{dS}}^2 - r^2} \cosh(t/L_{\text{dS}}), \quad (2.7)$$

$$X^i = r z_i \quad (2.8)$$

where z_i is coordinate on the unit sphere. In this coordinate, the metric becomes

$$ds_{d+1}^2 = -(1 - r^2/L_{\text{dS}}) dt^2 + \frac{dr^2}{1 - r^2/L_{\text{dS}}} + r^2 d\Omega_{d-1}^2 \quad (2.9)$$

The global coordinate covers the entire region in de Sitter spacetime, while the static patch only partially covers it. Specifically, in the static patch, there is a region that is causally disconnected from the expansion properties of de Sitter spacetime. It can be seen at first glance as a usual black hole, and the boundary $r = L_{\text{dS}}$ is generally called as a **cosmological horizon**.

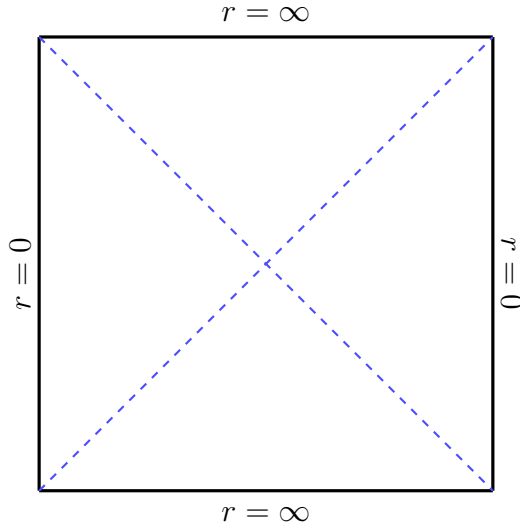


Figure 1: Penrose diagram for de Sitter spacetime in global coordinate. The blue dotted line is cosmological horizon. If a static patch describes dS spacetime, only a right or left Rindler patch can be described.

With the appropriate conformal transformations, the de Sitter spacetime in global coordinates can be rewritten into a Penrose diagram showing its global structure. Specifically, the diagram is shown in Figure 1. However, in the two-dimensional case, the Penrose diagram is further stretched horizontally by a factor of two, which is peculiar. The static patch can also be written as a region of the Penrose diagram. It will look like a Rindler patch, just like a usual black hole.

In addition, there may be Schwarzschild black holes in de Sitter spacetime (SdS). In such a case the metric is as follows (in $L_{\text{dS}} = 1$ units).

$$ds^2 = - \left(1 - \frac{2M}{r^{d-2}} - r^2 \right) dt^2 + \frac{dr^2}{1 - \frac{2M}{r^{d-2}} - r^2} + r^2 d\Omega_{d-1}^2 \quad (2.10)$$

On the other hand, we introduce an Anti-de Sitter (AdS) spacetime, which is in a sense the opposite of de Sitter spacetime. It is a spacetime with a negative cosmological constant

$$\Lambda = - \frac{d(d-1)}{2R^2}. \quad (2.11)$$

of the opposite sign to de Sitter, where R is called AdS scale. In this case, as in dS, it can also be defined as a region

$$-(X^0)^2 - (X^{d+1})^2 + (X^1)^2 + \dots + (X^d)^2 = -R^2, \quad (2.12)$$

embedded in a one-dimensional higher Minkowski spacetime $\mathbb{R}^{2,d}$

$$ds^2 = -(dX^0)^2 - (dX^{d+1})^2 + (dX^1)^2 + \dots + (dX^d)^2. \quad (2.13)$$

In this case, too, there are several useful coordinate systems. A good example is global coordinates (\tilde{t}, ρ, z_i) where we set the following.

$$X^0 = R \cosh \rho \cos \tilde{t}, \quad X^{d+1} = R \cosh \rho \sin \tilde{t}, \quad X^i = R z_i \sinh \rho, \quad (2.14)$$

where z_i are coordinates constrained on the unit sphere, $\sum_i z_i^2 = 1$. Then we have

$$\frac{ds^2}{R^2} = -\cosh^2 \rho d\tilde{t}^2 + d\rho^2 + \sinh^2 \rho d\Omega_{d-1}^2. \quad (2.15)$$

Or if we adopt $\tilde{r} = \sinh \rho$,

$$\frac{ds^2}{R^2} = -(\tilde{r}^2 + 1)d\tilde{t}^2 + \frac{d\tilde{r}^2}{\tilde{r}^2 + 1} + \tilde{r}^2 \rho d\Omega_{d-1}^2. \quad (2.16)$$

Another important coordinate system is the Poincaré coordinate. The definition is

$$X^0 = \frac{Rr}{2} \left(x_i^2 - t^2 + \frac{1}{r^2} + 1 \right), \quad (2.17)$$

$$X^{d+1} = Rrt, \quad (2.18)$$

$$X^i = Rtx_i \quad (i = 1, \dots, d-1), \quad (2.19)$$

$$X^d = \frac{Rr}{2} \left(x_i^2 - t^2 + \frac{1}{r^2} - 1 \right). \quad (2.20)$$

In this coordinate, the metric becomes

$$\frac{ds^2}{R^2} = r^2(-dt^2 + d\vec{x}_{d-1}^2) + \frac{dr^2}{r^2}. \quad (2.21)$$

In particular, the following metric with $z = 1/r$ is also used.

$$\frac{ds^2}{R^2} = \frac{-dt^2 + dz^2 + d\vec{x}_{d-1}^2}{z^2}. \quad (2.22)$$

Some important properties of coordinates should be mentioned here. First, global coordinate is a coordinate system that can describe the entire AdS spacetime. On the other hand, the Poincaré coordinate system can only describe a part of it. See Figure 2. Secondly, there is a boundary in the AdS spacetime. In global coordinates, it is $\rho \rightarrow \infty$ ($\tilde{r} \rightarrow \infty$) surface, while in Poincaré they are $r \rightarrow \infty$ ($z \rightarrow 0$) surface. What is important in this case is the spacetime structure of the boundary. This is closely related to the kind of spacetime on which the dual field theory is defined in the context of AdS/CFT. In the case of global coordinates, the boundary is $\mathbb{R} \times \mathbb{S}^{d-1}$, excluding the conformal factor. In the case of Poincaré coordinates the boundary is simply isomorphic to the Minkowski spacetime $\mathbb{R}^{1,d-1}$.

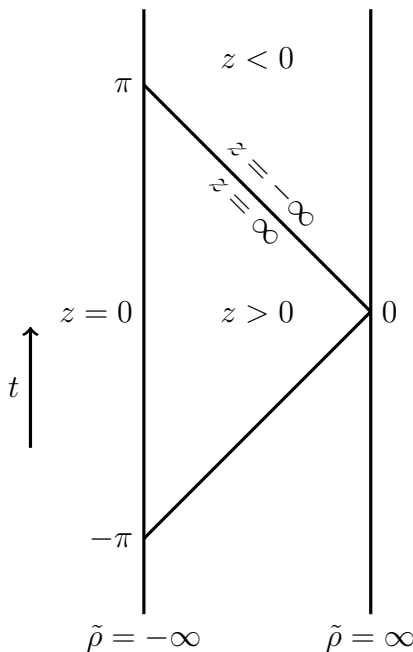


Figure 2: Penrose diagram for AdS spacetime.

2.2 DSSYK

In this section, we deal with the case where we consider the double-scaled limit SYK model where the p -point interaction is taken to be about $p \sim \mathcal{O}(\sqrt{N})$. In particular, it is expected that in this limit the theory may have some properties that we would like it to have as a dual theory of de Sitter spacetime. We will touch on them lightly in the next subsection. Starting from the conventional SYK model

$$H = \sum_{i_1 i_2 \dots i_p} j_{i_1 i_2 \dots i_p}^C \psi_{i_1} \psi_{i_2} \dots \psi_{i_p}. \quad (2.23)$$

Usually $j_{i_1 i_2 \dots i_p}^C$ is a random coupling constant with the following distribution.

$$\langle j_{i_1 i_2 \dots i_p}^C \rangle = 0 \quad (2.24)$$

$$\langle j_{i_1 i_2 \dots i_p}^{C^2} \rangle = \frac{J^2(p-1)!}{N^{p-1}} = \frac{2^{p-1}}{p} \frac{\mathcal{J}^2(p-1)!}{N^{p-1}} \quad (2.25)$$

In DSSYK, consider a scale change to $\chi = \sqrt{2}\psi$.

$$H_{\text{DS}} = 2^{-p/2} \sum_{i_1 i_2 \dots i_p} j_{i_1 i_2 \dots i_p}^C \chi_{i_1} \chi_{i_2} \dots \chi_{i_p} \equiv \sum_{i_1 i_2 \dots i_p} J_{i_1 i_2 \dots i_p} \chi_{i_1} \chi_{i_2} \dots \chi_{i_p} \quad (2.26)$$

In this way, $J_{i_1 i_2 \dots i_p}$ is a random coupling constant with the following distribution.

$$\langle J_{i_1 i_2 \dots i_p}^2 \rangle = 2^{-p} \langle j_{i_1 i_2 \dots i_p}^{C^2} \rangle = \frac{J^2(p-1)!}{2^p N^{p-1}} = \frac{\mathcal{J}^2(p-1)!}{2^p N^{p-1}} \quad (2.27)$$

This can also be described as

$$\langle J_{i_1 i_2 \dots i_p}^2 \rangle = \frac{N \mathcal{J}^2}{2p^2 {}_N C_p} = \frac{N \mathcal{J}^2}{2p^2 \frac{N!}{p!(N-p)!}} \simeq \frac{N \mathcal{J}^2 (p-1)!}{2p \frac{N!}{(N-p)!}} = \frac{\mathcal{J}^2 (p-1)!}{2p N^{p-1}} \quad (2.28)$$

The following convention is also used from here.

$$\langle J_{i_1 i_2 \dots i_p}^2 \rangle = \frac{\mathbb{J}^2}{{}_N C_p}, \quad \mathbb{J} = \frac{\mathcal{J}}{\sqrt{\lambda}} \quad (2.29)$$

where λ is

$$\lambda = \frac{2p^2}{N} \quad (2.30)$$

Under this, let us take the following Double Scaling limit.

$$N \rightarrow \infty, \quad p \rightarrow \infty, \quad q \equiv e^{-\lambda} = e^{-\frac{2p^2}{N}} = \text{fixed}. \quad (2.31)$$

This theory can also be treated by the method of $G\Sigma$, but the following methods are also known in [72] as a chord diagram method. First, consider the partition function. This corresponds to considering **moment** m_k such that

$$\langle Z \rangle_J \equiv \langle \text{Tr} e^{-\beta H} \rangle_J = \sum_{k=0}^{\infty} \frac{(-\beta)^k}{k!} m_k, \quad m_k = \langle \text{Tr} H^k \rangle_J \quad (2.32)$$

We take $\mathbb{J} = 1$ as in the convention of Berkooz et al. This is restored by dimensional analysis at the end. The dimension is Energy. Here, in the words of the Chord diagram, we can express

$$m_k = \sum_{\text{chord diagrams}} q^{\# \text{ intersections}} \quad (2.33)$$

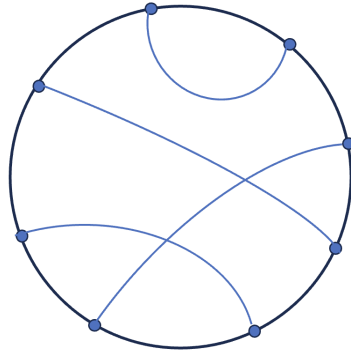


Figure 3: An example which contributes to $k = 8$ moment m_8

A chord diagram is a line drawn by writing several points on a circle and pairing two of each of them, as shown in Figure 3. To calculate m_k , we consider k dots. Each

dot represents one Hamiltonian $\sim J\psi^p$. Each line also represents an ensemble of random couplings in the Hamiltonian. Each intersection point corresponds to a sign change that appears when the fermions are interchanged, and in the double scaled limit this yields a factor of $q = e^{-\lambda}$. Furthermore, Berkooz et al. cut this diagram at an appropriate point and define a chord Hilbert space and tried to understand the moment as a certain amplitude there. As a result, they obtained

$$\langle Z \rangle_J = \int_0^\pi \frac{d\theta}{2\pi} \mu(\theta) e^{-\beta E(\theta)} \quad (2.34)$$

where $E(\theta)$ is a Hamiltonian on chord Hilbert space, a number understood as an energy eigenvalue in DSSYK, and can be written in terms of the parameter θ which can be regarded as an angle as follows.

$$E(\theta) = -\frac{2 \cos \theta}{\sqrt{1-q}}, \quad (2.35)$$

$$\mu(\theta) = (q, e^{\pm 2i\theta}; q)_\infty \quad (2.36)$$

where $(a)_q$ denotes q -Pochhammer symbol. When \mathbb{J} is restored, the energy levels are

$$E(\theta) = -\frac{2\mathbb{J} \cos \theta}{\sqrt{1-q}} = -\frac{2\mathcal{J} \cos \theta}{\sqrt{\lambda(1-q)}} \quad (2.37)$$

Berkooz et al. also calculated the two-point, four-point functions and OTOC for the following operators using the chord diagram.

$$M_A = i^{p_A/2} \sum_{1 \leq i_1 \leq \dots \leq i_{p_A} \leq N} J_{i_1 \dots i_{p_A}}^{(A)} \psi_{i_1} \dots \psi_{i_{p_A}} \quad (2.38)$$

where $J_{i_1 \dots i_{p_A}}^{(A)}$ is independent random coupling which has the same variance as (2.29). From this result, the following diagrammatic rule for the n -point correlation function can be given.

Diagrammatic rule

The correlation function can be calculated according to the following rules.

1. Draw a thermal circle with period $\beta = T^{-1}$.
2. Imprint on the thermal circle the position of Euclidean time at which the quantity M to be calculated, such as a correlation function, is inserted, and draw a chord diagram. The thermal circle is then divided by these insertions into line segments of length $\Delta\tau_i$. Each of them is labeled θ_i . Labels are equal if there is no other operator insertion before or after the pairing on the Chord diagram of M .
3. For each line segment, apply the following.

$$e^{\Delta\tau \cdot E(\theta)} = e^{\Delta\tau \cdot \frac{-2 \cos \theta}{\sqrt{\lambda(1-q)}}} \quad (2.39)$$

4. Apply the following to the boundary between θ_1 and θ_2

$$\sqrt{\frac{(\tilde{q}_A^2; q)_\infty}{(\tilde{q}_A e^{i(\pm\theta_1 \pm \theta_2)}; q)_\infty}} \quad (2.40)$$

where $\tilde{q}_A = e^{-\frac{2p \cdot p_A}{N}}$.

5. The intersection of the Chord is marked with R (Complex function. See [72]).
6. Apply the integral with respect to every θ .

$$\int \frac{d\theta}{2\pi} \mu(\theta) = \int \frac{d\theta}{2\pi} (q; q)_\infty (e^{2i\theta}; q)_\infty (e^{-2i\theta}; q)_\infty \quad (2.41)$$

As an example, let us consider two-point function of fermion chain M of length p' . By using the above diagrammatic rule, we can obtain

$$\langle \text{Tr} M e^{-\beta_2 H} M e^{-\beta_1 H} \rangle_J = \int \prod_{j=1}^2 \left\{ \frac{d\theta_j}{2\pi} (q, e^{\pm 2i\theta_j}; q)_\infty e^{\beta_j \cdot E(\theta_j)} \right\} \frac{(\tilde{q}^2; q)_\infty}{(\tilde{q} e^{i(\pm\theta_1 \pm \theta_2)}; q)_\infty} \quad (2.42)$$

where $\tilde{q} = e^{-\frac{2p \cdot p'}{N}}$.

Density

The probability of giving the energy $E(\theta)$ is, from the above discussion, obtained as

$$\rho(\theta) d\theta = \frac{1}{2\pi} (q, e^{\pm 2i\theta}; q)_\infty d\theta \quad (2.43)$$

$$\rho(E) dE = \frac{\sqrt{1-q}}{4\pi \sin \theta} (q, e^{\pm 2i\theta}; q)_\infty dE \quad (2.44)$$

By introducing, Jacobi's ϑ function defined by

$$\vartheta_1(z, q) = i \sum_{n=-\infty}^{\infty} (-1)^n e^{iz(n-\frac{1}{2})} q^{\frac{1}{2}(n-\frac{1}{2})^2}, \quad (2.45)$$

we see that

$$\rho(\theta) = \frac{\sin \theta}{\pi q^{1/8}} \vartheta_1(2\theta, q) \quad (2.46)$$

$$\rho(E) = \rho_0 \vartheta_1(2\theta(E), q), \quad \rho_0 = \frac{\sqrt{1-q}}{2\pi q^{1/8}} \quad (2.47)$$

Triple Scaling Limit

For $\lambda \rightarrow 0$, we see that the theory becomes Schwarzian dominated, as in ordinary SYK. Specifically, by applying the limit of $\lambda \rightarrow 0$, we find that

$$\rho(E) \propto e^{-\frac{2\pi^2}{\lambda}} e^{-\frac{2}{\lambda}(\theta-\frac{\pi}{2})^2} \sinh\left(\frac{2\pi\theta}{\lambda}\right) \sinh\left(\frac{2\pi(\pi-\theta)}{\lambda}\right) \quad (2.48)$$

More concretely, we can look at the behavior of the $O(1)$ energy region in $\lambda \rightarrow 0$ with fixed E limit. At this time $\theta \rightarrow \pi/2$, and using this we see that it is Gaussian, as the following.

$$\rho(E) \sim e^{-\frac{E^2}{2}}, \quad E = \frac{-2}{\sqrt{\lambda}} \left(\theta - \frac{\pi}{2}\right) \quad (2.49)$$

The triple scaling limit is an important limit, specifically it is argued that $\lambda \rightarrow 0$ and focusing only on the low energy part of the spectrum reproduces the usual JT gravity/SYK dual (NAdS/NCFT)[73]. In order to see the duality with de Sitter spacetime, one has to focus on the whole spectrum without zooming the spectrum to the low energy part.

2.3 Review of AdS/CFT

The next subsection is a review of the proposal by Susskind to adopt DSSYK as a dual of de Sitter spacetime. Before that, a light review of AdS/CFT will be given first as a comparison, followed by a description of dS/DSSYK. This subsection refers mainly to good reviews and lectures [77–83].

AdS/CFT correspondence

AdS/CFT is the current gold standard of quantum gravity theory and one of the excellent achievements of string theory [4]. In most formal form, the correspondence is as follows.

Large N and large $\lambda = g_{\text{YM}}^2 N$ limit of four dimensional $\mathcal{N} = 4$ SU(N) Super-Yang Mills theory is dual to Type IIB SUGRA on $\text{AdS}_5 \times \mathbb{S}^5$.

where $\mathcal{N} = 4$ SYM side has zero β -function and becomes Conformal Field Theory(CFT). This holds in quantum theory. Therefore, this correspondence is called AdS/CFT correspondence. First, I would like to comment on the symmetry of both theories. 5-dimensional AdS has $SO(2, 4)$ symmetry, which can be understood as an embedding of $\mathbb{R}^{2,4}$. This is the symmetry of the unit ball in \mathbb{R}^6 applied to the case of $\mathbb{R}^{2,4}$. On the other hand, it is known that the conformal symmetry of the 4-dimensional CFT can also be expressed by $SO(2, 4)$. From this point of view, this duality seem natural. Also, the symmetry ($SO(6)$) that \mathbb{S}^5 has on the gravity theory side corresponds to $SO(6) \simeq SU(4)$, which is a symmetry that appropriately replaces the four supersymmetries in the $\mathcal{N} = 4$ SYM. On the AdS side, sphere exists in the form of product. However, if the configuration of the field we will consider is even with respect to this sphere, the contribution in this direction can be neglected. Also, from the holographic principle, etc., CFT seems to live in the AdS boundary. (More specifically, the radial direction of the AdS spacetime corresponds to the energy scale of the theory. The AdS boundary corresponds to the physics on the UV energy scale, and the physics there has the physical meaning that the theory is UV complete = theory on a fixed point). Therefore, it can be regarded simply as a correspondence between 5-dimensional AdS spacetime and 4-dimensional CFT. Indeed, this is sufficient for the calculation of correlation functions. Extending the statement to a general dimension, it is possible to state in the following simple version.

Large N and strong coupling limit of CFT_d on the AdS boundary is dual to semiclassical theory on AdS_{d+1} .

In the following, we will give a brief review.

AdS/CFT - From string theory

AdS/CFT is obtained from string theory as follows. First, it is obtained by superposing many ($N \gg 1$) plane-like objects of $(3 + 1)$ -dimensions, called D3-branes. Brane sets the boundary conditions for the open strings and the edges of the open strings are fixed on the brane. This situation with a large number of branes on flat spacetime can be interpreted physically in two ways.

I. A curved spacetime without branes. Branes are very heavy objects and bend flat space-time. Superstring theory is formulated with $(9+1)$ -dimensional spacetime as the target space, and the distortion of spacetime when N D3-branes are placed on top of each other is known as black 3-brane spacetime, and is shown below [84].

$$ds^2 = H^{-1/2}(-dt^2 + d\vec{x}_3^2) + H^{1/2}(dr^2 + r^2 d\Omega_5^2), \quad (2.50)$$

$$H = 1 + \frac{R^4}{r^4}, \quad R = (4\pi g_s N)^{1/4} l_s. \quad (2.51)$$

where l_s is the string length scale, g_s is the string coupling constant and g_{YM} is the coupling constants of the corresponding gauge theory. This will be explained later.

II. $SU(N)$ gauge theory on D3 branes. The ends of the open strings are fixed

to branes, but if there are N branes, the ends of the open strings can be written as $N \times N$ matrices, depending on which of the N branes each of them is attached to. From this it is known that low-energy excitations of branes can be described by the $SU(N)$ gauge theory. In particular, a theory with N D3-branes collected can be described as a $\mathcal{N} = 4$ Super-Yang Mills theory in low-energy.

In description II, when the low-energy limit is not taken, there is an interaction between the degrees of freedom of gauge theory and gravity. Here we want to see the correspondence between gauge theory alone and gravity theory, so we must consider taking this coupling to zero. This corresponds to focusing on the spacetime near the black hole in the I picture. By taking the near horizon limit $r/R \rightarrow 0$,

$$ds^2 = \frac{r^2}{R^2} dx^\mu dx_\mu + \frac{R^2}{r^2} dr^2 + R^2 d\Omega_5^2 \quad (2.52)$$

and this is $AdS_5 \times S^5$. The relation between the parameters is given by

$$l_s^2 \mathcal{R} \sim \frac{l_s^2}{R^2} \sim \lambda^{-1/2}, \quad G_N \mathcal{R}^4 = N^{-2}. \quad (2.53)$$

where \mathcal{R} is scalar curvature and $\lambda = g_{YM}^2 N$ is 't Hooft coupling. Here, the relation $g_{YM}^2 \sim g_s$ is used. This is roughly obtained by writing the amplitude of the four-point function of the gauge field in open string terms. See Figure 4.

From the above relation of parameters, by taking $N \gg 1$, we can neglect the correction of G_N to the curvature of spacetime, i.e., the quantum gravity correction. Furthermore, by taking $\lambda \gg 1$, we can neglect the string length scale with respect to the curvature of spacetime. By taking these limits, the theory of gravity can be described in a semiclassical approximation.

AdS/CFT - correlation function

In the following, we will consider the most basic correspondence of AdS/CFT to the matching of correlation functions. For simplicity, consider the scalar operator \mathcal{O} . And specifically, we consider the following GKP-Witten correspondence [85, 86]. First, if we want to calculate the correlation function on the CFT side, consider the following generating function.

$$Z_{\text{CFT}}(\phi_s) = \left\langle \exp \left[- \int d^d x \phi_s(x) \mathcal{O}(x) \right] \right\rangle_{\text{CFT}} \quad (2.54)$$

Specifically using this, for example, a two-point function can be calculated as follows

$$\langle \mathcal{O}(x) \mathcal{O}(y) \rangle = \frac{\delta^2 Z_{\text{CFT}}(\phi_s)}{\delta \phi_s(x) \delta \phi_s(y)} \Big|_{\phi_s=0}. \quad (2.55)$$

Here, on the right-hand side, we have taken $\phi_s = 0$ at the end, after doing a variation. The above is a calculation from CFT side, but how can this be multiplied when considering the correspondence with AdS? The answer is

$$Z_{\text{CFT}}(\phi_s) = e^{-S_{\text{scalar in AdS}}} \Big|_{\phi_{\text{bdy}} \rightarrow \phi_s} \quad (2.56)$$

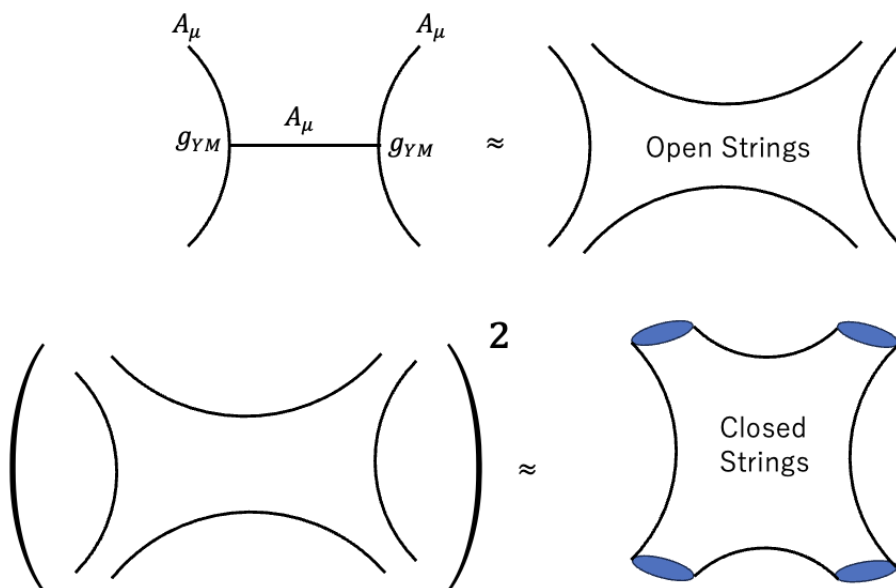


Figure 4: Conceptual diagram of the relationship between g_{YM} and g_s .

(upper) : Considering the upper left diagram contributing to the four-point amplitude of A_μ in pure Yang-Mills theory, it is of order g_{YM}^2 . Moreover, in string theory terms, this is scattering of open strings, corresponding to a diagram with open string connecting open strings.

(lower) : Let us consider the square of this amplitude. This corresponds to the pasting together of the diagram of the open string and corresponds to the 4-point amplitude of closed strings. Since this corresponds to g_s^2 as the order, $g_{YM}^2 \sim g_s^2$ can be roughly deduced.

This is equivalent to calculating the on-shell scalar action on the gravity side, finding the profile of the scalar field solved under the boundary condition that $\phi \rightarrow \phi_s$ near the AdS boundary. In general, this relation is systematically obtained from string theory. In the theory on brane, it is possible to derive the interaction between open strings, which are essentially gauge fields, and closed strings, which are gravitational fields. Specifically, coupled to the scalar field ϕ , one of the degrees of freedom in the theory of gravity, is $\mathcal{O} = \text{Tr}F^2$, glueball. ϕ is the dilaton value for string coupling, specifically $e^\phi \sim g_s \sim g_{YM}^2$. Thus, in gauge theory terms this corresponds to effectively changing the Yang Mills coupling g_{YM} . As one further comment, when solving for the equation of motion of the bulk scalar field, regularity inside the AdS spacetime is also imposed along with $\phi \rightarrow \phi_s$ near the boundary. This determines the scalar profile to be unique.

In the following we will see that the correlation function of CFT is reproduced

in the calculations on the gravity side. Starting from the scalar field in bulk side,

$$S = \int d^{d+1}x \sqrt{-g}(\partial_\mu\phi\partial^\mu\phi + m^2\phi^2) \quad (2.57)$$

$$= R^{d-1} \int dz d^d x \frac{1}{z^{d-1}} \left((\partial_z\phi)^2 + k^2\phi^2 + \frac{m^2 R^2}{z^2}\phi^2 \right) \quad (2.58)$$

where we adopt Poincaré coordinate (2.22) as AdS coordinate and k is momentum in direction x . Therefore the equation of motion becomes

$$\partial_z^2\phi - (d-1)\frac{1}{z}\partial_z\phi - \left(\frac{m^2 R^2}{z^2} + k^2 \right)\phi = 0. \quad (2.59)$$

It is possible to solve this equation exactly, but for simplicity let us focus on AdS boundary $z \ll 0$. By taking $\phi \simeq z^\Delta$ as the solution ansatz, we obtain

$$\Delta(\Delta-1) - (d-1)\Delta - m^2 R^2 = 0 \rightarrow \Delta_\pm = \frac{1}{2} \left(d \pm \sqrt{d^2 + 4m^2 R^2} \right). \quad (2.60)$$

$$\rightarrow \phi \simeq \phi_s z^{\Delta_-} + z^{\Delta_+} (A(x) + \dots) \quad (2.61)$$

It is important to note that $\Delta_+ > 0$, $\Delta_- < 0$ (suppose $m^2 > 0$). Therefore, the first term blows up near the boundary (Non-Normalizable mode). On the other hand, the second term converges (Normalizable mode). This means that the first term is uncontrollable on the gravity theory side, which corresponds to the source term in field theory terms. From the above deductions, the coefficient of the non-normalizable mode is identified as ϕ_s . More generally, the general solution can be written as

$$\phi(z, \vec{x}) = \int_{\text{bdy}} d^d \vec{y} K_{\Delta_+}(z, \vec{x}, \vec{y}) \phi_s(\vec{y}), \quad K_{\Delta}(z, \vec{x}, \vec{y}) = C \left(\frac{z}{z^2 + (\vec{x} - \vec{y})^2} \right)^\Delta \quad (2.62)$$

where C is the appropriate normalization factor. First, when $\vec{x} - \vec{y} \neq 0$, $K_{\Delta} \rightarrow 0$ is understood under the limit $z \rightarrow 0$. Only when $\vec{x} - \vec{y} = 0$ does the limit of $z \rightarrow 0$ diverge, and specifically considering the integral of \vec{x} we understand $K_{\Delta} \rightarrow z^{d-\Delta} \delta^d(\vec{x} - \vec{y})$. Hence, $\phi \rightarrow z^{d-\Delta_+} \phi_s(\vec{x}) = z^{\Delta_-} \phi_s(\vec{x})$ under the limit of $z \rightarrow 0$. This is consistent with (2.61). By considering this profile up to next leading term, this becomes

$$\phi(z, \vec{x}) \sim \phi_s(\vec{x}) z^{\Delta_-} + z^{\Delta_+} \int_{\text{bdy}} d^d \vec{y} \frac{\phi_s(\vec{y})}{(\vec{x} - \vec{y})^{2\Delta_+}} \equiv \phi_s(\vec{x}) z^{\Delta_-} + A(x) z^{\Delta_+}. \quad (2.63)$$

Next, let us substitute this into the scalar field action and calculate the on-shell action. Integrating scalar field action in AdS spacetime by parts,

$$S = R^{d-1} \int_{\text{bdy}} d^d x \frac{1}{z^{d-1}} (\phi \partial_z \phi) + R^{d-1} \int dz dx \text{ (EOM)} \quad (2.64)$$

Since we consider the on-shell action here, we have $(\text{EOM}) = 0$. Therefore, only the first term needs to be considered. Substituting (2.63) here,

$$S \sim \int_{\text{bdy}} d^d x \frac{1}{z^{d-1}} (\phi_s(x) z^{d-\Delta_+}) (A(x) \partial_z z^{\Delta_+}) \propto \int_{\text{bdy}} d^d x \phi_s(x) A(x) \quad (2.65)$$

$$= \int_{\text{bdy}} d^d x \int_{\text{bdy}} d^d \vec{y} \frac{\phi_s(x) \phi_s(\vec{y})}{(\vec{x} - \vec{y})^{2\Delta_+}} \quad (2.66)$$

where the term which is proportional to ϕ_s^2 is absorbed by renormalization. Note that all calculations up to now have been done in the bulk side. To recap what we have done, we have solved the equation of motion for the scalar field inside the bulk. However, we have imposed the boundary condition ϕ_s on the AdS boundary and also imposed regularity inside the AdS. This allows the solution to be obtained specifically as a function of ϕ_s as in (2.63). This is again substituted into the bulk scalar action to obtain the on-shell action. Since we have now substituted the on-shell bulk profile, we have used the fact that the part of action which is proportional to the equation of motion of the bulk vanishes and changed it to an integral only on the boundary. And the main claim is that $Z[\phi_s] \sim e^{-S}$ defined using this is the generating function of the CFT. Therefore, we obtain

$$Z_{\text{CFT}}[\phi_s] = \exp \left[\int_{\text{bdy}} d^d x \int_{\text{bdy}} d^d \vec{y} \frac{\phi_s(x) \phi_s(\vec{y})}{(\vec{x} - \vec{y})^{2\Delta_+}} \right] \quad (2.67)$$

as the CFT generating function. From this we obtain the CFT correlator as

$$\langle \mathcal{O}(x) \mathcal{O}(y) \rangle = \frac{1}{(\vec{x} - \vec{y})^{2\Delta_+}}, \quad \Delta_+ = \frac{1}{2} \left(d + \sqrt{d^2 + 4m^2 R^2} \right) \quad (2.68)$$

This has become a well-known formula for the operator's two-point function with conformal dimension Δ_+ in CFT. Since Δ is determined by the mass m of the scalar field, there is a one-to-one relationship between the scalar field inside the bulk and the conformal dimension Δ_+ of the CFT.

In the above, we considered the case where the bulk is strictly AdS spacetime, but we can also adopt the AdS black hole as the bulk. In this case, the condition of regularity inside the AdS spacetime corresponds to a different boundary condition, namely that the field is absorbed into the black hole, leaving the in-going mode of the field at the black hole horizon. As a reference to the mass spectrum of glueballs obtained using AdS/CFT, see [87–90].

AdS/CFT - Entanglement Entropy

Entanglement Entropy is a quantity naturally defined in field theory, and is specifically defined as follows. First, we start by dividing the spatial domain defined by the field theory into two (or more) parts. For example, in the case of a (1+1)-dimensional theory, the spatial direction is one-dimensional, so it can be taken, for example, as an

appropriate interval of length L , or as a half line of infinite length. Or, if we consider a system of two electron spins, then we can consider one electron spin as A and the other as B . Mathematically speaking, the Hilbert space \mathcal{H}_{tot} can be decomposed into the direct product of the Hilbert spaces \mathcal{H}_A and \mathcal{H}_B corresponding to system A and B as follows:

$$\mathcal{H}_A = \mathcal{H}_A \otimes \mathcal{H}_B \quad (2.69)$$

Secondly, we define the **reduced density matrix** ρ_A by taking Tr with respect to \mathcal{H}_B of the density matrix ρ_{tot} of the whole system as follows.

$$\rho_A = \text{Tr}_{\mathcal{H}_B}[\rho_{\text{tot}}]. \quad (2.70)$$

In general, however, even if the whole system is in a pure state, ρ_A traced with respect to B is in general a mixed state. In this case, Entanglement Entropy can be expressed as a von Neumann Entropy for the density matrix ρ_A restricted to A in this setting

$$S_A = -\text{Tr}_{\mathcal{H}_A}[\rho_A \log \rho_A]. \quad (2.71)$$

From now on, Entanglement Entropy is sometimes referred to as von Neumann Entropy when it is obvious. If the original system is in a pure state, the von Neumann Entropy for the whole system is zero. However, by taking Tr for a subsystem, the information of B is lost and the degree of loss is calculated as the deviation from the pure state in the form of S_A . Let us now calculate the Entanglement Entropy as a system consisting of electron spin. We will consider a pure state in which the wave function of the whole system is given by

$$|\Psi\rangle = \cos\theta|0\rangle_A|1\rangle_B + \sin\theta|1\rangle_A|0\rangle_B \quad (2.72)$$

If we calculate ρ_A for this state, we obtain

$$\rho_A = \text{Tr}_{\mathcal{H}_B}|\Psi\rangle\langle\Psi| = \cos^2\theta|0\rangle_A\langle 0|_A + \sin^2\theta|1\rangle_A\langle 1|_A \quad (2.73)$$

Thus, Entanglement Entropy is given by

$$S_A = -\cos^2\theta \log \cos^2\theta - \sin^2\theta \log \sin^2\theta \quad (2.74)$$

S_A is maximized at $\cos^2 = \frac{1}{2}$, an example of which is

$$|\Psi\rangle = \frac{1}{\sqrt{2}}(|0\rangle_A|1\rangle_B - |1\rangle_A|0\rangle_B) \quad (2.75)$$

In this case, if the spin of A is up (down), the spin of B is down (up), so the correlation between A and B becomes large. Such a phenomenon peculiar to quantum

mechanics is generally called quantum entanglement, and it is a phenomenon that does not exist in classical mechanics, as can be seen from the fact that it is caused by the superposition of quantum states. The entanglement entropy is a quantitative measure of how much correlation exists in the quantum entanglement. In this case, the entanglement entropy is $\log 2$. On the other hand, if $\theta = 0$, we can write $|\Psi\rangle = |0\rangle_A |1\rangle_B$ as a direct product, and there is no correlation between spin A and B . In fact, it is easy to see that the entanglement entropy is 0 in this case. When the whole system is in a pure state, the entanglement entropy generally represents the strength of the quantum entanglement. However, when the whole system is a mixed state, entanglement entropy includes not only quantum entanglement but also classical correlations. For example, when S_A is calculated for a many-body quantum system at finite temperature, the contribution of thermodynamic Entropy is also included.

Also, in general, when there is a system in a mixed state, the entire system can be made a pure state by introducing an auxiliary system and appropriately having entanglement with its degrees of freedom. The original mixed state is obtained by tracing out the auxiliary system. In general, this operation of making the whole system into a pure state by introducing auxiliary systems is called purification, which will be important in the next topic (TFD state).

As a generalization of field theory, the density matrix can be defined in field theory as well, so it is simply more difficult to compute. However, when focusing entanglement entropy in a vacuum state, the wavefunction method of path integral can be used. In particular, we use the following method called Replica trick. First, we calculate $\text{Tr}_{\mathcal{H}_A} \rho_A^n$ (hereafter abbreviated as $\text{Tr} \rho_A^n$) and obtain the following.

$$S_A = \lim_{n \rightarrow 1} \left[-\frac{\partial}{\partial n} \text{Tr} \rho_A^n \right] = \lim_{n \rightarrow 1} \left[-\frac{\partial}{\partial n} \log(\text{Tr} \rho_A^n) \right] \quad (2.76)$$

This can be obtained from the straightforward calculations

$$S_A = -\lim_{n \rightarrow 1} \frac{n \text{Tr} \rho_A^n \log \rho_A}{\text{Tr} \rho_A^n} = -\text{Tr} \rho_A \log \rho_A \quad (2.77)$$

Although n is usually a natural number, in the following calculation we will make an analytic continuation with respect to n and then differentiate n . Now we will calculate $\text{Tr} \rho_A^n$ concretely. It is convenient to use the concept of path integrals in field theory. First, we rotate the time coordinate t of the field theory by Wick and rewrite it as $x_0 = it$ and x_0 . If we write ϕ for the fields appearing in the theory, the field is a function of x_0 and other spatial coordinates x_i ($i = 1, 2, \dots, d$). For simplicity, we will consider a $d = 1$ theory, i.e., a two-dimensional field theory. In this field theory in Euclidean signature, the partition function Z for the whole spacetime

is given by the following path integral.

$$Z = \int \mathcal{D}\phi e^{-S[\phi]}. \quad (2.78)$$

Let us consider a state $|\Psi\rangle$ on $t = 0$. Then, the density matrix is given by

$$\rho_{\text{tot}} = |\Psi\rangle\langle\Psi| \quad (2.79)$$

To compute entanglement entropy, we consider the matrix element of the reduced density matrix

$$[\rho_A]_{\phi_A\phi'_A} = \langle\phi_A|\Psi\rangle\langle\Psi|\phi'_A\rangle \quad (2.80)$$

where $|\phi_A\rangle$ and $|\phi'_A\rangle$ are states on subsystem A ($t = 0$). If we rewrite this by using a complete set of subsystem B ,

$$[\rho_A]_{\phi_A\phi'_A} = \sum_{\phi_B} \langle\phi_A\phi_B|\Psi\rangle\langle\Psi|\phi'_A\phi_B\rangle \quad (2.81)$$

To compute $\langle\phi_A\phi_B|\Psi\rangle$, we have to translate this in language of Path integral

$$\Psi[\phi_0] = \langle\phi_0|\Psi\rangle = \frac{1}{\sqrt{Z}} \int_{t=-\infty}^{\phi(0)=\phi_0} \prod_{-\infty < x^0 < 0} \prod_{x^1} \mathcal{D}\phi(x^0, x^1) e^{-S[\phi(x^0, x^1)]} \delta[\phi(0, x^1) - \phi_0(x^1)]. \quad (2.82)$$

Thus the matrix element of the reduced density matrix is given by

$$\sum_{\phi_B} \langle\phi_A\phi_B|\Psi\rangle\langle\Psi|\phi'_A\phi_B\rangle \quad (2.83)$$

$$= \frac{1}{Z} \int \prod_{-\infty < x^0 < 0} \prod_{x^1} \mathcal{D}\phi(x^0, x^1) e^{-S[\phi(x^0, x^1)]} \prod_{x^1 \in A} \delta[\phi(-0, x^1) - \phi_A(x^1)] \delta[\phi(+0, x^1) - \phi'_A(x^1)]. \quad (2.84)$$

This expression is equivalent to performing path integration in Euclidean space under the boundary conditions $\phi(-0, x^1) = \phi_A(x^1)$, $\phi(+0, x^1) = \phi'_A(x^1)$. We can multiply this by n and take Tr , so

$$\text{Tr}\rho_A^n = \left(\prod_{j=1}^n \int \mathcal{D}\phi_j \right) \langle\phi_1|\rho_A|\phi_2\rangle\langle\phi_2|\rho_A|\phi_3\rangle \cdots \langle\phi_n|\rho_A|\phi_1\rangle = (Z)^{-n} \int_{\Sigma_n} \mathcal{D}\phi e^{-S[\phi]} \quad (2.85)$$

where Σ_n is n sheets glued in region B .

We will actually compute the Entanglement Entorpy using the Replica trick. For simplicity, we consider only the case of a two-dimensional complex scalar CFT.

We consider subsystem A as the single interval $x \in [u, v]$. There are n sheets, and we denote by ϕ_k ($k = 0, 1, \dots, n-1$) the field which you have in each sheet. k is the subscript that distinguishes the sheets. Then we can write down the boundary conditions to fields ϕ_k ($k = 0, 1, \dots, n-1$) as the following:

$$\phi_k(e^{2\pi i}(w-u)) = \phi_{k+1}(w-u), \quad \phi_k(e^{2\pi i}(w-v)) = \phi_{k-1}(w-v) \quad (2.86)$$

However, we redefine the boundary conditions to new fields $\tilde{\phi}_k = \frac{1}{\sqrt{n}} \sum_{l=0}^{n-1} e^{-2\pi i l k/n} \phi_l$,

$$\tilde{\phi}_k(e^{2\pi i}(w-u)) = e^{2\pi i k/n} \tilde{\phi}_k(w-u), \quad \tilde{\phi}_k(e^{2\pi i}(w-v)) = e^{-2\pi i k/n} \tilde{\phi}_k(w-v) \quad (2.87)$$

This follows the previous boundary conditions. In fact,

$$\begin{aligned} \tilde{\phi}_k(e^{2\pi i}(w-u)) &= \frac{1}{\sqrt{n}} \sum_{l=0}^{n-1} e^{-2\pi i l k/n} \phi_l(e^{2\pi i}(w-u)) = \frac{1}{\sqrt{n}} \sum_{l=0}^{n-1} e^{-2\pi i l k/n} \phi_{l+1}(w-u) \\ &= \frac{1}{\sqrt{n}} \sum_{l=1}^n e^{-2\pi i (l-1)k/n} \phi_l(w-u) = e^{2\pi i k/n} \frac{1}{\sqrt{n}} \sum_{l=1}^n e^{-2\pi i l k/n} \phi_l(w-u) = e^{2\pi i k/n} \tilde{\phi}_k(w-u) \end{aligned} \quad (2.88)$$

where we use the Replica symmetry $\phi_n = \phi_0$. In order to actually perform the Replica method, we define the Twist operator as follows. In free field theory, the Lagrangian is quadratic in ϕ and has no interaction, but when rewritten in $\tilde{\phi}$, it is also quadratic and has no interaction. Thus, there are n free fields in either case. Then we can conclude this system is equivalent to the n -sheets with two twist operators σ_k and σ_{-k} . Twist operator σ_k is an operator which induces the left-hand side of boundary conditions on the field ϕ . Thus, $\text{Tr} \rho_A^n$ is given by

$$\text{Tr} \rho_A^n = \prod_{k=0}^{n-1} \langle \sigma_k(u) \sigma_{-k}(v) \rangle \propto \prod_{k=0}^{n-1} \frac{1}{(v-u)^{2(h_k + \bar{h}_k)}} \quad (2.89)$$

where (h_k, \bar{h}_k) is conformal dimension of twist operators and it is

$$h_k = \bar{h}_k = -\frac{k^2}{2n^2} + \frac{k}{2n} \quad (2.90)$$

Taking the summation of h_k given in this way over k , we get

$$\sum_{k=0}^{n-1} h_k = \frac{c}{24} (n-1/n) \quad (2.91)$$

where c is the central charge. Then we get

$$\text{Tr} \rho_A^n \propto l^{-2 \sum (h_k + \bar{h}_k)} = l^{-\frac{c}{6} (n-1/n)}. \quad (2.92)$$

where $l(= v - u)$ is the length of subsystem A . To compute entanglement entropy, we have to differentiate with respect to n and set $n = 1$. Thus we get

$$S_A = \frac{c}{3} \log \frac{l}{\epsilon}, \quad (2.93)$$

where ϵ is UV-cutoff. This dependence of ϵ is hidden as a coefficient in this form, but it is clear from the fact that S_A is zero at $l = \epsilon \rightarrow 0$ and from dimensional analysis that it appears as this form.

Next, we would like to discuss how we calculate the Entanglement Entropy from the gravity side, which can be calculated properly in the CFT side. This answer is Ryu-Takayanagi formula,

$$S_A \sim \min_X \frac{\text{Area of } X}{4G_N}. \quad (2.94)$$

X is spatial curve in bulk such that it has ∂A as the boundary (cutoff surface). We have to search such a line which has the smallest area. Let us consider $\text{AdS}_3/\text{CFT}_2$. We define A is interval which has the length a on time slice $t = t_0$. AdS_3 metric is given by

$$ds^2 = \frac{R^2}{z^2} (-dt^2 + dz^2 + dx^2) \quad (2.95)$$

All we have to do is to calculate the length of geodesic line X which has the edges P and Q ,

$$P : (t, x, z) = \left(t_0, -\frac{a}{2}, \epsilon\right), \quad Q : (t, x, z) = \left(t_0, \frac{a}{2}, \epsilon\right) \quad (2.96)$$

where ϵ is cutoff. Then the geodesic line we want is semicircle connecting P and Q ,

$$z = \sqrt{\frac{a^2}{4} - x^2}. \quad (2.97)$$

The induced metric on this semicircle is

$$ds^2 = \frac{R^2 a^2 dz^2}{z^2 (a^2 - 4z^2)}. \quad (2.98)$$

Thus we can calculate the length of γ_A by integrating

$$\int_{\gamma_A} ds = 2 \times Ra \int_{\epsilon}^{a/2} \frac{dz}{z \sqrt{a^2 - 4z^2}}. \quad (2.99)$$

By using Brown-Henneaux formula

$$c = \frac{3R}{2G_N}, \quad (2.100)$$

Entanglement entropy is given by

$$S_A = \frac{Ra}{2G_N} \int_{\epsilon}^{a/2} \frac{dz}{z\sqrt{a^2 - 4z^2}} = \frac{R}{2G_N} \log \frac{a}{\epsilon} = \frac{c}{3} \log \frac{a}{\epsilon}, \quad (2.101)$$

this corresponds to entanglement entropy from CFT_2 .

AdS/CFT - Thermo-field double state

As relevant to this thesis, we consider the thermo-field double state. This is an important concept when considering two-sided black holes. See Figure 6.

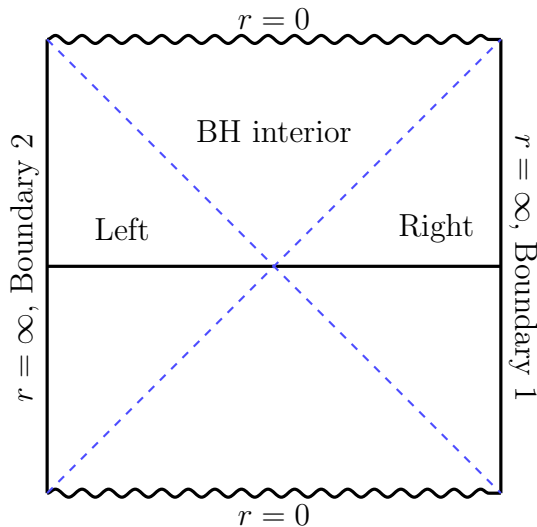


Figure 5: Penrose diagram for AdS black hole. Here, the wavy line with $r = 0$ corresponds to singularity. However, this situation varies depending on the dimension. If we consider, for example, a 3-dimensional AdS black hole = BTZ black hole, $r = 0$ simply corresponds to conical singularity, since we are simply considering different patches of 3-dimensional AdS. Furthermore, in the case of higher dimensional black holes the Penrose diagram may not be an exact square. However, Thermo-field double states can be discussed regardless of these details, so this is not a serious problem.

As can be seen from this Penrose diagram, this spacetime has two AdS boundaries. This implies that this bulk spacetime is described using two copies of the CFT. When we consider the CFT living in the right boundary, the region inside the bulk that can be reproduced from the theory does not include at least the left Rindler patch. This is because from the perspective of the right boundary this is not a causally connected region. Therefore, the theory cannot be dual to the whole two-sided black hole by considering only one CFT. Then, how can we reproduce the internal space-time by considering two CFTs? The answer is to entangle the two theories properly. This is the Thermo-field double(TFD) state [91].

We first look at one-sided theories. Let H denote the Hamiltonian of the system and let $|n\rangle$ denote its energy eigenstate

$$H|n\rangle = E_n|n\rangle. \quad (2.102)$$

Let us consider two of these theories, denoted by the subscripts L(ef) and R(igh) respectively. We now consider the following states using the respective systems of Energy eigenstates $\{|n\rangle_L\}$ and $\{|m\rangle_R\}$

$$|\text{TFD}\rangle = \frac{1}{\sqrt{Z(\beta)}} \sum_n e^{-\beta E_n/2} |n\rangle_L |n\rangle_R. \quad (2.103)$$

This is an element of the direct product of the left and right Hilbert spaces $|\text{TFD}\rangle \in \mathcal{H}_L \otimes \mathcal{H}_R$. Since this is a pure state and furthermore seems to be a one-sided purification of the theory. Specifically, consider the density matrix of this state.

$$\rho = |\text{TFD}\rangle\langle\text{TFD}|. \quad (2.104)$$

From this density matrix, a reduced density matrix can be calculated with one side (left CFT) traced out.

$$\rho_R \equiv \text{Tr}_L \rho = \frac{1}{Z(\beta)} \sum_{n,m,k} e^{-\beta(E_n+E_m)/2} \langle k| (|n\rangle_L |n\rangle_R) ({}_L\langle m| \langle m|) |k\rangle_L \quad (2.105)$$

$$= \frac{1}{Z(\beta)} \sum_k e^{-\beta E_k} |k\rangle_{RR} \langle k| \quad (2.106)$$

This is a simple thermal state. Therefore, if we focus only on one side of the CFTs, we observe thermal particle of the normal black hole. If we consider the expectation value of operator on the right CFT \mathcal{O}_R , it is equivalent to considering the thermal expectation value of the one CFT, as follows.

$$\langle\text{TFD}|\mathcal{O}_R|\text{TFD}\rangle = \frac{1}{Z(\beta)} \text{Tr}_R(e^{-\beta H_R} \mathcal{O}_R) \quad (2.107)$$

Also, considering left CFT operator \mathcal{O}_L , the expected value of the product of those operators $\langle\text{TFD}|\mathcal{O}_R\mathcal{O}_L|\text{TFD}\rangle$ is non-zero. Importantly, no correlation at the Lagrangian level is imposed between the two CFTs. More specifically, there is no interaction of both degrees of freedom in Lagrangian. This is a natural assumption, corresponding to the fact that these theories are causal apart. Therefore, it is nothing but the entangle between the states that generates the correlation between them. Quantum entanglement can produce correlations non-locally (note that this is by no means breaking the causality).

Next, consider the time evolution of this state. There are two ways to consider the time evolution in the combined Hamiltonian, either $H = H_L - H_R$ or $H = H_L + H_R$. Simply looking at the Unitary evolution of state, we can understand the following.

$$|\text{TFD}(t_L, t_R)\rangle = \frac{1}{\sqrt{Z(\beta)}} \sum_n e^{-\beta E_n/2} e^{-iE_n t_L} e^{-iE_n t_R} |n\rangle_L |n\rangle_R. \quad (2.108)$$

Here we see that the thermo-field double state does not evolve in time even with the following development.

$$t_L \rightarrow t_L + \Delta t, \quad t_R \rightarrow t_R - \Delta t. \quad (2.109)$$

This means TFD state does not change by Hamiltonian $H = H_L - H_R$. In two-sided black hole, this corresponds to boost symmetry on the Penrose diagram, where the time evolution is reversed on each of the left and right AdS boundaries. Therefore, when looking at the time evolution of TFD, the upper and lower sides must be clearly defined on the Penrose diagram, and both the left and right theories must be time evolved in that direction.

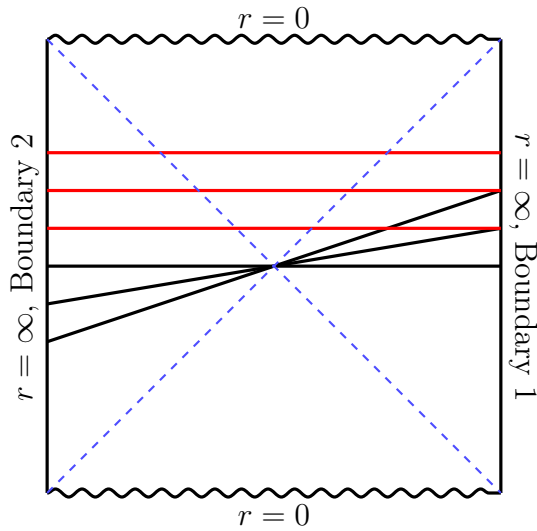


Figure 6: Two types of time evolution in AdS black hole. Black time foliation is boost evolution, TFD does not change. TFD changes with respect to red time foliation.

AdS/CFT - Beyond entanglement

we have understood from the above example that the entanglement entropy can probe the geometric structure of the bulk spacetime. It was discussed that we can probe the length of the Einstein-Rosen Bridge(ERB) in two-sided black hole by using entanglement [92]. The ERB is classically known to increase the length linearly with (appropriate) time $L \propto t$. As a result, we find that the effects of thermalization and scrambling saturate the entanglement entropy on a certain time scale, specifically, the polynomial time of the maximum entropy of the system. However, even after the scrambling time, ERB continues to increase, at least classically. A new attempt to solve the difficulties discussed here was made in [26]. This is the rise of complexity, but we will leave a detailed review of complexity to the next section.

Holographic principle

Originally, the duality between bulk gravity theory and boundary field theory, such as AdS/CFT, was known as the holographic principle. Therefore, note that AdS/CFT is an example of satisfying the holographic principle. The holographic principle claims that there is a corresponding boundary theory for any spacetime other than general AdS. This can be immediately deduced from the Bekenstein-Hawking entropy formula.

$$S_{\text{BH}} = \frac{A}{4G_N} \tag{2.110}$$

where A is an area of black hole horizon. It is important to note that the entropy of a black hole is proportional to its surface area, not to its volume. This is a situation that does not exist in general statistical mechanics. For example, let us consider a box of volume V in 3-dimensional space divided by a lattice of a on one side and a spin placed at each site. If each spin is simply distinguished between up and down states, the entropy of this system is $S \sim \log 2^{V/a^3} \sim \frac{V}{a^3} \log 2$, which is proportional to volume. Then, where does the specialness of black hole entropy come from? It is a fact that black holes are only recognized in systems in which gravity is taken into account. In addition, black holes are particularly high-energy objects in the gravity system. Black hole appears when an object is concentrated at a single point and an extremely large gravitational power is applied. From these circumstances, it is possible to consider that the essential degree of freedom of quantum gravity appears in the area of the system.

Further on, we can see the following description. It seems that the degrees of freedom per volume are only apparent and that the degrees of freedom essentially live on the surface area. Thus, a theory of gravity in a certain region can be replaced by a theory with the appropriate degrees of freedom on its surface! So what are these degrees of freedom? Are they degrees of freedom for which the effect of gravity should be taken into account? The answer is no. The system on the surface area can be treated simply as a field theory. Because then the entropy of the system on the surface area will be consistent with the volume of the system = the surface area of the gravity theory.

From the above, we can deduce that for a certain spacetime theory of gravity, an appropriate field theory of one dimension lower corresponds [5, 6]. Most importantly, this inference starts from the fact that the black hole entropy is proportional to the area, not to the volume, so it is a statement that does not rely on a specific spacetime such as AdS spacetime. Therefore, it seems that there should be a holographic dual theory for dS spacetime as well.

dS/DSSYK - Holographic screen

First, we have to answer the following question: if a dual quantum theory exists for de Sitter spacetime, on which surface should it live? Consider, for example, the case of AdS/CFT. In that case, the CFT would reside on the boundary of AdS, its bulk dual. The easiest way to explain why is the existence of the entanglement entropy and Bousso bound [93].

First, as the aspect of entanglement, we consider the states properly entangled between the left and right field theories (thermo-field double states) and understand the entropy of the black hole by considering the entanglement entropy between the left and right field theories. This can be interpreted in Ryu-Takayanagi surface terms by picking up extremal ones in the spacelike surface of the bulk. Considering the two-sided AdS black hole, which seems to be an Einstein-Rosen-bridge, it is roughly a hyperbolic surface, and properly contributes as the smallest surface near the horizon.

In addition, in the argument with Bousso bound, in a nutshell, the physics in the region covered by the sphere at a certain time should be holographically describable on the sphere. For example, in the case of AdS spacetime, the boundary with $r = \infty$ will play this role.

If we try to apply the same logic to the de Sitter case, for example, localising the field theory to a timelike surface with $r = 0$ as an analogue of the Penrose diagram in the case of AdS spacetime causes a contradiction. In dS spacetime, the time slice is a sphere, and if we try to adopt the surface with the smallest radius as the Ryu-Takayanagi surface, it will always pick up $r = 0$, it is not possible to reproduce the black hole entropy by the cosmological horizon. To avoid this, the holographic screen should be placed as close as possible to the cosmological horizon, and the prescription should be to pick up the cosmological horizon as the smallest surface between the right and left screens. Therefore, it is appropriate to adopt **Stretched horizon** as the screen. See Figure 7 and [3, 74, 94].

In this case, the argument with the Bousso bound has information about which regions of the bulk a single screen can reproduce. The region of the bulk that the stretched horizon can reproduce is a smaller radius than the stretched horizon, so it is simply the so-called Rindler patch from the stretched horizon to $r = 0$. However, the interior of de Sitter, especially the internal region of cosmological horizon, can be expected to be a spacetime that emerges by entanglement as in the usual AdS/CFT case.

2.4 dS/DSSYK conjecture

This subsection is a review of the dS/DSSYK conjecture by Susskind [15–17, 73–76]. Although this relationship is still under development and various calculations are not very rigorous, we will discuss the progress of the current research. Incidentally,

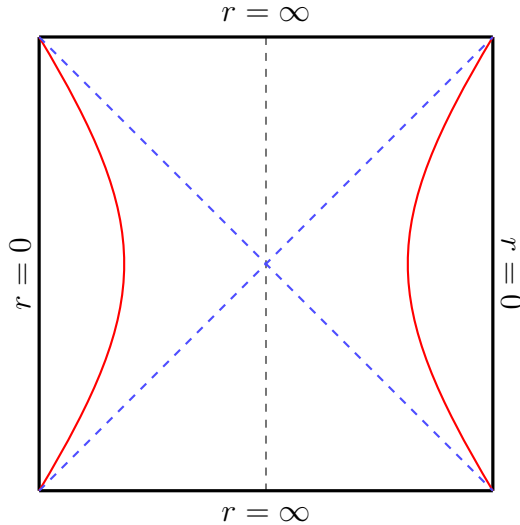


Figure 7: Penrose diagram for de Sitter with stretched horizon. The blue dotted line is cosmological horizon. The red curved line is stretched horizon where is close to the horizon. (In the figure, they are written slightly apart to avoid confusion.)

this subsection can be skipped because we do not proceed with the calculations in this thesis by explicitly using this correspondence. However, all our calculations are based on the assumption that some quantum mechanical system corresponds to de Sitter spacetime.

dS/DSSYK - Properties of de Sitter spacetime

From the above discussion, we have decided to adopt the stretched horizon as the holographic screen and will now look at what happens in de Sitter spacetime in that case. And it should simply be a property that a dual field theory should have. There are two main ones here.

1. OTOC(Out-Time-Orderd-Correlator) shows fast-scrambling
2. Complexity shows a property called hyperfast

It can be deduced from de Sitter's simple bulk argument.

First, OTOC is a quantity well known in conventional SYK and other systems, and is an important measure of the chaotic degree of a system. In general, the behavior of a chaotic system is exponential, and its exponent λ is called the Lyapunov exponent, which is a very important quantity. The larger it is, the more chaotic the system is. In general, the time for OTOC to saturate is called the scrambling time t_* . This is the time order in which the influence of chaos spreads sufficiently. In general, this is $t_* \sim \beta \log S$, where $\beta = T^{-1}$ is inverse temperature and S is the entropy of the system. OTOC can be replaced by a calculation with a bulk dual perturbed by shockwave [18]. The $\log S$ factor included in this scrambling time emerges from the

distance between the screen and the black hole horizon at the bulk in the holographic discussion. In the case of de Sitter spacetime, we can expect this $\log S$ factor to drop out because the screen is close to the horizon. This dramatic shortening of the scrambling time is called fast-scrambling, and we can predict that the corresponding field theory should also have this property.

Also, de Sitter spacetime is an expanding spacetime, which makes de Sitter spacetime a good model for our expanding universe. Therefore, at a properly defined time, the expansion of the volume of spacetime is beyond the scope of AdS/CFT. This corresponds to a dramatic increase in the quantity called complexity in the language of field theory. We call this hyperfast property.

dS/DSSYK - Properties of DSSYK

Having discussed above what happens when bulk is de Sitter, we will now consider DSSYK as a specifically proposed system. Here bulk is a two-dimensional de Sitter spacetime, formulated using JT gravity (or dimensional reduction of a three-dimensional de Sitter spacetime). Firstly, regarding the fast-scrambling property, this has been well investigated for some time. Starting from conventional SYK, if we fix p/N^α and take double scale, the scrambling time changes from $O(\log S)$ to $O(1)$ at $\alpha = 1/2$ [19, 95, 96]. This corresponds to the fact that as the number of interacting fermions is dramatically increased, the speed at which the chaos effect spreads increases significantly. As for complexity, Susskind himself predicts in [3]. However, there seems to be no concrete calculation in DSSYK.

dS/DSSYK - Temperature

Let us discuss the aspects of the entropy. For example, in the case of a three-dimensional Schwarzschild de Sitter spacetime with mass M , the metric is

$$ds^2 = -f(r)dt^2 + \frac{dr^2}{f(r)} + r^2d\phi^2, \quad f(r) = 1 - 8G_N M - r^2 \quad (2.111)$$

and the radius of horizon is given by $r = \sqrt{1 - 8G_N M} \ll 1$. Since the entropy is determined by the area of the black hole, the black hole entropy in de Sitter spacetime is always less than the entropy of the normal cosmological horizon. Conversely, pure de Sitter behaves as a state with maximum entropy. Chandrasekharan, Penington, and Witten studied von Neumann algebra in de Sitter spacetime as a study in this direction and argued that the formal temperature must be infinite [97]. From this point, Susskind considered that the formal high-temperature limit should be taken in DSSYK. In fact, this does not create any contradiction. This is because the effective temperature does not go to infinity. For example, the retarded two point function

$G_R(t) = \frac{1}{2^{N/2}} \text{Tr}(\chi(t)\chi(0))\theta(t)$ is as follows under DSSYK and high temperature limit

$$G_R(t_c)^p = \left(\frac{1}{\cosh(p\mathcal{J}t_c)} \right)^2 \quad (2.112)$$

where t_c is rescaled time $t = qt_c$.⁵ Retarded two-point functions generally decay with temperature scale $G \sim e^{-Tt}$. This is called thermalization. From the above, we can determine the effective temperature (Temperature \mathcal{T}) as

$$\mathcal{T} = 2\mathcal{J} \quad (2.113)$$

dS/DSSYK - Semiclassical approximation

Now, even in the case of de Sitter spacetime, it is tempting to search for a parameter region where the semiclassical approximation can be justified through a relation like (2.53). This is also known as

$$\frac{1}{L_{\text{dS}}} \sim \mathcal{J}, \quad \frac{L_{\text{dS}}}{G_N} \sim \frac{1}{\lambda} \quad (2.114)$$

The first correspondence is derived from the requirement that the temperature of the two-dimensional pure de Sitter spacetime and the temperature of DSSYK be the same, and the second equation is derived from the requirement that the deviation from the respective maximum entropy be the same. From this, we see that if we want to eliminate the quantum gravity correction, for example, we can take the limit of $\lambda \rightarrow 0$.

dS/DSSYK - Developments and Some references

In connection with the above, the quantity Krylov Complexity is known. This quantity is a physical quantity that describes the spread of the Operator (some also study the spread of the state). This is expected to give an upper bound on the Lyapunov exponent calculated from the OTOC. The Krylov Complexity in the case of DSSYK has been calculated in [14] and fast-scrambling can indeed be observed if the time scale is taken appropriately.

In addition, there is a discussion of two-point functions. In [98, 99], two DSSYK systems (left and right in Penrose diagram in de Sitter spacetime) are prepared and gauge invariant operators are constructed by gauging both of them with appropriate energy constraints. They then construct their two point functions entirely from the knowledge (Diagrammatic rule from chord diagram) of DSSYK and show that they can be reproduced from the equation of motion of the complex scalar field on de Sitter

⁵The justification and meaning of taking time in this way is discussed in [15, 16]. Simply, it seems that this scaling is necessary if one wants to describe the cosmic scale of de Sitter spacetime and to take the double-scaled limit well on this time scale. But in any case, it is not so important for this thesis, so I will not discuss it any further.

spacetime. However, in this discussion, we consider the parameter region $\lambda \rightarrow 0$ where the semiclassical description is valid. Other properties, e.g. the existence of the maximum entropy, type II_1 von Neumann algebra is also discussed [100].

As mentioned above, this conjecture is now in the process of being gradually confirmed. We consider in this context to develop our knowledge of the de Sitter spacetime complexity. It is not a question of whether or not we actually adopt DSSYK as the dual of de Sitter spacetime in the subsequent calculations. What matters is that there exists a corresponding field theory and that the dual theory lives on a stretched horizon.

3 Holographic Complexity

In the history of the holographic principle, a number of physical quantities probing the bulk have been considered. One great example is the Entanglement Entropy. In this context, Ryu-Takayanagi (RT) prescription relates entanglement entropy in a CFT to the area of extremal codimension-two bulk surfaces anchored at the AdS boundary [101–103]. However, in terms of the dual theory in AdS, entanglement entropy does not suffice [92] to capture the growth of the Einstein-Rosen bridge inside a black hole, which continues even after the thermalization time. The appropriate dual quantity to be considered is quantum complexity, which keeps growing for an exponentially large time [25, 26].

3.1 Basics of Complexity

Definition and basic properties

Computational complexity is a quantity originally formulated in the field of computational science. It is the “effort” it takes to obtain the state of the system (classically, this is n -bit). More specifically, it is the computational effort required to achieve the desired state, starting from a simple state.

First, let us consider the classical example. The classical state is represented by n -bit (e.g. 0101100 \dots). In this case, there are 2^n different states. We take 0000 \dots or 111111 \dots as a simple state. It’s possible to include the equivalence \mathbb{Z}_2 for all n -bit flips. Anyway, we define a simple state. In addition, we consider an operation that flips one of the bits ($0 \leftrightarrow 1$) as a possible operation in unit time. In this case, the time to reach the most laborious state (maximum complexity) is $\mathcal{C}_{\max} \sim n/2$. The maximum entropy of the system is also $S_{\max} = \log 2^n = n \log 2$ and is an order of n . Also, the physical evolution to a state with maximum entropy is thermalization, which generally saturates in polynomial time of the system size n . Thus, classically, the time at which these are headed is not much different. However, things change drastically in quantum theory.

In quantum theory, an n -bit is generally described by the following quantum state

$$|\Psi\rangle = \sum_{i=1}^{2^n} \alpha_i |i\rangle \quad (3.1)$$

where $|i\rangle$ denotes all possible 2^n states from $0000\dots$ to $11111\dots$. Thus, in this case, 2^n complex numbers α_i correspond to the classical bits mentioned earlier. In this case, the typical maximum complexity is $\mathcal{C}_{\max} \sim 2^n \sim e^n$. Incidentally, as a basic operation, we cannot adopt here only the operation of changing the state of one qubit. It is necessary to have an operation that generates an entanglement between two qubits. This is formulated in quantum information as quantum gates. However, even in this case, the maximum entropy is scaled by $S_{\max} \sim n \log 2$ as is well known. Of course, this is typically achieved after only thermalization time (or scrambling time).

Furthermore, it should be noted that there is also a time scale called recurrence time. This is the time scale from the initial condition to the time when the system evolves and returns to the original initial condition. Since it depends approximately on the degrees of freedom and the number of possible states, it can be estimated to be on the scale of $t_{\text{rec}} \sim e^n$ classically and $t_{\text{rec}} \sim e^{e^n}$ in quantum theory.

Another extremely important property of typical chaotic theory is that it keeps increasing with respect to time until saturation.

$$\frac{d\mathcal{C}}{dt} = TS \quad (3.2)$$

where T is the temperature and S is entropy. This is proved by the geometry formulation of Nielsen and collaborators [24, 104]. This is also a formulation of complexity for continuous Hamiltonian deformations, moving away from the discrete definition of complexity. Specifically, we consider the change of state by k gates.

$$|\Psi(k)\rangle = U(k)|\Psi(0)\rangle \quad (3.3)$$

where $U(k)$ is an element of $\text{SU}(2^n)$ (Now dimension of this Hilbert space is 2^n). And they properly introduced the inner product in this $\text{SU}(N)$ space and properly introduced the notion of distance. As a result, the equation of evolution from the origin (the unit matrix I) in $\text{SU}(N)$ as

$$\frac{dU(s)}{ds} = -ih(s)U(s) \quad (3.4)$$

$$U(s) = P \exp \left[-i \int_0^s h(s') ds' \right] \quad (3.5)$$

where $s \sim$ time is parameter on the line connecting I and $U(s)$ and $h(s)$ is generator (hamiltonian with respect to $s \sim$ time). It's possible to define the complexity as the

length of the shortest of all paths that reproduce $U(s)$. This definition is continuous and allows us to describe the actual time evolution of the black hole, etc. In [104], they showed that “if Hamiltonian is relatively easy, then the Hamiltonian $h(s)$ on $SU(N)$ is independent of s and $U(s)$ can be written as follows.

$$U(s) = e^{-ihs} \tag{3.6}$$

and becomes shortest path before the saturation.” Therefore, in this case, the complexity is simply proportional to s . Since this is time along the path, in this case complexity is proportional to time. In $SU(2)$ geometry, the distance from the unit matrix I is linearly increasing with time. After the saturation, we can find paths shorter than this.

These two properties: 1. entanglement entropy continues to increase beyond the typical time scale of saturation. 2. its evolution is proportional to time. From the above two properties, Susskind considered that these properties probe the long linear growth of the ERB [26]. In the following, we present the more general case of bulk dual beyond ERB. Several correspondences are proposed. Complexity calculated in terms of holography in this way is also called holographic complexity.

Holographic complexity

There are two definitions of complexity, strictly speaking, one for operator and the other for state, but when we consider holographic complexity, we mainly consider state complexity. In this case, complexity $\mathcal{C}(|\psi\rangle)$ for the target state $|\psi\rangle$ is the minimum number of elementary gates required to build that state from a reference one. We can consider the case where the target state $|\psi\rangle$ is an entangled state of two boundary theories, that live on the left and right boundaries. Given the target state $|\psi\rangle$, which is a function of both the left and right boundary time t_l, t_r , then Σ is a codimension one bulk Cauchy surface anchored at the boundary state t_l and t_r . There are three main holographic proposals that are dual to holographic complexity $\mathcal{C}[|\psi\rangle]$.

CA (Complexity=Action)

This is the gravitational bulk action I_{WdW} of the Wheeler-de Witt (WdW) patch of bulk causal diamond of Cauchy slice Σ ,

$$\mathcal{C}_A(\Sigma) = \frac{I_{\text{WdW}}}{\pi} \tag{3.7}$$

The WdW patch is given by a causal region (diamond-shaped region) inside the bulk, whose edge is anchored to the boundary time slice. In the case of de Sitter, it is anchored to the time slice defined on the stretched horizon. See Figure 8.

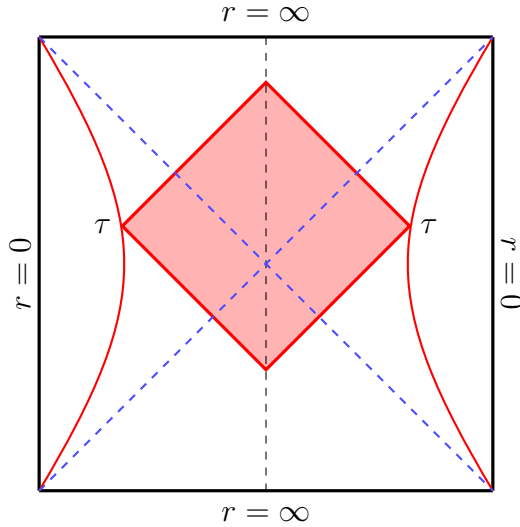


Figure 8: Penrose diagram for dS spacetime showing the WdW patch (red region).

CV2.0

This conjecture is similar to CA, but the difference is in CV2.0. The holographic Complexity is the space-time volume of the WdW patch

$$\mathcal{C}_W(\Sigma) = \frac{V_{\text{WdW}}}{G_N \ell_{\text{bulk}}^2} \quad (3.8)$$

instead of the action. In pure dS and pure AdS case, Lagrangian density is constant and proportional to ℓ_{bulk}^{-2} , therefore both CA and CV2.0 behave in similar ways⁶. Here ℓ_{bulk} is the length scale set by the cosmological constant.

CV (Complexity=Volume)

In this conjecture, the Complexity is evaluated by the maximal volume of codimension one surface Σ ,

$$\mathcal{C}_V = \max \left[\frac{V(\Sigma)}{G_N \ell_{\text{bulk}}} \right] \quad (3.9)$$

The maximization should be conducted under the condition that the boundary time t_l and t_r are fixed.

3.2 Holographic Complexity in AdS

The most famous holographic calculation of complexity is probing Einstein-Rosen bridge. As mentioned earlier, the Einstein-Rosen bridge continues to grow infinitely

⁶Precisely speaking, the behavior is generally different because of the boundary terms. However, the critical time τ_∞ given in (3.15) is determined by the WdW patch in both CA and CV2.0, as examined by [47].

long [25, 26]. Let us look at this. This calculation has been done in many places, but is most educational, for example in the case of 2D JT gravity. We can calculate the renormalized length of Einstein-Rosen bridge as the following.

$$L_{\text{ren}}(t) = 2 \log \left(2 \cosh \frac{t}{2} \right) + \dots \quad (3.10)$$

where \dots means small correction in large R_b (IR cutoff in AdS bulk). In the late time, this becomes $\sim t$, linear growth. On the other hand, it is known that the computational complexity (on the field theory side) generally increases linearly.

Switch back effect

In addition, we will briefly mention the switchback effect [48, 105], which is relevant for our purposes in this thesis. This considers the behaviour of complexity when perturbations are added on the field theory side. In AdS/CFT a two-sided black hole is supposed to emerge with appropriate entanglement on the CFT side. Specifically, it's described as Thermofield-double state $|\text{TFD}\rangle \in \mathcal{H}_L \otimes \mathcal{H}_R$.

$$|\text{TFD}\rangle = \sum_n e^{-\frac{\beta E_n}{2}} |E_n\rangle_L |E_n\rangle_R \quad (3.11)$$

When perturbations are mixed in $-t_w$ (early time, $t_w > 0$), we can write perturbed state as

$$W(-t_w)|\text{TFD}\rangle = U(t_w)WU^\dagger(t_w)|\text{TFD}\rangle \quad (3.12)$$

where U is the usual Unitary operator. This corresponds to the operation of going back in time by t_w , inserting an operator and finally advancing time by t_w . If the operator to be inserted is the unit operator 1, they all cancel each other. That is, the developments of time-reversal and time-forward exactly cancel each other. However, if the inserted operator is not 1, they generally do not cancel each other, since it can happen that the developments on the way there and on the way back are completely different. Thus naively, the complexity of the precursor is $2Kt_w$.

However, until scrambling comes, it is not possible to distinguish whether the inserted operator is 1 or not. Therefore, U and U^\dagger cancel each other until scrambling time, but after that they do not cancel each other because they are completely different developments in chaotic systems. Therefore, it is possible to consider that the increase in complexity is delayed by the scrambling time. Therefore, the actual value is $2K(t - t_*)$. This is called the switchback effect.

In bulk side, let us consider AdS spacetime with shockwave at the time $-t_w$ in the theory of boundary. If the inserted energy is E , the shockwave gains energy by the gravitational potential and reaches the following energy scale by reaching $t = 0$.

$$\frac{E}{M} e^{\frac{2\pi t_w}{\beta}} \quad (3.13)$$

where M is the mass of the black hole. This becomes $O(1)$ from the time order $t_* \sim \frac{\beta}{2\pi} \log \frac{M}{E}$. where E is the energy of a single particle being thermalized by the black hole, $E \sim T_H$ and

$$t_* \sim \frac{\beta}{2\pi} \log S \quad (3.14)$$

Thus, we can see that this energy changes significantly after t_* . Shockwaves inserted after t_* do not acquire the gravitational potential well and do not cause significant changes in complexity (U and U^\dagger cancel). Shockwaves inserted before t_* will result in a significant change in geometry. See for example [18, 106, 107].

3.3 Holographic Complexity in dS

Using all three (CA, CV2.0, CV) methods, the complexity calculations in general dS_{d+1} ($d \geq 2$) were made in [47]. As a result, they found that complexity and its growth rate diverge when a certain critical time τ_∞ is reached, no matter which conjecture is followed,

$$\lim_{\tau \rightarrow \tau_\infty} \mathcal{C} \rightarrow \infty, \quad \lim_{\tau \rightarrow \tau_\infty} \frac{d\mathcal{C}}{d\tau} \rightarrow \infty. \quad (3.15)$$

This is typical hyperfast behavior in dS_{d+1} ($d \geq 2$). The main contribution to this divergence is r_f reaches infinity, where r_f is the radius of the conical point at the most future tip of the WdW patch. In other words, the fact that the radius $r = r_f$ at the top vertex of the diamond-shaped-WdW patch diverges causes the volume of S^{d-1} to diverge, and as a result, causes the complexity diverges. In the case of CV, $r = r_{\text{turn}}$ diverges, which we will define later but r_{turn} is the radius of most future tip in Σ slice. See Figure 20 and 23.

In particular, let us look at the time dependence of the WdW patch. Note here that the holographic screen is on the stretched horizon $r = \rho \ell$, which is close to the cosmological horizon. Here $r = \ell$ is the cosmological horizon for pure dS and ρ is a parameter for the stretched horizon, *i.e.*, $0 < \rho < 1$ and $\rho \rightarrow 1$. We choose the boundary time increases upward on both the left and right stretched horizons such that $t_R = -t_L \propto \tau$ on the stretched horizon. As τ increase, the radius r at the top vertex of the diamond-shaped-WdW patch also increases. Then at some finite time, r_f will eventually reach infinity, and then, at the moment of arrival, the volume of the WdW patch also grows rapidly and diverges in dS_{d+1} ($d \geq 2$). Therefore, the critical time can be estimated as the time when $r_f = \infty$.

4 CA in JT gravity

In this section, we calculate the action complexity of the de Sitter spacetime considered in the two-dimensional JT gravity theory and show that it satisfies the hyperfast

property. Specifically, we define the Action of JT gravity in de Sitter spacetime as a dimensional reduction of 3-dimensional Einstein gravity. We consider reduction from three dimensions, partly because of Susskind's Motivation and partly because we will later reconsider the dual of two-dimensional complexity in terms of reduction in three dimensions. The divergence of the concrete complexity comes from the dilaton value.

4.1 Setup

According to the CA conjecture, the complexity of a state with a holographic realization is proportional to the full gravitational action of the Wheeler-DeWitt (WDW) patch:

$$\mathcal{C}_A = \frac{I_{\text{WDW}}}{\pi}. \quad (4.1)$$

We compute action complexity in Jackiw-Teitelboim (JT) gravity, whose bulk action is

$$I_{\text{JT}} = \frac{1}{8G} \int_{\mathcal{W}} d^2x \sqrt{-g} (\phi R + L^{-2} U(\phi)) + \frac{1}{4G} \int_{\partial\mathcal{W}} dy \sqrt{-h} \phi_b K, \quad (4.2)$$

with ϕ the dilaton and ϕ_b its value at the boundary $\partial\mathcal{W}$. The dilaton potential is $U(\phi) = 2\phi$ for anti-de Sitter (AdS) spacetime and $U(\phi) = -2\phi$ for de Sitter (dS) spacetime. The boundary term represents the Gibbons-Hawking-York (GHY) action [108, 109], where $K = h^{\mu\nu} K_{\mu\nu}$ is the trace of the extrinsic curvature. The latter is defined as $K_{\mu\nu} = h_{\mu}^{\rho} h_{\nu}^{\sigma} \nabla_{\rho} n_{\sigma}$, with n_{σ} the outward-directed normal to $\partial\mathcal{W}$.

The equations of motion for the dilaton and the metric are

$$R = -\frac{U'(\phi)}{L^2}, \quad (4.3)$$

$$0 = \nabla_a \nabla_b \phi - g_{ab} \nabla^2 \phi + \frac{g_{ab}}{2L^2} U(\phi). \quad (4.4)$$

In this paper, we work in dS spacetime, so we choose

$$U(\phi) = -2\phi. \quad (4.5)$$

With this choice, the equations of motion are solved by the following metric and dilaton

$$ds^2 = -f(r) dt^2 + \frac{dr^2}{f(r)}, \quad \phi = \frac{r}{L}, \quad (4.6)$$

where the blackening factor $f(r)$ is

$$f(r) = 1 - \frac{r^2}{L^2}. \quad (4.7)$$

In the following, we focus on the portion of spacetime with $0 \leq r < \infty$ (for the reason we shall explain at the beginning of subsection 4.2). Therefore, the position of the cosmological horizon is $r_h = L$. It is convenient to introduce the tortoise coordinate

$$r^*(r) = \int^r \frac{d\hat{r}}{f(\hat{r})}. \quad (4.8)$$

Taking as a boundary condition $r^*(0) = 0$, we get

$$r^*(r) = \frac{L}{2} \log \left| \frac{r+L}{r-L} \right|. \quad (4.9)$$

The Eddington-Finkelstein (EF) coordinates are given by

$$v = t + r^*(r), \quad u = t - r^*(r). \quad (4.10)$$

To describe the whole of spacetime, we need to consider two copies of EF coordinates, one for the right (R) and one for the left (L) side of the Penrose diagram, see figure 9. Note that u_R is constant along null rays falling into the cosmological horizon, whereas v_R is constant along outgoing null rays. The reverse behavior applies to the EF coordinates for the left side of the Penrose diagram.

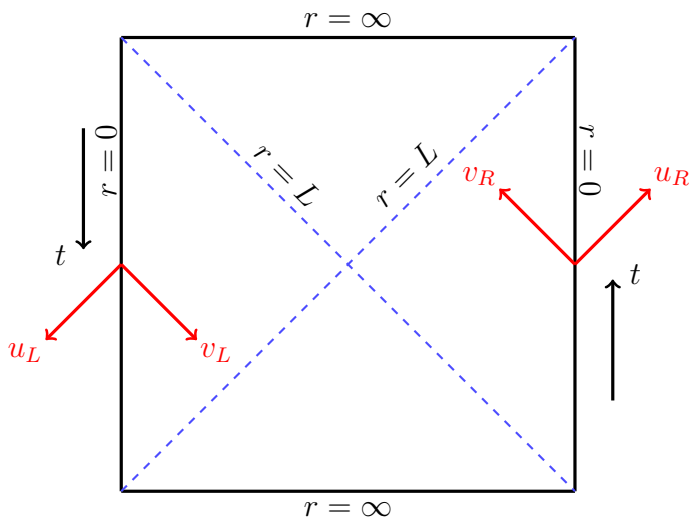


Figure 9: Penrose diagram for dS spacetime. The time coordinate t runs upwards on the right and downwards on the left. Coordinate axes for the EF coordinates on the right and the left are shown in red.

4.2 Action manual and dimensional reduction

Action complexity is obtained by evaluating the full gravitational action of the WDW patch as in eq. (4.1). The question of which action should be considered is non-trivial since the full JT gravity action of the relevant spacetime region is not just given by I_{JT} in eq. (4.2). In fact, there are several additional boundary contributions. In order to determine the right action, we exploit the fact that the dS JT gravity action in two dimensions can be obtained by dimensional reduction from three-dimensional pure dS, starting from the Einstein-Hilbert (EH) action plus boundary terms [110].⁷ We employ this procedure to explicitly compute action complexity in dS_2 .

⁷The dimensional reduction allows us to circumvent the study of the variational problem in JT gravity, leading to the same result for the full gravitational action.

Before we proceed, we point out that there are two ways to obtain dS₂ JT gravity from dimensional reduction. One is half reduction from pure dS₃ [110] and the other is full reduction from Schwarzschild-dS_d ($d \geq 4$) in the near-Nariai limit [111, 112] (see [110, 113, 114] as well). For our analysis, we use half reduction from pure dS₃, which automatically reduces to the $r \geq 0$ range. The dS₂ spacetime obtained from Schwarzschild-dS_d ($d \geq 4$) in the near-Nariai limit also includes $r < 0$ and a horizon at negative r . In this limit, we are zooming in on the very tiny region near the black hole and cosmological horizons, and the r -negative horizon corresponds to the original black hole one. Since our main interest is holographic complexity beyond the cosmological horizon, rather than black hole complexity, we focus on $r > 0$. For this purpose, half reduction from three-dimensional pure dS is enough. In three dimensions, the full gravitational action is [115]

$$\begin{aligned}
I_{\text{tot}} &= I_{\text{EHGHY}} + I_{\text{null}} + I_{\text{joint}} + I_{\text{ct}}, \\
I_{\text{EHGHY}} &\equiv \frac{1}{16\pi G_{(3)}} \int_{\tilde{\mathcal{W}}} d^3 X \sqrt{-g_{(3)}} (R_{(3)} - 2\Lambda_{(3)}) + \frac{1}{8\pi G_{(3)}} \int_{\partial\tilde{\mathcal{W}}} d^2 Y \sqrt{-h_{(3)}} K_{(3)}, \\
I_{\text{null}} &\equiv \frac{1}{8\pi G_{(3)}} \int_{\tilde{\mathcal{B}}} dS d\lambda \sqrt{\gamma} k, \quad I_{\text{joint}} \equiv \frac{1}{8\pi G_{(3)}} \int_{\tilde{\mathcal{J}}} d\theta \sqrt{\gamma} \tilde{\mathbf{a}}, \\
I_{\text{ct}} &\equiv \frac{1}{8\pi G_{(3)}} \int_{\tilde{\mathcal{B}}} dS d\lambda \sqrt{\gamma} \Theta \log |\tilde{L} \Theta|.
\end{aligned} \tag{4.11}$$

The term I_{EHGHY} contains the EH and the GHY actions, the latter coming from spacelike and timelike codimension-one boundaries. Contributions from codimension-one null surfaces $\tilde{\mathcal{B}}$ are given by I_{null} [115, 116]. In I_{joint} , we have the contributions from codimension-two joints $\tilde{\mathcal{J}}$ [115, 117] at the intersection between codimension-one surfaces. Finally, I_{ct} is a counterterm for null boundaries $\tilde{\mathcal{B}}$ [115] which ensures invariance of the full action under reparameterization of null normals. In what follows, we analyze each term separately and we apply dimensional reduction to determine the right action for holographic complexity in dS₂ JT gravity.

The EH-GHY action in three dimensions with positive cosmological constant reads

$$\begin{aligned}
I_{\text{EHGHY}} &= \frac{1}{16\pi G_{(3)}} \int_{\tilde{\mathcal{W}}} d^3 X \sqrt{-g_{(3)}} (R_{(3)} - 2\Lambda_{(3)}) \\
&\quad + \frac{1}{8\pi G_{(3)}} \int_{\partial\tilde{\mathcal{W}}} d^2 Y \sqrt{-h_{(3)}} K_{(3)},
\end{aligned} \tag{4.12}$$

where

$$\Lambda_{(3)} = \frac{1}{L_{(3)}^2}. \tag{4.13}$$

This admits a three-dimensional dS spacetime solution

$$ds_{(3)}^2 = g_{(3)MN} dX^M dX^N = -f(r) dt^2 + \frac{dr^2}{f(r)} + r^2 d\theta^2, \quad f(r) = 1 - \frac{r^2}{L_{(3)}^2}. \tag{4.14}$$

In the GHY boundary term in eq. (4.12), $h_{(3)}$ is the determinant of the induced metric on $\partial\tilde{\mathcal{W}}$ and $K_{(3)}$ denotes the trace of the extrinsic curvature.

We now introduce the metric ansatz

$$ds_{(3)}^2 = g_{(2)\mu\nu} dx^\mu dx^\nu + L_{(3)}^2 \phi^2(x) d\theta^2, \quad (4.15)$$

where we have expressed $X^M = (t, r, \theta) = (x^\mu, \theta)$ with $M = 0, 1, 2$ and $\mu = 0, 1$. As in eq. (4.6), we consider a solution for the dilaton $\phi(x)$ depending just on the radial coordinate: $\phi = \phi(r)$. From the metric ansatz (4.15), we get [110]

$$\begin{aligned} R_{(3)} &= R_{(2)} - \frac{2}{\phi} \square_{(2)} \phi, \\ K_{(3)} &= K_{(2)} + \frac{1}{\phi} n^\mu \nabla_{(2)\mu} \phi, \\ \sqrt{-g_{(3)}} &= L_{(3)} \phi \sqrt{-g_{(2)}}, \end{aligned} \quad (4.16)$$

with n^μ the normal vector to the two-dimensional boundary $\partial\tilde{\mathcal{W}}$. Plugging into eq. (4.12), we obtain

$$\begin{aligned} I_{\text{JT}} &= \frac{L_{(3)}}{8G_{(3)}} \int_{\mathcal{W}} d^2x \sqrt{-g_{(2)}} [\phi (R_{(2)} - 2\Lambda_{(3)}) - 2 \square_{(2)} \phi] \\ &\quad + \frac{L_{(3)}}{4G_{(3)}} \int_{\partial\mathcal{W}} dy \sqrt{-h_{(2)}} (\phi K_{(2)} + n^\mu \nabla_{(2)\mu} \phi), \end{aligned} \quad (4.17)$$

where \mathcal{W} and $\partial\mathcal{W}$ are the manifolds endowed with metric $g_{(2)\mu\nu}$ and $h_{(2)\mu\nu}$, respectively. Defining $G \equiv G_{(2)} = G_{(3)}/L_{(3)}$ and $L \equiv L_{(3)}$, we recognize the JT gravity action I_{JT} in eq. (4.2) with some additional terms. Three comments regarding the EH-GHY contributions are in order:

- According to the CA conjecture, we must evaluate the full gravitational action of the WDW patch. Such a spacetime region, which we denote by \mathcal{W} , is bounded by null codimension-one surfaces. Since there are neither timelike nor spacelike boundaries, the GHY term in eq. (4.17) vanishes.
- With the metric ansatz in eq. (4.15), the three-dimensional dS spacetime solution in eq. (4.14) comes down to the two-dimensional dS solution with linear dilaton given in eqs. (4.6) and (4.7). On-shell we have

$$R_{(2)} = 2\Lambda_{(3)} = \frac{2}{L_{(3)}^2}, \quad (4.18)$$

so the bulk contribution I_{JT} in eq. (4.17) reduces to

$$I_{\text{bulk}} = -\frac{1}{4G_{(2)}} \int_{\mathcal{W}} d^2x \sqrt{-g_{(2)}} \square_{(2)} \phi. \quad (4.19)$$

Even though we refer to this expression as two-dimensional “bulk” action, I_{bulk} is in fact a boundary term since it comprises a total divergence.⁸

- We can integrate the term $\square_{(2)}\phi$ getting a codimension-one contribution for the null boundaries of the WDW patch distinct from I_{null} in eq. (4.11):

$$I_{\text{bulk}} = -\frac{1}{4G_{(2)}} \int_{\tilde{\mathcal{B}}} d\lambda k^\mu \nabla_{(2)\mu} \phi = -\frac{1}{4G_{(2)}} \int_{\tilde{\mathcal{B}}} d\lambda \partial_\lambda \phi, \quad (4.20)$$

where k^μ is the null normal to $\tilde{\mathcal{B}}$, see [34] for an analog analysis in AdS₂ JT gravity. As we will see, this term yields nonzero contribution and is important to get consistency with the three-dimensional CA result.

Besides the bulk term, the full gravitational action of the WDW patch contains boundary terms for null codimension-one surfaces and joint terms for codimension-two surfaces at the intersection of null bounding surfaces, which we consider next.

The contribution from null boundaries has been originally studied in [115, 116]. In three-dimensional spacetime it is

$$I_{\text{null}} = \frac{1}{8\pi G_{(3)}} \int_{\tilde{\mathcal{B}}} dS d\lambda \sqrt{\gamma} k, \quad (4.21)$$

where λ is a parameter running along the null geodesics generating the surface $\tilde{\mathcal{B}}$, S is the transverse spatial direction to such generators, and γ is the determinant of the induced metric in the S direction. The constant κ is defined by the geodesic equation

$$\tilde{k}^M \nabla_{(3)M} \tilde{k}^N = \kappa \tilde{k}^N, \quad (4.22)$$

with $\tilde{k}^M = \frac{dX^M(\lambda)}{d\lambda}$ the null generator. In other words, κ measures the failure of λ to be an affine parameter. Consequently, we can set $\kappa = 0$ by a wise parameterization choice, getting rid of the I_{null} contribution.

At the intersection between bounding codimension-one surfaces, where the boundary is non-smooth, the joint term comes into play. The joint contributions involving just timelike and spacelike intersecting surfaces have been investigated in [117], while joints involving at least one null boundary have been studied in [115]. In our computation we will meet only joints involving two null boundaries, which in three-dimensional spacetime are given by

$$I_{\text{joint}} = \frac{1}{8\pi G_{(3)}} \int_{\tilde{\mathcal{J}}} d\theta \sqrt{\gamma} \tilde{\mathbf{a}}, \quad (4.23)$$

$$\sqrt{\gamma} = \sqrt{g_{(3)\theta\theta}}, \quad \tilde{\mathbf{a}} = \text{sign}(\text{joint}) \times \log \left| \frac{\tilde{\mathbf{k}}_1 \cdot \tilde{\mathbf{k}}_2}{2} \right|_{\tilde{\mathcal{J}}},$$

⁸As it will be clear later, at late times all contributions to the full action have the same divergence structure. Therefore, by neglecting I_{bulk} the qualitative behavior of action complexity at late times does not change.

where $\tilde{\mathbf{k}}_1, \tilde{\mathbf{k}}_2$ denote the one-forms normal to null boundaries, which are taken to be outward-directed from the spacetime region of interest. The sign of the joint term is fixed by the following rule. Choosing either of the two null boundaries intersecting at the joint, the sign of the corresponding contribution (4.23) is positive if the bulk region \mathcal{W} is at the future (past) of the segment and the joint itself is located at the past (future) edge of the selected segment. In the remaining configurations, the joint term has a negative sign [115].

Applying the dimensional reduction, we obtain

$$I_{\text{joint}} = \frac{1}{4G_{(2)}} \sum_{\mathcal{J}} \phi(r_{\mathcal{J}}) \mathbf{a}_{\mathcal{J}}, \quad \mathbf{a}_{\mathcal{J}} = \text{sign}(\text{joint}) \times \log \left| \frac{\mathbf{k}_1 \cdot \mathbf{k}_2}{2} \right|_J. \quad (4.24)$$

Here $r = r_{\mathcal{J}}$ is the radial position of the joint, and we consider one-forms $\mathbf{k}_1, \mathbf{k}_2$ normal to one-dimensional boundaries. By spherical symmetry of the dS_3 geometry, we trivially have $\tilde{\mathbf{k}}_i = \mathbf{k}_i$ and $\tilde{k}_i^M = (k_i^M, 0)$, with $i = 1, 2$.

The joint contributions in eq. (4.24) are affected by the arbitrariness of choosing the normalization of null normals $\mathbf{k}_1, \mathbf{k}_2$. Such ambiguity can be partially removed by requiring that $\mathbf{k}_i \cdot \partial_t = \pm\alpha$ at the spacetime boundary [118–120], with ∂_t the timelike Killing vector in the boundary theory and α a positive constant. Still, the constant α can be arbitrarily chosen. For the gravitational action to be invariant under the reparameterization of null generators, a counterterm must be added for each null boundary [115]. In three-dimensional spacetime, the counterterm has the following form

$$I_{\text{ct}} = \frac{1}{8\pi G_{(3)}} \int_{\tilde{\mathcal{B}}} dS d\lambda \sqrt{\gamma} \Theta \log \left| \tilde{L} \Theta \right|, \quad (4.25)$$

where \tilde{L} is an arbitrary length scale. In the above expression, Θ is the expansion of null geodesics given by $\Theta = \partial_\lambda \log \sqrt{\gamma}$. An explicit calculation with the metric ansatz (4.15) leads to

$$\Theta = \partial_\lambda \log \sqrt{g_{(3)\theta\theta}} = \partial_\lambda \log \phi = \frac{\partial_\lambda \phi}{\phi}. \quad (4.26)$$

Therefore, in JT gravity the counterterm reads

$$I_{\text{ct}} = \frac{1}{4G_{(2)}} \int_{\mathcal{B}} d\lambda \partial_\lambda \phi \log \left| \tilde{L} \partial_\lambda \log \phi \right|. \quad (4.27)$$

Summarizing, the full gravitational action for holographic complexity in dS_2 JT is given by

$$\begin{aligned} I_{\text{JTdS}_2} &= I_{\text{bulk}} + I_{\text{joint}} + I_{\text{ct}} \\ &= -\frac{1}{4G_{(2)}} \int_{\tilde{\mathcal{B}}} d\lambda \partial_\lambda \phi + \frac{1}{4G_{(2)}} \sum_{\mathcal{J}} \phi(r_{\mathcal{J}}) \mathbf{a}_{\mathcal{J}} \\ &\quad + \frac{1}{4G_{(2)}} \int_{\mathcal{B}} d\lambda \partial_\lambda \phi \log \left| \tilde{L} \partial_\lambda \log \phi \right|. \end{aligned} \quad (4.28)$$

The lesson we learn from the dimensional reduction analysis is that the effects of the dilaton, which explicitly appears in all terms of the full action (4.28), are important for the evaluation of holographic complexity. This is consistent with the discussion in the introduction. Note that in JT gravity the value of dilaton varies, and as a result, one has an effective Newton “constant”

$$\frac{1}{G_{(2)\text{eff}}} \equiv \frac{\phi}{G_{(2)}}. \quad (4.29)$$

We recall that in two dimensions there is no “area” for a black hole horizon, but instead, there is a dilaton. The dilaton plays the role of area. In fact, in $d(\geq 3)$ -dimensional dS spacetime, the orthogonal S^{d-2} area grows to infinity near the future spacelike infinity, and by dimensional reduction the size factor of the S^{d-2} area becomes the dilaton. Since the divergence of complexity in higher-dimensional dS is associated with the growth of the orthogonal S^{d-2} area [47], without taking into account the dilaton one cannot see the divergence of complexity in two-dimensional dS spacetime in JT gravity.

4.3 Action evaluation

We now move to the explicit computation of the full gravitational action, mainly following [47]. To ease the notation, we set $L_{(3)} \equiv L$. First, we introduce the stretched horizons for both the left and the right sides of the Penrose diagram. These are r -constant surfaces described by

$$r_{st} = \rho L, \quad 0 < \rho < 1, \quad (4.30)$$

where the limit $\rho \sim 1$ is intended. We then attach the WDW patch to the two stretched horizons, and we define the anchoring times as t_L and t_R for the left and the right horizons, respectively. It is not restrictive to focus on the symmetric case $t_R = -t_L$. For convenience, we define a dimensionless time as $t_R = L\tau$. We focus on the case where the tip of the WDW patch does not meet the future spacelike infinity at $r = \infty$.

For the right side of the geometry, the future boundary of the WDW patch is at constant u_R , whereas the past boundary is at constant v_R . From eq. (4.10), the defining equations are

$$\begin{aligned} u_{FR} &= t_R - r^*(r_{st}) = L\tau - \frac{L}{2} \log \left(\frac{1+\rho}{1-\rho} \right), \\ v_{PR} &= t_R + r^*(r_{st}) = L\tau + \frac{L}{2} \log \left(\frac{1+\rho}{1-\rho} \right). \end{aligned} \quad (4.31)$$

Let us denote by $r = r_{\pm}$ the position of the future and past tip of the WDW patch, respectively. By symmetry, both tips are located on the vertical axis in the middle

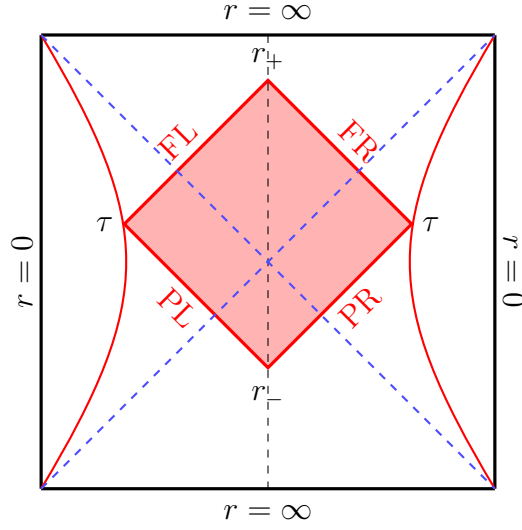


Figure 10: Penrose diagram for dS spacetime showing the WDW patch (red region). The stretched horizons at $r = \rho L$ are represented by red curves.

of the Penrose diagram, which is described by $t = 0$. So, evaluating u_{FR} defined in eq. (4.31) at the future tip, from eq. (4.10) we get

$$L\tau - \frac{L}{2} \log \left(\frac{1+\rho}{1-\rho} \right) = -\frac{L}{2} \log \left(\frac{r_+ + L}{r_+ - L} \right), \quad (4.32)$$

which leads to

$$\frac{r_+}{L} = \frac{\cosh \tau - \rho \sinh \tau}{\rho \cosh \tau - \sinh \tau}. \quad (4.33)$$

Similarly, computing v_{PR} defined in eq. (4.31) at the past tip we obtain

$$L\tau + \frac{L}{2} \log \left(\frac{1+\rho}{1-\rho} \right) = \frac{L}{2} \log \frac{r_- + L}{r_- - L}, \quad (4.34)$$

from which

$$\frac{r_-}{L} = \frac{\cosh \tau + \rho \sinh \tau}{\rho \cosh \tau + \sinh \tau}. \quad (4.35)$$

The time $\tau = \tau_\infty$ at which the future tip meets the future spacelike infinity $r \rightarrow \infty$ can be obtained by eq. (4.33) as

$$\tau_\infty = \tanh^{-1} \rho. \quad (4.36)$$

We can thus rewrite eqs. (4.32) and (4.34) as

$$\tau_\infty - \tau = \tanh^{-1} \left(\frac{L}{r_+} \right), \quad \tau + \tau_\infty = \tanh^{-1} \left(\frac{L}{r_-} \right), \quad (4.37)$$

or equivalently

$$r_\pm = L \coth(\tau_\infty \mp \tau). \quad (4.38)$$

Since we are interested in how complexity grows as τ approaches τ_∞ , we focus on $\tau \leq \tau_\infty$. We now evaluate the gravitational action in eq. (4.28) term by term.

Explicit computation of the boundary term in eq. (4.20) gives

$$\begin{aligned} I_{\text{bulk}} &= \frac{\phi}{2G_{(2)}} \Big|_{\rho L}^{r_+} + \frac{\phi}{2G_{(2)}} \Big|_{\rho L}^{r_-} = \frac{1}{G_{(2)}} \left(\frac{r_+ + r_- - 2\rho L}{2L} \right) \\ &= \frac{1}{G_{(2)}} \frac{\rho(1 - \rho^2) \cosh^2 \tau}{1 - (1 - \rho^2) \cosh^2 \tau}, \end{aligned} \quad (4.39)$$

where in the last step eqs. (4.33) and (4.35) has been used.

We now move to the boundary terms. The null normals $\mathbf{k} = k_\mu dx^\mu$ to the four codimension-one boundaries of the WDW patch are

$$\begin{aligned} \mathbf{k}_{FR} &= \alpha du_R = \alpha \left(dt - \frac{dr}{f(r)} \right), \\ \mathbf{k}_{PR} &= -\beta dv_R = \beta \left(-dt - \frac{dr}{f(r)} \right), \\ \mathbf{k}_{FL} &= -\alpha' dv_L = \alpha' \left(-dt - \frac{dr}{f(r)} \right), \\ \mathbf{k}_{PL} &= \beta' du_L = \beta' \left(dt - \frac{dr}{f(r)} \right), \end{aligned} \quad (4.40)$$

where $\alpha, \beta, \alpha', \beta'$ are positive arbitrary constants and F (P) stands for future (past), see figure 10. This choice corresponds to an affine parameterization of null normals, thus the boundary term (4.21) for null surfaces vanishes. To compute the four joint terms in eq. (4.24) we need

$$\begin{aligned} \mathbf{a}_+ &= + \log \left| \frac{\mathbf{k}_{FR} \cdot \mathbf{k}_{FL}}{2} \right|_{r=r_+} = \log \left| \frac{\alpha\alpha'}{f(r_+)} \right|, \\ \mathbf{a}_- &= + \log \left| \frac{\mathbf{k}_{PR} \cdot \mathbf{k}_{PL}}{2} \right|_{r=r_-} = \log \left| \frac{\beta\beta'}{f(r_-)} \right|, \\ \mathbf{a}_{st,R} &= - \log \left| \frac{\mathbf{k}_{FR} \cdot \mathbf{k}_{PR}}{2} \right|_{r=r_{st}} = - \log \left| \frac{\alpha\beta}{f(\rho L)} \right|, \\ \mathbf{a}_{st,L} &= - \log \left| \frac{\mathbf{k}_{FL} \cdot \mathbf{k}_{PL}}{2} \right|_{r=r_{st}} = - \log \left| \frac{\alpha'\beta'}{f(\rho L)} \right|. \end{aligned} \quad (4.41)$$

Then, the total joint contribution is

$$\begin{aligned} I_{\text{joint}} &= I_+ + I_- + I_{st,R} + I_{st,L} \\ &= \frac{1}{4G_{(2)}L} \left(r_+ \log \frac{\alpha\alpha' L^2}{r_+^2 - L^2} + r_- \log \frac{\beta\beta' L^2}{r_-^2 - L^2} - \rho L \log \frac{\alpha\beta\alpha'\beta'}{(1 - \rho^2)^2} \right). \end{aligned} \quad (4.42)$$

Finally, we have to calculate the counterterm for null boundaries given by eq. (4.27). We start from the FR boundary. The null vector orthogonal to this surface

is

$$k_{FR}^\mu = g^{\mu\nu} k_{FR\nu} = -\alpha \left(\frac{1}{f(r)}, 1 \right). \quad (4.43)$$

By definition, the null vector is $k^\mu = \partial_\lambda x^\mu = (\dot{t}, \dot{r})$, where the dot denotes a derivative with respect to the affine parameter λ . We thus conclude that $\dot{r} = -\alpha$, implying that $r = -\alpha \lambda$ is an affine parameter too which increases when λ decreases. Putting all together, we get

$$\begin{aligned} I_{ct,FR} &= \frac{1}{4G_{(2)}L} \int_{r_+}^{\rho L} dr \log \frac{\tilde{L} \alpha}{r} \\ &= \frac{1}{4G_{(2)}L} \left(\rho L - r_+ + \rho L \log \left(\frac{\tilde{L} \alpha}{\rho L} \right) - r_+ \log \left(\frac{\tilde{L} \alpha}{r_+} \right) \right). \end{aligned} \quad (4.44)$$

By symmetry, the contribution on the future left boundary is simply $I_{ct,FL} = I_{ct,FR}(\alpha \rightarrow \alpha')$. Similarly, the counterterm for the right past boundary is

$$\begin{aligned} I_{ct,PR} &= \frac{1}{4G_{(2)}L} \int_{r_-}^{\rho L} dr \log \frac{\tilde{L} \beta}{r} \\ &= \frac{1}{4G_{(2)}L} \left(\rho L - r_- + \rho L \log \left(\frac{\tilde{L} \beta}{\rho L} \right) - r_- \log \left(\frac{\tilde{L} \beta}{r_-} \right) \right), \end{aligned} \quad (4.45)$$

and the contribution from the past left boundary is $I_{ct,PL} = I_{ct,PR}(\beta \rightarrow \beta')$. So, the total counterterm reads

$$\begin{aligned} I_{ct} &= I_{ct,FR} + I_{ct,FL} + I_{ct,PR} + I_{ct,PL} \\ &= \frac{1}{4G_{(2)}L} \left(4\rho L - 2r_+ - 2r_- + \rho L \log \left(\frac{\tilde{L}^4 \alpha \beta \alpha' \beta'}{\rho^4 L^4} \right) - r_+ \log \left(\frac{\tilde{L}^2 \alpha \alpha'}{r_+^2} \right) - r_- \log \left(\frac{\tilde{L}^2 \beta \beta'}{r_-^2} \right) \right). \end{aligned} \quad (4.46)$$

Note that the terms containing the arbitrary constants $\alpha, \beta, \alpha', \beta'$ cancel the corresponding terms in the joint contribution (4.42). In details,

$$\begin{aligned} I_{\text{joint}} + I_{ct} &= \frac{1}{2G_{(2)}L} \left(2\rho L - r_+ - r_- + r_+ \log \frac{r_+ L}{\tilde{L} \sqrt{r_+^2 - L^2}} + r_- \log \frac{r_- L}{\tilde{L} \sqrt{r_-^2 - L^2}} - \rho L \log \frac{\rho^2 L^2}{\tilde{L}^2 (1 - \rho^2)} \right) \\ &= \frac{1}{2G_{(2)}L} \left(L \coth(\tau_\infty - \tau) \left(\log \left(\frac{L \cosh(\tau_\infty - \tau)}{\tilde{L}} \right) - 1 \right) + (\tau \rightarrow -\tau) \right. \\ &\quad \left. - 2L \tanh(\tau_\infty) \left(\log \left(\frac{L \sinh(\tau_\infty)}{\tilde{L}} \right) - 1 \right) \right), \end{aligned} \quad (4.47)$$

where in the second equality eqs. (4.36) and (4.38) have been used.

Summing up eqs. (4.39) and (4.47), we finally get the action complexity

$$\begin{aligned} \mathcal{C}_A &= \frac{I_{\text{JTdS}_2}}{\pi} = \frac{I_{\text{bulk}} + I_{\text{joint}} + I_{ct}}{\pi} \\ &= \frac{1}{2\pi G_{(2)}} \left(\frac{2\rho(1-\rho^2)\cosh^2\tau}{1-(1-\rho^2)\cosh^2\tau} - 2\tanh(\tau_\infty) \left(\log\left(\frac{L\sinh(\tau_\infty)}{\tilde{L}}\right) - 1 \right) \right. \\ &\quad \left. + \coth(\tau_\infty - \tau) \left(\log\left(\frac{L\cosh(\tau_\infty - \tau)}{\tilde{L}}\right) - 1 \right) + (\tau \rightarrow -\tau) \right), \end{aligned} \quad (4.48)$$

which matches the dS_3 result found in [47], with $G_{(2)} = G_{(3)}/L$.

Some comments are in order:

- The \mathcal{C}_A given by eq. (4.48) diverges at the critical time

$$\cosh^2\tau_\infty = \frac{1}{1-\rho^2}, \quad (4.49)$$

which is exactly eq. (4.36). In the limit $\tau \rightarrow \tau_\infty$, both r_+ and \mathcal{C}_A diverge at the leading order. In particular,

$$r_+ = \frac{L}{(\tau_\infty - \tau)} + (\text{subleading}) \quad \text{as } \tau \rightarrow \tau_\infty, \quad (4.50)$$

where we have used eq. (4.33), and

$$\mathcal{C}_A = \frac{1}{\pi G_{(2)}} \frac{1}{\sqrt{2-\rho^2}} \frac{1}{(\tau - \tau_\infty)} \propto \frac{r_+}{G_{(2)}} + (\text{subleading}) \quad \text{as } \tau \rightarrow \tau_\infty. \quad (4.51)$$

Therefore, the late-time behavior of \mathcal{C}_A is

$$\mathcal{C}_A \sim \frac{\phi}{G_{(2)}} \equiv \frac{1}{G_{(2)\text{eff}}}. \quad (4.52)$$

As discussed in the introduction, this is exactly what we expect in JT gravity.

- As first pointed out in [3], in $d \geq 3$ dimensions volume complexity diverges at the critical time. This can be understood from the fact that maximal slices anchored at the two stretched horizons bend upwards to the future spacelike infinity, where local $(d-2)$ -spheres exponentially expand. In JT gravity, the effect of such an exponential expansion appears in the linear dilaton. Note that the static coordinate r behaves as time beyond the cosmological horizon $r \geq L$ and it diverges at the future spacelike infinity.
- Even though τ_∞ diverges in the limit $\rho \rightarrow 1$, it does as

$$\rho \equiv 1 - \epsilon, \quad \tau_\infty = \frac{1}{2} \log \frac{2}{\epsilon} + O(\epsilon). \quad (4.53)$$

So, the τ_∞ dependence on the stretched horizon parameter ϵ is very mild [3, 47].

- Without taking into account the dilaton, volume complexity in dS_2 remains finite due to the lack of a local exponentially expanding $(d-2)$ -sphere in two dimensions [39, 47].

5 Geodesics, Volume and Weyl dependence

In this section, we point out that volume is not a well-defined quantity in JT gravity, focusing on the intrinsic properties of JT gravity theory, and discussing the superiority of action complexity over volume complexity.

5.1 Volume complexity in dS₂

First, we discuss the complexity of the two-dimensional de Sitter spacetime.

5.2 Weyl field redefinition

In this section, we discuss volume complexity and its subtleties. Before we proceed, we review the basic point.

The most general two-dimensional dilaton gravity bulk action up to two derivatives can be written in the form

$$S = \frac{1}{8G} \int_{\mathcal{W}} d^2x \sqrt{-\tilde{g}} \left(U_1(\Phi) \tilde{R} + U_2(\Phi) \tilde{g}^{\mu\nu} \tilde{\nabla}_\mu \Phi \tilde{\nabla}_\nu \Phi + L^{-2} U_3(\Phi) \right). \quad (5.1)$$

We can perform a Weyl field redefinition

$$\tilde{g}_{\mu\nu} = e^{2\omega} g_{\mu\nu}, \quad \nabla_\mu \omega = -\frac{U_2(\Phi)}{2U_1'(\Phi)} \nabla_\mu \Phi, \quad (5.2)$$

to get rid of the kinetic term. Then, by doing a simple field redefinition $\phi = U_1(\Phi)$, we can remove U_1 as well. Note that this Weyl field redefinition does not change the coefficient of the $\sqrt{-\tilde{g}}\tilde{R}$ terms and we are left with just one function of ϕ which is related to U_3 as $U(\phi) = U_3(\Phi)$. Therefore, a general dilaton gravity system can be brought to the form

$$S = \frac{1}{8G} \int d^2x \sqrt{-g} (\phi R + L^{-2} U(\phi)), \quad (5.3)$$

which admits the two-dimensional dS solution with linear dilaton in eq. (4.6).

Note that even though the intermediate Weyl transformation done above is *just a field redefinition*, and hence should not affect physical quantities, it has significant influence in the context of the CV conjecture, since the volume changes by Weyl transformation. In this section, we study the effects of Weyl transformations on the CV conjecture. To evaluate volume complexity, it is convenient to use the metric ansatz

$$ds^2 = -f(r) dt^2 + \frac{dr^2}{f(r)}. \quad (5.4)$$

In fact, by starting with the dS₂ solution in eq. (4.6) and by applying the Weyl transformation-like field redefinition

$$g_{\mu\nu} \equiv \Omega(\phi) \hat{g}_{\mu\nu}, \quad (5.5)$$

one can always put the metric in the form of eq. (5.4) by a coordinate change, as we will show soon. Here we always assume $\Omega(\phi)$ is regular. In what follows, we set $L = 1$ for convenience. The L scale can always be recovered by dimensional analysis.

Since $\phi = r$, we have $\Omega(\phi) = \Omega(r)$. Starting from $f(r) = 1 - r^2$, the Weyl-transformed metric is given by

$$ds^2 = \Omega(r) \left(-f(r)dt^2 + \frac{dr^2}{f(r)} \right) = -\Omega(r)f(r)dt^2 + \frac{\Omega^2(r)dr^2}{\Omega(r)f(r)}. \quad (5.6)$$

Defining the coordinate \tilde{r} in terms of r as

$$\tilde{r}(r) = \int^r \Omega(\hat{r})d\hat{r}, \quad (5.7)$$

the line element can be written as

$$ds^2 = -\tilde{f}(\tilde{r})dt^2 + \frac{d\tilde{r}^2}{\tilde{f}(\tilde{r})}, \quad \tilde{f}(\tilde{r}) = \Omega(r(\tilde{r}))f(r(\tilde{r})). \quad (5.8)$$

One can check that the temperature of the solution remains unchanged upon Weyl transformation-like field redefinition because t is unmodified. In this way, we can always make the metric in the form eq. (5.4). However, note that the dilaton is no more linear in terms of the new radial coordinate \tilde{r}

$$\phi = r(\tilde{r}). \quad (5.9)$$

In the end, this is just a field-redefinition, so physics should not be modified. Since the vacuum of JT gravity is characterized by both the metric and the dilaton, reasonable physical quantities should be determined by taking into account both. While the on-shell action is invariant under such field-redefinitions, the volume is not, because it is determined by the metric only. In other words, action complexity is invariant, but the volume (precisely, geodesic length) changes, as we will see explicitly.

Given the metric ansatz in eq. (5.4), we now present the procedure to compute the length of geodesic following the approach of [39, 47]. As in the action computation, we focus on the portion of spacetime with $0 \leq r < \infty$.

In EF coordinates (4.10), the line element on the right side of the Penrose diagram covered by (v_R, r) or (u_R, r) coordinates is

$$ds^2 = -f(r)dv_R^2 + 2dv_Rdr = -f(r)du_R^2 - 2du_Rdr. \quad (5.10)$$

The length of geodesics in this geometry reads

$$V = \int ds \sqrt{-f\dot{v}_R^2 + 2\dot{v}_R\dot{r}} = \int ds \sqrt{-f\dot{u}_R^2 - 2\dot{u}_R\dot{r}}, \quad (5.11)$$

where the dot denotes the derivative with respect to the geodesic parameter s . Since the geodesic is spacelike, we can always choose a parameterization such that the integrand in eq. (5.11) is unity:

$$\begin{aligned} -f\dot{v}_R^2 + 2\dot{v}_R\dot{r} &= 1 \quad \rightarrow \quad \dot{r} = \frac{1 + f\dot{v}_R^2}{2\dot{v}_R}, \\ -f\dot{u}_R^2 - 2\dot{u}_R\dot{r} &= 1 \quad \rightarrow \quad \dot{r} = -\frac{1 + f\dot{u}_R^2}{2\dot{u}_R}. \end{aligned} \quad (5.12)$$

The equations of motion obtained from eq. (5.11) by varying u_R, v_R lead to the conserved quantity

$$\begin{aligned} P &= \frac{\delta V}{\delta \dot{v}_R} = -f\dot{v}_R + \dot{r} = \frac{1 - f\dot{v}_R^2}{2\dot{v}_R}, \\ P &= \frac{\delta V}{\delta \dot{u}_R} = -f\dot{u}_R - \dot{r} = \frac{1 - f\dot{u}_R^2}{2\dot{u}_R}. \end{aligned} \quad (5.13)$$

We can thus express \dot{u}_R, \dot{v}_R , and \dot{r} in terms of the conserved quantity P as

$$\dot{r}_\pm = \pm\sqrt{f + P^2}, \quad \dot{u}_{R\pm} = \frac{-P - \dot{r}_\pm}{f}, \quad \dot{v}_{R\pm} = \frac{-P + \dot{r}_\pm}{f}. \quad (5.14)$$

The sign \pm in the above equation indicates whether the parameter s increases or decreases along the direction of increasing r . There is a turning point where $f(r_t) + P^2 = 0$. We consider geodesics anchored at the left and right stretched horizons $r = r_{st}$, defined in eq. (4.30). We take by convention the parameter s to increase from the left stretched horizon to the right one. In the chosen gauge, the volume is given by

$$V(P) = \int ds = 2 \int_{r_{st}}^{r_t} \frac{dr}{\dot{r}_+} = 2 \int_{r_{st}}^{r_t} \frac{dr}{\sqrt{f(r) + P^2}}, \quad (5.15)$$

where by symmetry we integrate over the left half of the geodesic and we introduce a multiplicative factor of 2. The dependence of volume on the stretched horizon time $t_R = -t_L = \tau$ is encoded in the conserved quantity P . For $P > 0$, geodesics explore the region beyond the future cosmological horizon [39, 47]. In this case, the right portion of geodesics is fully covered by the EF coordinate u_R , while the left portion is fully described by v_L , see figure 9. The time dependence of P can thus be computed by

$$u_R(r_{st}) - u_R(r_t) = \int_{r_t}^{r_{st}} \frac{\dot{u}_{R-}}{\dot{r}_-} dr = \int_{r_{st}}^{r_t} T(P, r) dr, \quad (5.16)$$

$$v_L(r_t) - v_L(r_{st}) = \int_{r_{st}}^{r_t} \frac{\dot{v}_{L+}}{\dot{r}_+} dr = \int_{r_{st}}^{r_t} T(P, r) dr, \quad (5.17)$$

where

$$T(P, r) \equiv \frac{\sqrt{f(r) + P^2} - P}{f(r)\sqrt{f(r) + P^2}}. \quad (5.18)$$

Summing up eqs. (5.16) and (5.17) and using the definition of the EF coordinates, we end up with

$$\tau(P) = r^*(r_{st}) - r_t^* + \int_{r_{st}}^{r_t} T(P, r) dr = - \int_{r_{st}}^{r_t} \frac{P}{f(r)\sqrt{f(r) + P^2}} dr, \quad (5.19)$$

where we have defined $r_t^* \equiv r^*(r_t)$. Note that the case $P < 0$ corresponds to a time-reflection $\tau \rightarrow -\tau$.

As we have seen, the metric resulting from Weyl field-redefinition is given by eq. (5.6). So, eqs. (5.15) and (5.19) still hold true, provided that we replace $r, f(r) \rightarrow \tilde{r}, \tilde{f}(\tilde{r})$ given by eqs. (5.7) and (5.8). Therefore, after the Weyl field-redefinition, the volume and the stretched horizon time are given by

$$V(P) = 2 \int_{\tilde{r}_{st}}^{\tilde{r}_t} \frac{d\tilde{r}}{\sqrt{\tilde{f}(\tilde{r}) + P^2}} = 2 \int_{r_{st}}^{r_t} \frac{\Omega(r)}{\sqrt{\Omega(r)f(r) + P^2}} dr, \quad (5.20)$$

$$\tau(P) = \tilde{r}^*(\tilde{r}_{st}) - \tilde{r}_t^* + \int_{\tilde{r}_{st}}^{\tilde{r}_t} \tilde{T}(P, \tilde{r}) d\tilde{r} = - \int_{r_{st}}^{r_t} \frac{P}{f(r)\sqrt{\Omega(r)f(r) + P^2}} dr, \quad (5.21)$$

where \tilde{r}_t is the turning point obtained by

$$\tilde{f}(\tilde{r}_t) + P^2 = 0, \quad (5.22)$$

and \tilde{r}^* is the tortoise coordinate defined by

$$\tilde{r}^*(\tilde{r}) = \int^{\tilde{r}} \frac{d\hat{r}}{\tilde{f}(\hat{r})}. \quad (5.23)$$

To illustrate the Weyl dependence of the volume, we consider $\Omega(\phi) = \Omega(r)$ of the form

$$\Omega(\phi) = \phi^w = r^w, \quad (5.24)$$

so that we get

$$\tilde{r} = \frac{r^{w+1}}{w+1}. \quad (5.25)$$

By choosing a few specific values of w , we now show in detail how the volume in dS spacetime changes as we change w .

• $w = 0$

We consider the dS blackening factor given by eq. (4.7) with $L = 1$. Thus, the cosmological horizon is at $r = 1$. The stretched horizon is specified by the location where the dilaton takes the fixed value

$$\phi_{st} = r_{st} = \rho. \quad (5.26)$$

The turning point of the geodesic elongating between the right and left stretched horizons is

$$r_t = \sqrt{1 + P^2}. \quad (5.27)$$

The volume and the boundary time can be computed explicitly and are given by

$$\begin{aligned} V(P) &= 2 \int_{\rho}^{\sqrt{1+P^2}} \frac{dr}{\sqrt{f(r) + P^2}} = \pi - 2 \arctan \left[\frac{\rho}{\sqrt{P^2 + 1 - \rho^2}} \right], \\ \tau(P) &= - \int_{\rho}^{\sqrt{1+P^2}} \frac{P}{f(r)\sqrt{f(r) + P^2}} dr = \operatorname{arctanh} \left[\frac{P\rho}{\sqrt{P^2 + 1 - \rho^2}} \right], \end{aligned} \quad (5.28)$$

as found in [47]. If we set $\rho = 0$, geodesics stretch between the poles of dS spacetime. In this case, we get $V(P) = \pi$ and $\tau(P) = 0$, which is consistent with the result of [39].

• $w = 2$

For the case $w = 2$, we have

$$\tilde{r} = \frac{r^3}{3}, \quad (5.29)$$

so the blackening factor becomes

$$\tilde{f}(\tilde{r}) = (3\tilde{r})^{2/3}(1 - (3\tilde{r})^{2/3}). \quad (5.30)$$

The turning point in terms of the original coordinate r is given by

$$r_t = \frac{1}{\sqrt{2}} \sqrt{1 + \sqrt{1 + 4P^2}}. \quad (5.31)$$

Since the Weyl transformation only changes the metric, and not the dilaton, the location of the stretched horizon is still given by eq. (4.30). The expressions for the volume and the boundary time are given by

$$\begin{aligned} V(P) &= 2 \int_{\tilde{r}_{st}}^{\tilde{r}_t} \frac{d\tilde{r}}{\sqrt{\tilde{f}(\tilde{r}) + P^2}} = 2 \int_{\rho}^{r_t} \frac{r^2}{\sqrt{r^2(1 - r^2) + P^2}} dr, \\ \tau(P) &= - \int_{\tilde{r}_{st}}^{\tilde{r}_t} \frac{P}{\tilde{f}(\tilde{r})\sqrt{\tilde{f}(\tilde{r}) + P^2}} d\tilde{r} = - \int_{\rho}^{r_t} \frac{P}{(1 - r^2)\sqrt{r^2(1 - r^2) + P^2}} dr. \end{aligned} \quad (5.32)$$

In order to compare the cases $w = 0, 2$ described above, in figure 11 we present some plots of the volume as a function of time on the stretched horizon.

Remarkably, for $w = 2$ the volume diverges at the critical time, qualitatively matching the behavior of action complexity. Below, we consider refined volume for complexity.

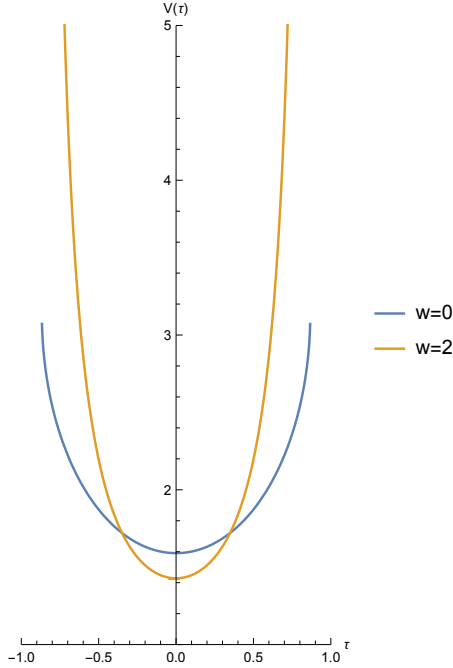


Figure 11: Plot of $V(\tau)$ for fixed values of w . As $\tau \rightarrow \tau_\infty$, the refined volume behaves differently depending on w . The $w = 0$ result is bounded by π . Instead, the refined volume for $w = 2$ diverges, due to the additional Weyl (dilaton) contribution from the point near the future infinity. We set $\rho = 0.7$ and $\tau_\infty = \operatorname{arctanh}(\rho) = 0.88$.

5.3 Refined volume for complexity

As we have seen, despite a field redefinition should not influence physics, volume complexity is clearly modified by this kind of transformation. Moreover, there is a discrepancy between volume complexity and action complexity in JT gravity. In this subsection, we look for a Weyl factor of the form in eq. (5.24) with an appropriate parameter w for which the transformed volume complexity behaves qualitatively as action complexity. We refer to the volume with this specific choice of w as refined volume.

This can be easily done as follows. We recall that the action complexity we computed in section 4 is obtained by dimensional reduction from dS_3 . Therefore, action complexity in dS_2 JT gravity is essentially the same as in dS_3 Einstein gravity. For Einstein gravity in dS_{d+1} , both CV and CA conjectures are studied in detail in [47], where the authors have found

$$V \sim \int_\rho^{r_t} dr \frac{(r/L)^{2(d-1)}}{\sqrt{P^2 + f(r)} (r/L)^{2(d-1)}}, \quad \tau \sim \int_\rho^{r_t} \frac{dr}{L} \frac{-P}{f(r) \sqrt{P^2 + f(r)} (r/L)^{2(d-1)}}, \quad (5.33)$$

see eq. (5.9) and (5.11) in [47]. In dS_{d+1} ($d \geq 2$), both volume and action complexity grow as r_+^{d-2} . Therefore, a direct comparison of the above result with our eqs. (5.20)

and (5.21) for dS_3 determines

$$\Omega(\phi) = \phi^2. \quad (5.34)$$

With this choice, corresponding to $w = 2$ in eq. (5.24), the refined volume matches volume complexity in Einstein gravity dS_3 , which reduces to JT gravity dS_2 . In this way, in JT gravity one can define the Weyl transformed refined volume which behaves as action complexity.⁹

We end this section by pointing out that, in a similar spirit as the refined volume we have discussed, modifications of the CV conjecture in non-Einstein gravity theories with higher derivative terms have been proposed in [121–124].

6 BTZ/dS spacetime with shock waves

In this section, we review the spacetime metric when a shockwave is inserted as a preparation for the next section, which examines the response of hyperfast properties to shockwaves. To understand the effects of shock waves, we will study the geometry of AdS and dS in single shock wave case and double shock waves case. There are two ways that we consider for our analysis.

- *Method 1*

Finding a shock wave geometry on the horizon through the Einstein equation

One way is considering a shock wave on the horizon, which is induced by the delta-function stress tensor. Einstein equation determines the resultant back-reacted metric of the shock wave, and the effect of the shock wave is restricted only on the shock wave, *i.e.*, horizon. Even though the metric is unchanged by the shock wave except on the horizon, in this case, the two metric coordinates, one above and the other below the shock wave, are connected by a simple translational constant shift on the horizon.

- *Method 2*

Cutting and connecting different solutions

Another way is preparing the two different geometry, and cutting them at a null surface but that null surface is not necessarily the horizon, and connecting the two geometry at the null surface. In this case, the stress tensor is not simply a delta functional. Although it is proportional to a delta function, its magnitude is a function of the radial coordinate. The difference of coordinates at the connecting null surface is not as simple as above *Method 1*. However, in certain limits, one can see the consistency with the *Method 1*.

⁹More generally, to get the volume complexity result of conventional JT gravity to match with the corresponding result of Einstein gravity in dS_{d+1} , the Weyl factor should be taken to be $\Omega(\phi) = \phi^{2(d-1)}$.

Hence we will analyze shock waves following these two methods for the BTZ case and dS case respectively. We will also check the consistency between *Method 1* and *2* as well.

6.1 BTZ spacetime

We first consider the case of BTZ with shock waves.

The BTZ black hole metric is

$$ds^2 = -f(r)dt^2 + \frac{dr^2}{f(r)} + r^2d\phi^2, \quad (6.1)$$

$$f(r) = \frac{r^2 - R^2}{\ell^2}, \quad (6.2)$$

where $f(r)$ is blackening factor and ℓ is AdS-radius. R is the horizon radius which is related to the BTZ black hole mass M as

$$R^2 = 8G_N M \ell^2. \quad (6.3)$$

Let us rewrite this in Kruskal coordinates defined by

$$U_R = -e^{-\frac{R}{\ell^2}(t_R - r^*)}, \quad V_R = e^{\frac{R}{\ell^2}(t_R + r^*)}, \quad (6.4)$$

where $r^*(r)$ is a tortoise coordinate,

$$r^*(r) = \int \frac{dr}{f(r)} = \frac{\ell^2}{2R} \log \left| \frac{r - R}{r + R} \right|. \quad (6.5)$$

The subscript R in t_R indicates that this definition only covers the right Rindler patch. At the black hole horizon $r \rightarrow R$, $r^*(r) \rightarrow -\infty$. To describe the black hole patch, the left patch, and the white hole patch, we need to perform analytic continuation for t in eq. (6.4) as

$$t \rightarrow t + \frac{i\beta}{4}, \quad t \rightarrow t + \frac{i\beta}{2}, \quad t \rightarrow t + \frac{3i\beta}{4}, \quad \text{where } \beta = \frac{2\pi\ell^2}{R} \quad (6.6)$$

respectively. In this coordinate, the BTZ metric is

$$ds^2 = \frac{-4\ell^2 dU dV}{(1 + UV)^2} + R^2 \left(\frac{1 - UV}{1 + UV} \right)^2 d\phi^2, \quad (6.7)$$

and the black hole horizon is $U = 0$ or $V = 0$.

One can define the null coordinates (u, v) as follows.

$$u_R = t - r^*, \quad v_R = t + r^*. \quad (6.8)$$

Again, R stands for the right patch. On the left patch, we can define

$$u_L = t - r^*, \quad v_L = t + r^*, \quad (6.9)$$

where on the left, t goes backward. Unlike (U, V) coordinates, these (u_R, v_R) null coordinates are not defined smoothly beyond the horizon and thus cover only the right patch in Figure 12. Note that on the right boundary, $r^* = 0$ and $u_R = v_R = t$ ranges from $-\infty$ to ∞ .

The ingoing Eddington-Finkelstein coordinates are

$$ds^2 = -f(r)dv_R^2 + 2dv_Rdr + r^2d\phi^2 \quad (6.10)$$

where (v_R, r) coordinates cover the right and black hole patch. See figure 12.

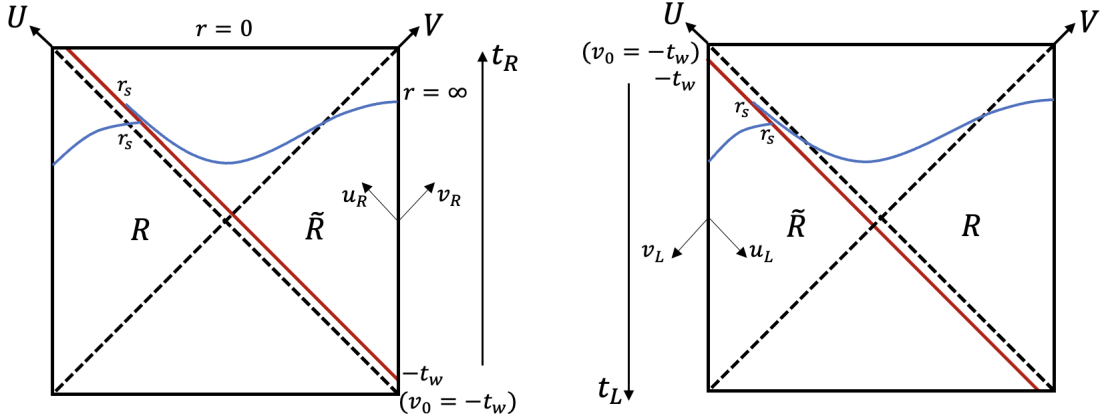


Figure 12: Penrose diagram of single shock wave on BTZ geometry. Here we consider the case where a single shock wave is inserted at $t = -t_w$ on the right or left boundary. The horizons are R and \tilde{R} before and after the shock wave passes through. Here before and after are for the right (left) boundary time, $t_R = -t_w$ ($t_L = -t_w$) for the left (right) figure. On this geometry, a geodesic jump at the shock wave. For example, a blue geodesic starting from the left boundary intersects a shock wave at $r = r_s$, but it emerges from the same $r = r_s$ but different U , because r is continuously connected to the other geometry but U is not.

6.1.1 Single shock wave

We would now like to study the BTZ black hole metric with a single shock wave. As we mentioned, we study the shock wave geometry based on two ways;

Method 1

Suppose a shock wave is launched along $V = 0$. Then we want to find the solution of the Einstein Equation with the following stress tensor,

$$T_{VV} = \frac{\alpha}{4\pi G_N} \delta(V), \quad (6.11)$$

where $\alpha > 0$ due to the averaged null energy condition (ANEC). The resultant metric is as follows

$$ds^2 = \frac{-4\ell^2 dU dV}{(1 + UV)^2} + 4\ell^2 \alpha \delta(V) dV^2 + R^2 \left(\frac{1 - UV}{1 + UV} \right)^2 d\phi^2. \quad (6.12)$$

Clearly, this metric is the same as eq. (6.7) except $V = 0$. It is convenient to rewrite this metric as follows.

$$ds^2 = \frac{-4\ell^2 dU dV}{(1 + (U + \alpha\theta(V))V)^2} + R^2 \left(\frac{1 - (U + \alpha\theta(V))V}{1 + (U + \alpha\theta(V))V} \right)^2 d\phi^2 \quad (6.13)$$

Setting $U \rightarrow U - \alpha\theta(V)$ (where $\theta(V)$ is step function), eq. (6.13) becomes (6.12), therefore they are equivalent. However written the metric as eq. (6.13), the spacetime structure becomes clearer. The spacetime is divided into two parts by the shock wave which is on the horizon $V = 0$. The metric is unmodified by the shock wave at $V > 0$ and $V < 0$, namely if $V = 0$ is avoided, there is no effect of the shock wave. However, at $V = 0$, U coordinate is shifted by the amount of $\alpha > 0$. See Figure 13 for the Penrose diagram. These two black holes have the same mass, and this corresponds to inducing a time delay on the horizon. As a result, the distance between the left boundary to the right boundary becomes longer by the shock wave [18] as butterfly effects.

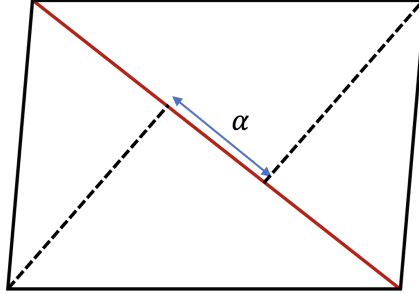


Figure 13: Penrose diagram of BTZ geometry with single shock wave which is inserted on the horizon. The red line represents a shock wave. In this case, a time delay of $\alpha > 0$ is generated. This can be interpreted as a simple constant shift only when the shock wave is as close as possible to the horizon.

Method 2

The second way is preparing the black hole geometry with different masses. In this case, the shock wave is not necessary on the horizon. For example, we can consider the case that a shock wave is released at the time $-t_w$ from the right/left boundary. More concretely, we consider the situation where the mass of the BTZ black hole is modified from M to $M + E$ by the insertion of a shock wave. This has a natural

interpretation that the mass has increased due to the insertion of a shock wave. Each black hole is described by (U, V) and (\tilde{U}, \tilde{V}) coordinates respectively. See figure 12.

In this case, the shock wave trajectory can be described in UV coordinates as

$$V = \pm e^{-\frac{Rt_w}{\ell^2}}, \quad \tilde{V} = \pm e^{-\frac{\tilde{R}t_w}{\ell^2}} \quad (6.14)$$

where we take the positive sign for the situation in the left figure in figure 12, and the negative sign for the one in the right figure. In the uv coordinate system, it is given as a constant surface where

$$v_{R(L)} = v_0 \equiv -t_w. \quad (6.15)$$

The (U, V) and (\tilde{U}, \tilde{V}) coordinates are connected at this shock wave trajectory, and r must be continuous there such that the metric is C^0 . The smoothness of r at the shock wave trajectory requires

$$R \frac{1 - UV}{1 + UV} = \tilde{R} \frac{1 - \tilde{U}\tilde{V}}{1 + \tilde{U}\tilde{V}} \quad (6.16)$$

where V and \tilde{V} are given by eq. (6.14) and

$$R^2 = 8G_N M \ell^2, \quad \tilde{R}^2 = 8G_N (M + E) \ell^2. \quad (6.17)$$

Thus, the metric is C^0 and it can also be written in the Vaidya metric as

$$ds^2 = -\frac{1}{\ell^2} (r^2 - R^2 \theta(v_0 - v) - \tilde{R}^2 \theta(v - v_0)) dv^2 + 2dvdr + r^2 d\phi^2 \quad (6.18)$$

$$= -\frac{1}{\ell^2} (r^2 - R^2 - 8G_N E \ell^2 \theta(v - v_0)) dv^2 + 2dvdr + r^2 d\phi^2 \quad (6.19)$$

Here v means v_R ($v = v_L$) in the left (right) figure 12. This is the solution of the Einstein equation under the following stress tensor.

$$T_{vv} = \frac{E}{2\pi r} \delta(v - v_0). \quad (6.20)$$

The ANEC requires $E > 0$. This shock wave has some strange properties since it is induced by the stress tensor whose magnitude depends on r . However, as we will see below, this is consistent with *Method 1* in certain limits.

Consistency check

We now check the consistency that the metric obtained with *Method 2* matches the one obtained with *Method 1*, *i.e.*, the shock wave geometry eq. (6.13) in a certain limit.

As described earlier, in *Method 2*, the shock wave propagates not necessarily on the horizon. To see the consistency with the metric obtained in *Method 1*, we need to take the limit large t_w so that the shock wave approaches the horizon. Furthermore,

in *Method 1*, the geometry is unmodified except for the horizon. This implies that E must be small.

Thus we are led to the following double scaling limit,

$$t_w \rightarrow \infty, \quad \frac{E}{M} \rightarrow 0, \quad \text{where} \quad \frac{E}{M} e^{\frac{R}{\ell^2} t_w} = \text{fixed}. \quad (6.21)$$

Under this double scaling limit, using eq. (6.14), (6.16) and (6.17), we can obtain the relationship between U and \tilde{U} , which turns out

$$\tilde{U} = U \pm \alpha, \quad \alpha = \frac{E}{4M} e^{\frac{R}{\ell^2} t_w} > 0. \quad (6.22)$$

Here $+$ ($-$) is for the left (right) figure 12. This corresponds to the extreme case where the shock wave is localized on the horizon and $\tilde{R} \rightarrow R$. This is simply a black hole geometry with the same mass connected by constant shift translation obtained in *Method 1*.

Note that in the case where the shock wave is inserted on the left boundary at $t_L = -t_w$, the region where the tilde coordinates are defined is the exact opposite of the case where the shock wave is inserted on the right boundary at $t_R = -t_w$, as shown in figure 12. Then U and \tilde{U} are switched and eq. (6.22) is exactly what we obtained in the metric eq. (6.13). In this way, the shock wave geometry inserted at time $-t_w$ from the right/left boundary gives essentially the same shift between different coordinates U and \tilde{U} under the double scaling limit eq. (6.21).

The stress tensor eq. (6.20) is also consistent with eq. (6.11). To see this, we have

$$T_{VV} = \left(\frac{dv}{dV} \right)^2 T_{vv}(v), \quad \frac{dV}{dv} = \frac{R}{\ell^2} e^{\frac{R}{\ell^2} v} \quad (6.23)$$

and in the double scaling limit $v = v_0 = -t_w \rightarrow -\infty$, $r \rightarrow R$ and

$$\delta(v - v_0) = \left(\frac{dv}{dV} \right)^{-1} \delta(V - e^{-\frac{R}{\ell^2} t_w}) \rightarrow \left(\frac{dv}{dV} \right)^{-1} \delta(V) \quad (6.24)$$

thus, starting from eq. (6.20),

$$\begin{aligned} T_{VV} &= \left(\frac{dv}{dV} \right)^2 \frac{E}{2\pi r} \delta(v - v_0) \\ &\rightarrow \left(\frac{dv}{dV} \right) \frac{E}{2\pi R} \delta(V) = \frac{E}{16G_N \pi M} e^{\frac{R}{\ell^2} t_w} \delta(V) = \frac{\alpha}{4\pi G_N} \delta(V). \end{aligned} \quad (6.25)$$

we obtain eq. (6.11).

6.1.2 Double shock waves

Next, we consider the case where two shock waves are inserted. We will describe the metric based on the two previous methods.

Method 1

First, we consider the case where two shock waves pass over two horizons. *i.e.*, $V = 0$ and $U = 0$, where the following stress tensors are inserted,

$$T_{VV} = \frac{\alpha}{4\pi G_N} \delta(V), \quad T_{UU} = \frac{\alpha}{4\pi G_N} \delta(U). \quad (6.26)$$

Just like the single shock wave case, we can find the following solution

$$ds^2 = \frac{-4\ell^2 dU dV}{(1 + UV)^2} + 4\ell^2 \alpha \delta(U) dU^2 + 4\ell^2 \alpha \delta(V) dV^2 + R^2 \left(\frac{1 - UV}{1 + UV} \right)^2 d\phi^2. \quad (6.27)$$

However, this is a solution only in the leading order of α , neglecting $O(\alpha^2)$. On the other hand, the single shock wave solution eq. (6.12) is an exact solution. Therefore we assume α is small enough to justify this perturbative solution in α .

At constant $U (\neq 0)$ surface, (or constant $V (\neq 0)$ surface), this geometry is a solution with a single shock wave at $V = 0$ (or $U = 0$). Therefore, if we leave aside the points where the shock waves intersect, we will see a shift of coordinates on each shock wave, as seen in the single shock wave solution.

Method 2

Next, let us consider the method connecting two black hole geometries with different masses. The same continuity condition for r as a single shock wave case must be imposed across shock waves.

However, a nontrivial additional condition is required at the point where shock waves intersect each other, which is Dray-'t Hooft-Redmount (DTR) condition [125–127]. DTR condition is the consequence of the C^0 property of metric at the intersection point of delta-functional shock waves. Suppose dividing the spacetime into 4 regions at the intersection of shock waves, a(bove), b(elow), r(ight), and l(eft) of the intersection in the Penrose diagram, then the blackening factor for f_a, f_b, f_r, f_l must satisfy

$$f_a(r_c) f_b(r_c) = f_l(r_c) f_r(r_c) \quad (6.28)$$

at the shock wave intersection radius $r = r_c$.

Let us consider this condition more concretely. Suppose that the below part of the Penrose diagram divided by shock waves is a black hole geometry with mass $M - E$ and that the left and right parts are mass M as a result of inserting energy E . See Figure the left figure in figure 14.

The DTR condition (6.28) at the intersection radius $r = r_c$ becomes

$$(r_c^2 - 8G_N \ell^2 M_l)(r_c^2 - 8G_N \ell^2 (M - E)) = (r_c^2 - 8G_N \ell^2 M)^2 \quad (6.29)$$

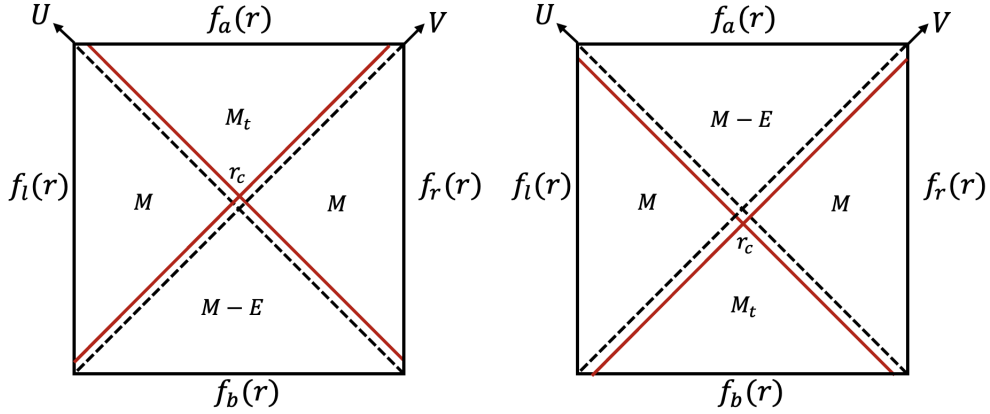


Figure 14: BTZ space-time divided by two shock waves (red solid lines). For simplicity, we consider the insertion of double shock waves in such a way that the Penrose diagram is left-right symmetrical. There is a choice to be made as to which boundary to insert the shock wave from $t = -t_w$. In the left figure, one shock wave is inserted at the right boundary time $t_R = -t_w$. Another shock wave reaches the left boundary at $t_L = +t_w$. In the right figure, the situation is the other way around; one shock wave reaches the right boundary at $t_R = +t_w$, and one shock wave is inserted at $t_L = -t_w$ on the left boundary. Shock waves divide the spacetime into four distinguished region as a (bove), b (elow), l (eft), r (ight), and their masses are M_t , $M - E$, M and M respectively in the left figure. Two shock waves intersect at $r = r_c$.

which determines the relation between M_t and r_c as

$$M_t = M + E + \frac{8G_N \ell^2 E^2}{8G_N(M - E)\ell^2 - r_c^2} \quad (6.30)$$

In the right figure 14, simply the role of above and below patches is flipped.

Consistency check

The left/right patch and the below patch have masses M and $M - E$, respectively in the left figure 14. This mass difference is the same as the single shock wave case. Therefore, the continuity of r across the shock wave reproduces the constant shift of α given in (6.22) in the double scaling limit eq. (6.21).

Next, let us look at the relationship between the left (or right) and the above patch in the left figure 14. In the double scaling limit eq. (6.21),

$$r_c^2 \rightarrow R^2 = 8G_N \ell^2 M, \quad G_N E \rightarrow 0, \quad (6.31)$$

then, the denominator of the last term in (6.30) becomes zero and we need careful analysis in that limit.

To understand M_t in detail, let us first determine r_c as a function of t_w . Since both shock waves are inserted at $t = t_w$ on the left and right boundary, we have

$$U = V = \pm e^{-\frac{Rt_w}{\ell^2}} \quad (6.32)$$

at the intersection $r = r_c$. Here again, the positive and negative signs represent the case in the left and right figures of figure 14, respectively.

Therefore, we have

$$UV = e^{-2Rt_w/\ell^2} = e^{2Rr^*(r_c)/\ell^2} = \frac{R - r_c}{R + r_c} \quad (6.33)$$

which determines t_w dependence of r_c as

$$r_c = R \tanh \frac{R}{\ell^2} t_w \quad (6.34)$$

From this, M_t in (6.30) becomes

$$M_t = M + E + \frac{E^2 \cosh^2 \frac{R}{\ell^2} t_w}{M - E \cosh^2 \frac{R}{\ell^2} t_w}. \quad (6.35)$$

Let us consider the double scaling limit (6.21), which is $E/M \rightarrow 0$ with $t_w \rightarrow \infty$ where α is fixed. In this limit

$$M \ll E \cosh^2 \frac{R}{\ell^2} t_w \quad (6.36)$$

and therefore M_t becomes

$$M_t \rightarrow M \quad (6.37)$$

Therefore, the effects of the shock waves are restricted only on the horizon $U = 0$ and $V = 0$ in the double scaling limit (6.21) which is consistent with the metric eq. (6.27).

6.2 de Sitter spacetime

We now consider the case of dS. The method is the same as for the BTZ case. However, the results are different in a very interesting way.

The (Schwarzschild) dS spacetime [128, 129] can be written as

$$ds^2 = -f(r)dt^2 + \frac{dr^2}{f(r)} + r^2 d\phi^2, \quad (6.38)$$

$$f(r) = \frac{L^2 - r^2}{\ell^2}. \quad (6.39)$$

where ℓ is dS-radius. L is a parameter for the cosmological horizon, such that

$$L^2 = \ell^2 \quad (\text{for pure dS}) \quad (6.40)$$

$$L^2 = (1 - 8G_N M)\ell^2 \quad (\text{for Schwarzschild dS}) \quad (6.41)$$

Note that even though we call Schwarzschild dS (or SdS in short), only a cosmological horizon exists and there is no black hole horizon in three dimensions.

Let us rewrite this in Kruskal coordinates defined by

$$U_R = e^{\frac{L}{\ell^2}(t_R - r^*)}, \quad V_R = -e^{-\frac{L}{\ell^2}(t_R + r^*)}, \quad (6.42)$$

where $r^*(r)$ is a tortoise coordinate,

$$r^*(r) = \int \frac{dr}{f(r)} = \frac{\ell^2}{2L} \log \left| \frac{L+r}{L-r} \right|. \quad (6.43)$$

at the cosmological horizon $r \rightarrow L$, $r^*(r) \rightarrow +\infty$. Note that the sign in eq. (6.42) is different from that of AdS in eq (6.4).

Again the subscript R in t_R indicates that this definition only covers the right static patch. We sometimes call the right static patch $r = 0$ a south pole and the left static patch $r = 0$ a north pole. In this coordinate, the dS metric is

$$ds^2 = \frac{-4\ell^2 dU dV}{(1 - UV)^2} + L^2 \left(\frac{1 + UV}{1 - UV} \right)^2 d\phi^2 \quad (6.44)$$

and the cosmological horizon is $U = 0$ or $V = 0$.

It is also useful to define the null coordinates (u, v) as follows,

$$u_R = t - r^*, \quad v_R = t + r^*, \quad u_L = t - r^*, \quad v_L = t + r^* \quad (6.45)$$

Note that this definition of (u, v) is the same as that of AdS in eq. (6.8), however, the orientations of the u and v coordinates are switched compared to the AdS case, and so are (U, V) coordinates. See figure 16 for the orientations of the coordinates. Note that in the right static patch, the south pole, $r = 0$, corresponds to $r^* = 0$, and there, $u_R = v_R = t$ ranges from $-\infty$ to ∞ .

The ingoing Eddington-Finkelstein coordinates are

$$ds^2 = -f(r)du_R^2 - 2du_R dr + r^2 d\phi^2. \quad (6.46)$$

where (u_R, r) coordinates the right static patch and future patch which is $r \geq L$.

6.2.1 Single shock wave

Method 1

As is the case of BTZ, we can find the solution of the Einstein equation under the stress tensor

$$T_{UU} = \frac{\beta}{4\pi G_N} \delta(U) \quad (6.47)$$

where $\beta > 0$ due to ANEC. For simplicity, we are considering a 2 + 1 dimensional solution, but the solutions in higher dimension were specifically constructed in [130–132]. These solutions can be obtained by appropriately boosting the solution for a point particle.

The Einstein equation with stress tensor eq. (6.47) yields

$$ds^2 = \frac{-4\ell^2 dU dV}{(1 - UV)^2} - 4\ell^2 \beta \delta(U) dU^2 + L^2 \left(\frac{1 + UV}{1 - UV} \right)^2 d\phi^2 \quad (6.48)$$

In this metric, the effects of the shock wave are restricted only on the horizon $U = 0$. It is convenient to rewrite this metric as follows.

$$ds^2 = \frac{-4\ell^2 dU dV}{(1 - U(V - \beta\theta(U)))^2} + L^2 \left(\frac{1 + U(V - \beta\theta(U))}{1 - U(V - \beta\theta(U))} \right)^2 d\phi^2 \quad (6.49)$$

Setting $V \rightarrow V + \beta\theta(U)$, eq. (6.49) becomes (6.48). Note that compared with the BTZ case in eq. (6.12) and (6.13), the effect of the shock wave is exactly the *opposite*. This reverse shift behaves as if it induces a time advance. However, this is causally consistent [65, 69]. Shock wave makes the universe shrink gravitationally and allows a causal connection between the left and right patch. See figure 15.

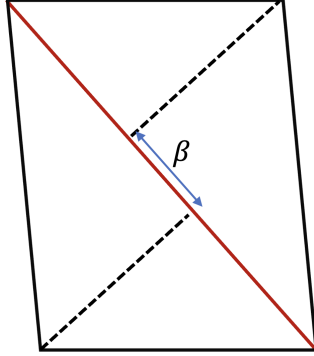


Figure 15: Penrose diagram of dS with single shock wave which is inserted on the cosmological horizon. The shift is exactly the opposite compared with the BTZ case as Figure 13. In this case, effectively a time advance of β is generated.

Method 2

Now let us see the second method by preparing Schwarzschild dS spacetime with different masses and connecting them at the shock wave. In the case of dS, the mass shift is nontrivial, so we will use (U, V) for the upper part and (\tilde{U}, \tilde{V}) for the lower part as in Penrose diagram in the left figure of figure 16. Again, in the right figure, the role of U and \tilde{U} is reversed. The connection condition is the same as BTZ, making r continuous on the shock wave,

$$L \frac{1 + UV}{1 - UV} = \tilde{L} \frac{1 + \tilde{U}\tilde{V}}{1 - \tilde{U}\tilde{V}} \quad (6.50)$$

Thus, the metric must be C^0 and it can also be written in the Vaidya metric as

$$ds^2 = -\frac{\left(L^2\theta(u-u_0) + \tilde{L}^2\theta(u_0-u) - r^2\right)}{\ell^2} du^2 - 2dudr + r^2 d\phi^2 \quad (6.51)$$

where u implies u_R (u_L) in the left (right) figure in Figure 16. u_0 is a parameter for the shock wave trajectory; the shock wave is on the constant surface

$$u_{R(L)} = u_0 = -t_w \quad (6.52)$$

in uv coordinates, and $t = -t_w$ is the time on the south (north) pole, *i.e.*, right (left) patch $r = 0$, and

$$U = \pm e^{-\frac{L}{\ell^2}t_w}, \quad \tilde{U} = \pm e^{-\frac{\tilde{L}}{\ell^2}t_w} \quad (6.53)$$

where we take the positive (negative) sign for the case in the left (right) figure in figure 16.

This metric is the solution of Einstein equation with the stress tensor

$$T_{uu} = \frac{L^2 - \tilde{L}^2}{16\pi G_N \ell^2 r} \delta(u - u_0) \quad (6.54)$$

Setting

$$L^2 = \ell^2 - 8G_N M \ell^2, \quad \tilde{L}^2 = \ell^2 - 8G_N \tilde{M} \ell^2 \quad (6.55)$$

we obtain

$$T_{uu} = \frac{\tilde{M} - M}{2\pi r} \delta(u - u_0) \equiv \frac{E}{2\pi r} \delta(u - u_0). \quad (6.56)$$

Therefore the ANEC requires

$$\tilde{M} > M \Leftrightarrow E > 0. \quad (6.57)$$

Thus, after the shock wave, the mass should *decrease* in the dS case. For example, if $M = 0$, the L is for the dS cosmological horizon. Then $\tilde{M} > 0$, where \tilde{L} is for SdS.

Consistency check

As is the case of AdS, we also check if *Method 1* and *Method 2* are consistent in the case of dS, and for that purpose, we need the following double scaling limit

$$G_N E \rightarrow 0, \quad t_w \rightarrow \infty \quad \text{where} \quad G_N E e^{\frac{L}{\ell^2}t_w} = \text{fixed}. \quad (6.58)$$

Under the double scaling limit eq. (6.58), we can solve r -coordinate continuity condition eq. (6.50) for \tilde{U} , with (6.53) and (6.55) and we obtain β as

$$\tilde{V} = V \pm \beta, \quad \beta = \frac{2G_N E}{1 - 8G_N M} e^{\frac{L t_w}{\ell^2}} = \frac{2G_N E \ell^2}{L^2} e^{\frac{L t_w}{\ell^2}} > 0. \quad (6.59)$$

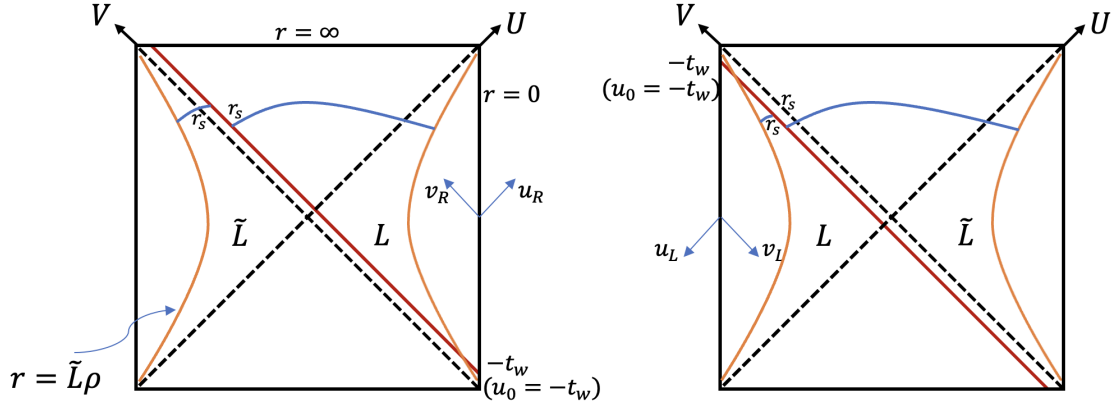


Figure 16: Penrose diagram of single shock wave on dS geometry. Note that our convention of U and V orientation is switched compared with the BTZ case as Figure 12. We treat the case where a single shock wave is inserted at $t_R = -t_w$ ($t_L = -t_w$) in the south pole (north pole). The stretched horizon is drawn in the orange curve, which is $r = \rho L$ and $\rho \rightarrow 1$. L and \tilde{L} are shifted by the inserted energy E . Note, however, that the relationship is inverse compared with the BTZ case. For example, if L is for pure dS, then \tilde{L} is for SdS. r is again continuously connected in this case.

Again, the positive (negative) sign for the left (right) figure in figure 16. Since L and \tilde{L} are switched between the left and right figure, eq. (6.59) is exactly what we obtained in the metric eq. (6.49).

The other thing to check is that the stress tensor of the Vaidya metric, which describes the mass shift in an obvious way, does indeed match that of *Method 1*. One can also check the stress tensor (6.56) matches with (6.47) in the double scaling limit (6.58), where $r \rightarrow L$ as follows

$$T_{UV} = \left(\frac{du}{dU} \right)^2 T_{uu} \rightarrow \left(\frac{du}{dU} \right) \frac{E}{2\pi L} \delta(U) = \frac{\beta}{4\pi G_N} \delta(U) \quad \text{at } r \rightarrow L \quad (6.60)$$

where β is given by (6.59). This is indeed consistent with the stress tensor in (6.47).

Before we go on to double shock waves, we summarize the results and emphasize the difference between BTZ and dS. First of all, the shift of coordinate translation at the shock wave in dS is the exact opposite of that in the BTZ, which allows a time advance. In this way, it is possible to travel from the south pole to the north pole. Second, the mass shift is also the exact opposite of the BTZ. In other words, in the Penrose diagram, the lower part is the Schwarzschild dS spacetime which has a larger mass compared with the upper part. For example, the lower part is the Schwarzschild dS spacetime and the upper part can be pure de Sitter spacetime, see the left figure 16.

6.2.2 Double shock waves

Method 1

As in the case of AdS, we consider following stress tensors

$$T_{VV} = \frac{\beta}{4\pi G_N} \delta(V), \quad T_{UU} = \frac{\beta}{4\pi G_N} \delta(U). \quad (6.61)$$

which yields the solution as follows

$$ds^2 = \frac{-4\ell^2 dU dV}{(1 - UV)^2} - 4\ell^2 \beta \delta(U) dU^2 - 4\ell^2 \beta \delta(V) dV^2 + L^2 \left(\frac{1 + UV}{1 - UV} \right)^2 d\phi^2 \quad (6.62)$$

Again this is the solution only in the leading order of β , neglecting $O(\beta^2)$. Therefore we assume β is small. As in the BTZ case, this should be a shift solution similar to the single shock wave case if we consider $V \neq 0$ or $U \neq 0$.

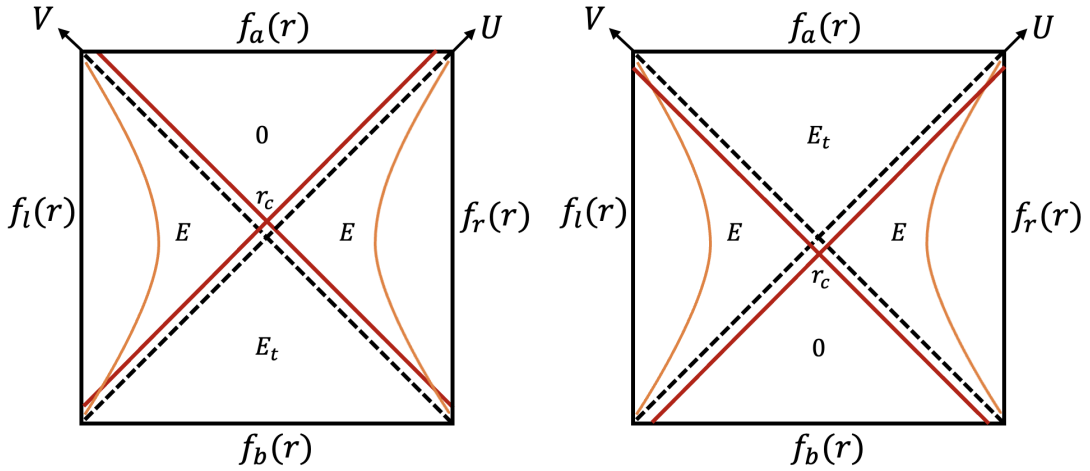


Figure 17: dS space-time divided by two shock waves (red solid lines). For simplicity, we consider the insertion of symmetric double shock waves. Again there are two choices for the shock waves, as left and right figures. On the left (right) figure, the shock wave is inserted $t_R = -t_w$ ($t_L = -t_w$). Another shock wave is determined such that the Penrose diagram is symmetric between l (eft) and r (ight) as these two figures. Shock waves divide the spacetime into four distinguished region as a (bove), b (elow), l (eft), r (ight), and their masses are 0 , E_t , E and E respectively in the left figure. Two shock waves intersect at $r = r_c$.

Method 2

In the case of dS with double shock waves, we need to consider the DTR condition. We consider the case where one shock wave is inserted from the past on the south (or north) pole at $t_R = -t_w$ ($t_L = -t_w$) in the left (right) figure in figure 17. The other shock wave position is automatically determined so that the Penrose diagram is symmetrical between left and right.

For simplicity, let us consider the setting of the left figure 17, and we take the above part of the shock wave as simply pure dS, and set the mass of Schwarzschild

de Sitter in the below part as E_t , then

$$f_a(r) = 1 - \frac{r^2}{\ell^2}, \quad (6.63)$$

$$f_l(r) = f_r(r) = 1 - 8G_N E - \frac{r^2}{\ell^2}, \quad (6.64)$$

$$f_b(r) = 1 - 8G_N E_t - \frac{r^2}{\ell^2}. \quad (6.65)$$

In this case, the DTR condition becomes,

$$\left(1 - \frac{r_c^2}{\ell^2}\right) \left(1 - 8G_N E_t - \frac{r_c^2}{\ell^2}\right) = \left(1 - 8G_N E - \frac{r_c^2}{\ell^2}\right)^2 \quad (6.66)$$

at the shock wave intersection $r = r_c$.

In the case of the right figure 17, the a(bove) and b(elow) parts are exchanged, but the DTR condition is the same.

Therefore in both left and right figures in figure 17, we can calculate E_t

$$E_t = 2E + \frac{8G_N \ell^2 E^2}{r_c^2 - \ell^2}. \quad (6.67)$$

Here r_c is

$$r_c = \frac{\tilde{L}}{\tanh \frac{\tilde{L} t_w}{\ell^2}} \quad (6.68)$$

with

$$\tilde{L}^2 = \ell^2 (1 - 8G_N E). \quad (6.69)$$

This can be seen since the two shock waves intersect at

$$U = V = \pm e^{-\frac{\tilde{L} t_w}{\ell^2}} \quad (6.70)$$

where the positive (negative) sign is for the left (right) figure in figure 17. Then at the shock wave intersect,

$$UV = e^{-\frac{2\tilde{L} t_w}{\ell^2}} = e^{-\frac{2\tilde{L} r^*(r_c)}{\ell^2}} = \frac{r_c - \tilde{L}}{r_c + \tilde{L}}, \quad (6.71)$$

which gives eq. (6.68).

Plugging eq. (6.68) and (6.69) into (6.67), we obtain

$$E_t = 2E + \frac{8G_N \ell^2 E^2}{r_c^2 - \ell^2}. \quad (6.72)$$

Consistency check

In the double scaling limit eq. (6.58), $\tilde{L} \rightarrow \ell$ and (6.72) goes to

$$G_N E_t \rightarrow 2G_N^2 E^2 e^{\frac{2t_w}{\ell}} = \frac{\beta^2}{2} \ll 1 \quad (6.73)$$

which is $O(\beta^2)$ and negligible, where β is given by eq. (6.59) with $L = \ell$. This is consistent since eq. (6.62) is a solution neglecting this order.

7 Delay of Hyperfast

We will now study how this critical time is affected by shock waves. Even in the absence of a shock wave, the critical time can be calculated by the time when r_f becomes infinite [3, 47]. However, the shock waves affect the critical time because the shape of the WdW patch is modified. We are particularly interested in, by the shock wave perturbation, how the dS complexity critical time τ_∞ is modified, especially whether τ_{infy} becomes greater or lesser by shock waves. Our argument is based on both the WdW patch, which is for CV2.0 and CA, and also the complexity = volume (CV) method. We will find in both methods, the results are the same and therefore consistent.

7.1 BTZ case

Before we proceed to the dS case, let us calculate the critical time in the BTZ case as a warm-up.

Single shock wave

Given the boundary time t_L and t_R , the WdW patch extends from there. See Figure 18, where the future null boundaries of the WdW patch are drawn. The value of U or V on each null boundary is determined by the boundary time. Note that t_L goes backward on the left boundary. However, due to the shock wave, the value of U is not continuous. To distinguish before and after the shock wave, we use (\tilde{U}, \tilde{V}) coordinate after the shock wave and (U, V) before the shock wave.

As Figure 18, let us define the r_f as the radius where the $U = \text{constant}$ and $V = \text{constant}$ null lines meet, namely the top “tip” of WdW patch where the radius r becomes the smallest. Even in the BTZ case, we can define the “critical time” as the boundary time when the intersection point, r_f , reaches the singularity, *i.e.*, $r_f = 0$. In BTZ, this does not give a significant contribution, since the volume near the singularity $r = 0$ vanishes¹⁰. However, the shape of the WdW patch will change after this time.

Under this setting, we can write down the relationship between r_f and t_w , the boundary time shock wave is inserted, and t_R and t_L . It is also convenient to define r_s as a radius where the shock wave and null line of fixed U from the left time t_L , intersect, denoted as point A in Figure 18.

When $U = \text{constant}$ and $V = \text{constant}$ null lines intersect at a certain radius r ,

¹⁰Because of this, although $r = 0$ is a region where the semiclassical approximation inherently breaks down, formally one can compute the critical time. More specifically, even if we introduce an appropriate cutoff such as $r > \epsilon$, the main contribution to the Complexity is the volume away from the small r region.

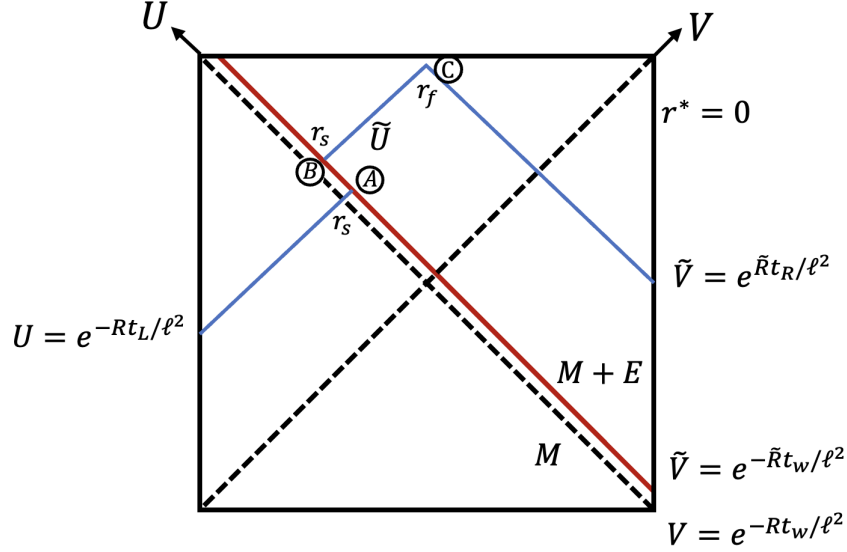


Figure 18: The future null boundaries of the WdW patch are drawn in BTZ geometry. We use $(\tilde{U}, \tilde{V})/(U, V)$ after/before the shock wave (red line). r_f is the radius of conical point where fixed \tilde{U} and fixed \tilde{V} of the null boundaries (blue line) meet. Point A and B have the same radius $r = r_s$, but U is shifted by the shock wave. The “critical time” is the time at the boundary where $r_f \rightarrow 0$.

the following holds,

$$UV = \pm e^{\frac{2Rr^*(r)}{\ell^2}}, \quad (7.1)$$

$$\tilde{U}\tilde{V} = \pm e^{\frac{2\tilde{R}\tilde{r}^*(r)}{\ell^2}} \quad (7.2)$$

where $\tilde{r}^*(r)$ is a tortoise coordinate as eq. (6.5) but in terms of \tilde{R} instead of R . For \pm , we choose $-$ if $r > R$ and $+$ if $r < R$. Eq. (7.1) is valid in (U, V) coordinate patch, and (7.2) is in (\tilde{U}, \tilde{V}) coordinate patch. Note that the shock wave is inserted at $t_R = -t_w$, which is the boundary between (U, V) and (\tilde{U}, \tilde{V}) coordinate patch. Therefore, there are two definitions of V here, one using R and the other using \tilde{R} as

$$V = e^{-\frac{Rt_w}{\ell^2}}, \quad \tilde{V} = e^{-\frac{\tilde{R}t_w}{\ell^2}} \quad (\text{on the shock wave}) \quad (7.3)$$

Before proceeding to the evaluation of the critical time, we first confirm a constant shift occurs between U and \tilde{U} in the double scaling limit (6.21). Since $U = \text{constant}$ and $\tilde{U} = \text{constant}$ intersect with the shock wave given by eq. (7.3) at $r = r_s$, using (7.1) and (7.2), we have

$$\tilde{U} - U = e^{\frac{\tilde{R}(t_w + 2\tilde{r}^*(r_s))}{\ell^2}} - e^{\frac{R(t_w + 2r^*(r_s))}{\ell^2}} \quad (7.4)$$

Substituting $\tilde{R} = \sqrt{\frac{M+E}{M}}R$, using the fact that in the double scaling limit (6.21), $r_s \rightarrow R$, the right hand side of (7.4) becomes

$$\tilde{U} - U = e^{\frac{\tilde{R}(t_w+2\tilde{r}^*(r_s))}{\ell^2}} - e^{\frac{R(t_w+2r^*(r_s))}{\ell^2}} \rightarrow \frac{E}{4M} e^{\frac{Rt_w}{\ell^2}} = \alpha \quad (7.5)$$

which is exactly what we have seen in (6.22).

Now, let's calculate the critical time τ_∞ . It must be clear from Figure 18 that the critical time is smaller than that without a shock wave. In particular, since critical time is zero without a shock wave, it must be negative. In order to evaluate the time shift, using eq. (7.1) for point A and (7.2) for point B and C,

$$e^{-\frac{Rt_L}{\ell^2}} e^{-\frac{Rt_w}{\ell^2}} = e^{\frac{2Rr^*(r_s)}{\ell^2}} \quad (\text{point A}) \quad (7.6)$$

$$\tilde{U} e^{-\frac{\tilde{R}t_w}{\ell^2}} = e^{\frac{2\tilde{R}r^*(r_s)}{\ell^2}} \quad (\text{point B}) \quad (7.7)$$

$$\tilde{U} e^{\frac{\tilde{R}t_R}{\ell^2}} = e^{\frac{2\tilde{R}r^*(r_f)}{\ell^2}} \quad (\text{point C}) \quad (7.8)$$

where \tilde{U} is the coordinate value on the null line between points B and C, and we use

$$U = e^{-\frac{Rt_L}{\ell^2}}, \quad \tilde{V} = e^{\frac{\tilde{R}t_R}{\ell^2}} \quad (7.9)$$

as shown in figure 18.

Eq. (7.6), and the equation (7.8) divided by (7.7) yield,

$$t_L + t_w = -2r^*(r_s), \quad (7.10)$$

$$t_R + t_w = 2(\tilde{r}^*(r_f) - \tilde{r}^*(r_s)) \quad (7.11)$$

respectively. Eliminating t_w from the above and setting $-t_L = t_R \equiv \tau$, we have

$$2\tau = t_R - t_L = 2(\tilde{r}^*(r_f) + r^*(r_s) - \tilde{r}^*(r_s)) \quad (7.12)$$

Since at $r_f \rightarrow 0$, $\tilde{r}^*(r_f) \rightarrow 0$, this leads to the following as the advanced part of critical time.

$$\Delta\tau_\infty = \tau_\infty = r^*(r_s) - \tilde{r}^*(r_s) \quad (7.13)$$

$\Delta\tau_\infty = \tau_\infty$ because critical time without shock wave is at $\tau = 0$.

To see $\tau_\infty < 0$, we need to evaluate the right-hand side of eq. (7.13). Since this is the difference of tortoise coordinates for the difference between R and \tilde{R} , the derivative r^* with respect to R is

$$\frac{dr^*(R)}{dR} = \frac{\ell^2}{2R^2} \left(\frac{2rR}{R^2 - r^2} + \log\left(\frac{R+r}{R-r}\right) \right) > 0 \quad (\text{for } r < R) \quad (7.14)$$

Thus, we see that r^* increases by increasing R at $r = r_f < R$, and therefore $\tilde{r}^*(r_s) > r^*(r_s)$ and thus, $\Delta\tau_\infty$ is negative.

We can also examine $\tau_\infty < 0$ in the double scaling limit (6.21). For that purpose, we set $\tilde{R} = \sqrt{1 + \frac{E}{M}}R$. Furthermore, we use

$$r_s = R \tanh \frac{R}{2\ell^2}(t_w + t_L) \quad (7.15)$$

This can be obtained by solving (7.10) for r_s . In the double scaling limit (6.21),

$$R^2 - r_s^2 \rightarrow 4R^2 e^{-\frac{R}{\ell^2}(t_w+t_L)}, \quad (7.16)$$

$$\frac{E}{M} \frac{R^2}{R^2 - r_s^2} \rightarrow \frac{E}{4M} e^{+\frac{R}{\ell^2}(t_w+t_L)} = e^{+\frac{R}{\ell^2}t_L} \alpha. \quad (7.17)$$

Thus, we obtain the following

$$\Delta\tau_\infty = r^*(r_s) - \tilde{r}^*(r_s) \rightarrow -\frac{\ell^2}{2R}\alpha + O(\alpha^2) < 0. \quad (7.18)$$

Thus $\Delta\tau_\infty$ is negative.

Double shock wave

Next, we calculate the critical time in the case where two shock waves are inserted from both boundaries. For simplicity, we insert two shock waves in such a way that the resultant Penrose diagram is symmetric between left and right, see figure 19. Note that, as we did in section 6.1.2 and figure 14, there are two ways to put shock wave in the symmetry, but this time we consider the situation as shown in figure 19 in order to perform the calculation unambiguously. Then we can use (U, V) for the left and right region, which is separated by double shock waves (red line in the figure).

Again, $U = \text{constant}$ and $V = \text{constant}$ null lines (blue line) are determined by the left boundary time t_L and right boundary time t_R . As in the single shock wave case, there are two different coordinate descriptions for a single shock wave, such as (7.3). However, $\tilde{R} = 8G_N M_t \ell^2$ now. As in the single shock wave case, the following conditions are derived using eq. (7.1) for points A and E, and (7.2) for points B, C, D,

$$-e^{-\frac{Rt_L}{\ell^2}} e^{-\frac{Rt_w}{\ell^2}} = -e^{\frac{2Rr^*(r_s)}{\ell^2}} \quad (\text{point A}) \quad (7.19)$$

$$-\tilde{U} e^{-\frac{\tilde{R}t_w}{\ell^2}} = -e^{\frac{2\tilde{R}\tilde{r}^*(r_s)}{\ell^2}} \quad (\text{point B}) \quad (7.20)$$

$$\tilde{U}\tilde{V} = e^{\frac{2\tilde{R}\tilde{r}^*(r_f)}{\ell^2}} \quad (\text{point C}) \quad (7.21)$$

$$-e^{-\frac{\tilde{R}t_w}{\ell^2}} \tilde{V} = -e^{\frac{2\tilde{R}\tilde{r}^*(r_s)}{\ell^2}} \quad (\text{point D}) \quad (7.22)$$

$$-e^{-\frac{Rt_w}{\ell^2}} e^{\frac{Rt_R}{\ell^2}} = -e^{\frac{2Rr^*(r_s)}{\ell^2}} \quad (\text{point E}) \quad (7.23)$$

where \tilde{U} is the coordinate value on the null line between point B and C, and \tilde{V} is the one between C and D. Just as a single shock wave case, in the double scaling

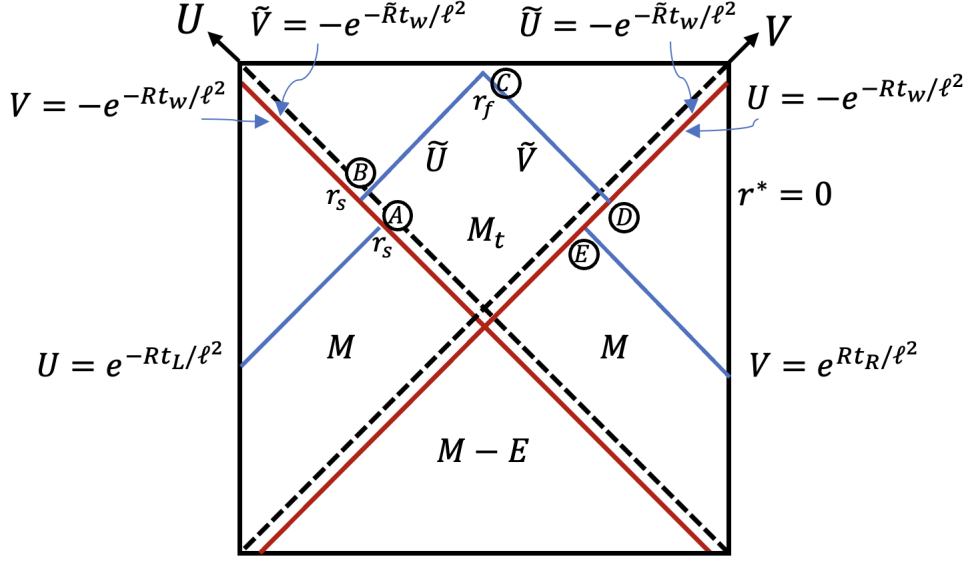


Figure 19: Future boundary of WdW patch in the case of a double shock wave in AdS. Double shock waves (red line) divide the region into left, right, above, and below. We use (U, V) coordinates for left and right and (\tilde{U}, \tilde{V}) on the above region. M_t in (\tilde{U}, \tilde{V}) coordinates is determined by the DTR condition.

limit (6.21), the effect of shock waves is simply the coordinate shift in U and V by α . Again setting $-t_L = t_R \equiv \tau$, and from the symmetry, $\tilde{U} = \tilde{V}$, (7.19) and (7.23), and (7.20) and (7.22) are the same. Therefore from (7.19),

$$\tau - t_w = 2r^*(r_s), \quad (7.24)$$

and from (7.20) and (7.21),

$$\tilde{U} = e^{\frac{2\tilde{R}\tilde{r}^*(r_s) + \tilde{R}t_w}{\ell^2}} = e^{\frac{\tilde{R}\tilde{r}^*(r_f)}{\ell^2}} \Rightarrow t_w + 2\tilde{r}^*(r_s) = \tilde{r}^*(r_f). \quad (7.25)$$

From these, we obtain

$$\tau = 2r^*(r_s) - 2\tilde{r}^*(r_s) + \tilde{r}^*(r_f) \quad (7.26)$$

Since $r_f \rightarrow 0$, $\tilde{r}^*(r_f) \rightarrow 0$, we obtain

$$\Delta\tau_\infty = 2(r^*(r_s) - \tilde{r}^*(r_s)). \quad (7.27)$$

This is twice as large as (7.13). Thus in the double scaling limit (6.21),

$$\Delta\tau_\infty = -\frac{\ell^2}{R}\alpha + O(\alpha^2) < 0. \quad (7.28)$$

Let us understand this in terms of constant shift. By using formula (7.21), we have at point C,

$$\tilde{U}\tilde{V} = 1 \quad (7.29)$$

where we take $r_f \rightarrow 0$. Using eq. (6.22)¹¹, $\tilde{U} = U + \alpha$, and left right symmetry of the Penrose diagram, $\tilde{V} = \tilde{U}$. After setting $-t_L = t_R = \tau$, we can solve this for τ , and we obtain

$$U = e^{-\frac{Rt_L}{\ell^2}} = 1 - \alpha \quad \Rightarrow \quad \tau = \frac{\ell^2}{R} \log(1 - \alpha) = -\frac{\ell^2}{R} \alpha + O(\alpha^2) < 0 \quad (7.30)$$

This is the same quantity as in (7.28). Here, in the last equality, we used the fact that the solution of the shift is satisfied in the limit where α is small.

7.2 de Sitter case

Now let us discuss complexity in the dS case. As we said earlier, we consider the stretched horizon as a holographic screen [3]. Furthermore, we consider the effects of the shock waves which are inserted at times $t_L = -t_w$ on the north pole (left patch $r = 0$). In the case of dS, even without the shock wave, the critical time for complexity divergence is nontrivial.

As BTZ case, in dS, when $U = \text{constant}$ and $V = \text{constant}$ null lines intersect at a certain radius r , the following holds

$$UV = \pm e^{-\frac{2Lr^*(r)}{\ell^2}}, \quad (7.31)$$

$$\tilde{U}\tilde{V} = \pm e^{-\frac{2\tilde{L}\tilde{r}^*(r)}{\ell^2}} \quad (7.32)$$

For \pm , we choose $-$ if $r < L$, and $+$ if $r > L$. $\tilde{r}^*(r)$ is a tortoise coordinate as eq. (6.43) but in terms of \tilde{L} instead of L . Eq. (7.31) is valid in (U, V) coordinate patch, and (7.32) is in (\tilde{U}, \tilde{V}) coordinate patch.

No shock wave

First, let us calculate the critical time without a shock wave. The discussion in this case is based on [47].

In figure 20, the point r_f is the location where U and V are determined on the stretched horizon. At the $r = r_f > L$ point, using eq. (7.31) we have

$$UV = e^{-\frac{L(t_L - t_R + 2r^*(r_{st}))}{\ell^2}} = e^{-\frac{2Lr^*(r_f)}{\ell^2}} \quad (7.33)$$

Note, however, in dS, the coefficient in front of r^* on the right-hand side is negative. Therefore, it follows that

$$-t_L + t_R - 2r^*(r_{st}) = -2r^*(r_f). \quad (7.34)$$

¹¹Note that \tilde{U} and U are switched between the right figure 12 and 19.

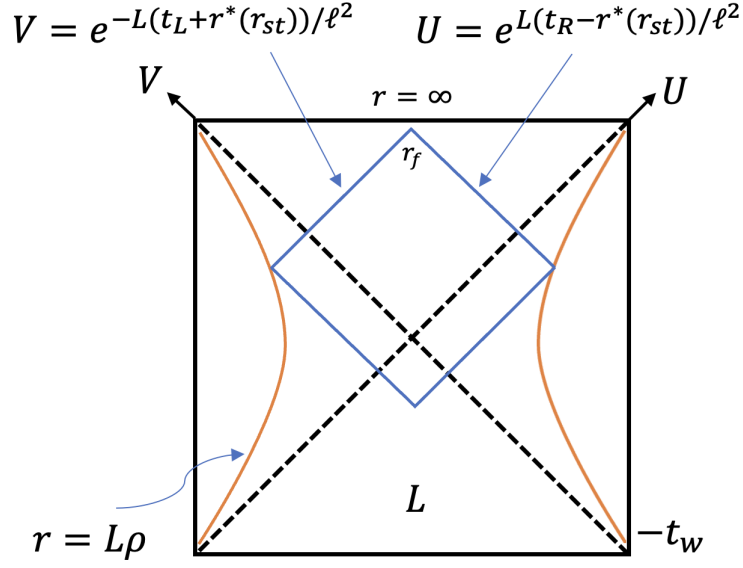


Figure 20: The WdW patch is anchored by the time on the stretched horizon, where t_L and t_R is the time on the stretched horizon $r = \rho\ell$, where $\rho \rightarrow 1$. If this WdW patch reaches the depth of r_f , the critical time is the stretched horizon time when $r_f \rightarrow \infty$.

Setting $-t_L = t_R = \frac{\ell^2}{L}\tau$ and considering the pure dS case, $L = \ell$, and we obtain the critical time $\tau = \tau_\infty^{(0)}$ when $r_f \rightarrow \infty$ as,

$$\begin{aligned} \ell\tau_\infty^{(0)} &= r^*(r_{st}) - r^*(r_f \rightarrow \infty) \rightarrow r^*(r_{st}), \\ \tau_\infty^{(0)} &= \frac{r^*(r_{st})}{\ell} = \frac{1}{2} \log \left| \frac{1+\rho}{1-\rho} \right| = \text{Arctanh}\rho. \end{aligned} \quad (7.35)$$

This is the same result as in [47]. Here $\tau_\infty^{(0)}$ represents the critical time without shock waves.

Single shock wave

Next, let us consider the case where a shock wave is inserted at the time $t_L = -t_w$ on the north pole. As shown in Section 6.2, in this case, the lower part of the Penrose diagram is pure dS.

Similarly in this case, the following equation holds eq. (7.31) for point A and (7.32) for point B and C,

$$-e^{-\frac{t_w}{\ell}} V = -e^{-\frac{2r^*(r_s)}{\ell}} \quad (\text{point A}) \quad (7.36)$$

$$-e^{-\frac{\tilde{L}t_w}{\ell^2}} \tilde{V} = -e^{-\frac{2\tilde{L}r^*(r_s)}{\ell^2}} \quad (\text{point B}) \quad (7.37)$$

$$e^{\frac{\tilde{L}(t_R - r^*(r_{st}))}{\ell^2}} \tilde{V} = e^{-\frac{2\tilde{L}r^*(r_f)}{\ell^2}} \quad (\text{point C}) \quad (7.38)$$

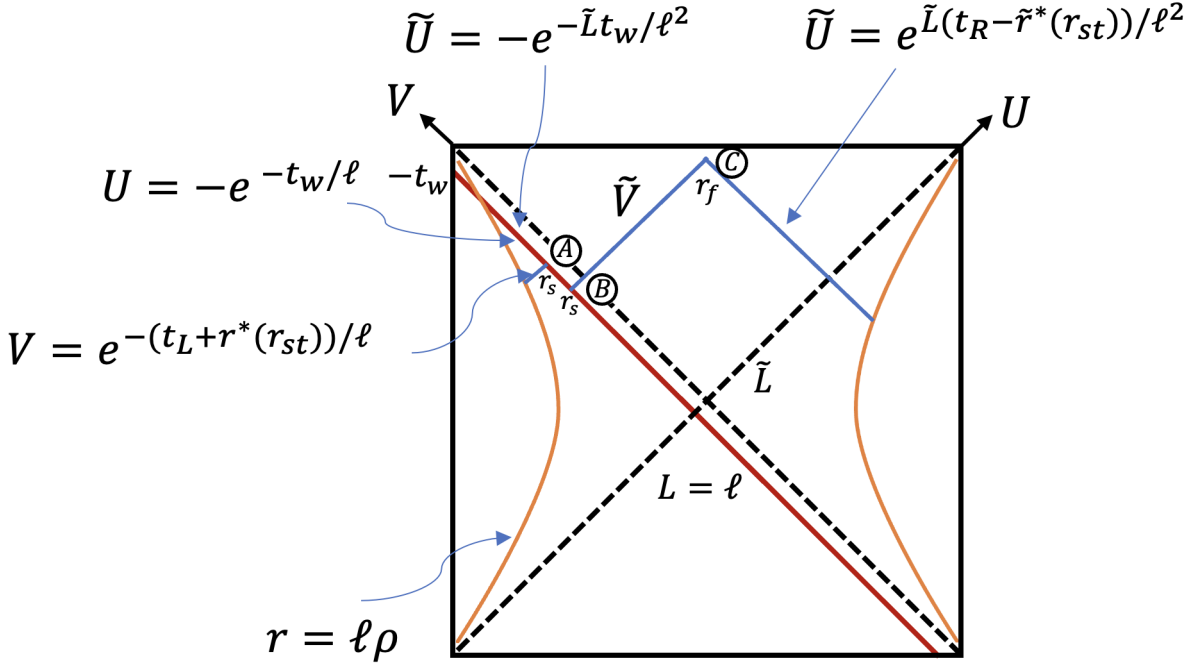


Figure 21: Consider the future boundary of the WdW patch in dS. If this patch reaches the depth of r_f ($=$ point C), the critical time is the boundary time when $r_f = \infty$. The stretched horizon is $r_{st} = \rho \ell$, with $\rho \rightarrow 1$.

where \tilde{V} is the coordinate value on the null line between points B and C, and we have

$$V = e^{-\frac{t_L + r^*(r_{st})}{\ell}} \quad (7.39)$$

for the coordinate value on the null line between point A.

Using eq. (7.36) and (7.37), in this case too, the shift can be understood under the limit as follows.

$$\tilde{V} - V = e^{\frac{\tilde{L}(t_w - 2\tilde{r}^*(r_s))}{\ell^2}} - e^{\frac{t_w - 2r^*(r_s)}{\ell}} \quad (7.40)$$

$$= e^{\tilde{L}t_w/\ell^2} \frac{\tilde{L} - r_s}{\tilde{L} + r_s} - e^{t_w/\ell} \frac{\ell - r_s}{\ell + r_s} \quad (7.41)$$

Substituting $\tilde{L} = \ell\sqrt{1 - 8G_N E}$, and taking the double scaling limit (6.58), with $r_s \rightarrow \ell$, we obtain

$$\tilde{V} - V \rightarrow -2G_N E e^{t_w/\ell} = -\beta \quad (7.42)$$

which matches the (6.59).

The calculation of the critical time is straightforward, however, it must be clear from the figure 20 that the critical time is *greater* than the one without a shock

wave. Using eq. (7.36) with (7.39), and the eq. (7.37) divided by (7.38) become, respectively

$$t_L + t_w + r^*(r_{st}) = 2r^*(r_s) \quad (7.43)$$

$$t_R + t_w - r^*(r_{st}) = -2\tilde{r}^*(r_f) + 2\tilde{r}^*(r_s) \quad (7.44)$$

Eliminating t_w from the above and setting $-t_L = t_R = \ell\tau$, and using at $r_f \rightarrow \infty$, $\tilde{r}^*(r_f) \rightarrow 0$, we obtain the following

$$\ell\tau_\infty = r^*(r_{st}) + \tilde{r}^*(r_s) - r^*(r_s) \quad (7.45)$$

The term $r^*(r_{st})$ is the critical time without shock waves, (7.35), therefore $\ell\tau_\infty^{(0)} = r^*(r_{st})$, and the delay of critical time is given by

$$\Delta\tau_\infty \equiv \tau_\infty - \tau_\infty^{(0)} = \frac{1}{\ell} (\tilde{r}^*(r_s) - r^*(r_s)) \quad (7.46)$$

To understand what eq. (7.46) implies, we need to consider the difference of torse coordinate between L and \tilde{L} . In our setting $r_s < L = \ell$, and $\tilde{L} = \ell\sqrt{1 - 8G_N E}$. Since

$$\begin{aligned} \frac{d\tilde{r}^*(r_s)}{dE} &= \frac{d\tilde{L}}{dE} \times \frac{d\tilde{r}^*(r_s)}{d\tilde{L}} \\ &= - \left(\frac{4\ell G_N}{\sqrt{1 - 8G_N E}} \right) \times - \left(\frac{\ell^2 r_s}{L(L^2 - r_s^2)} + \frac{\ell^2}{2L^2} \log \frac{L + r_s}{L - r_s} \right) > 0 \end{aligned} \quad (7.47)$$

Therefore, the critical time becomes greater by the shock wave.

In the double scaling limit (6.58), $r_s \rightarrow L$. To analyze this carefully, using (7.43),

$$t_L + t_w + r^*(r_{st}) = 2r^*(r_s) = \ell \log \frac{\ell + r_s}{\ell - r_s} \quad (7.48)$$

$$\Rightarrow r_s = \ell \tanh \frac{t_L + t_w + r^*(r_{st})}{2\ell}. \quad (7.49)$$

Therefore in the double scaling limit (6.58), we can derive the delay of critical time as

$$\Delta\tau_\infty \rightarrow \frac{\beta}{2} + O(\beta^2) > 0. \quad (7.50)$$

Thus $\Delta\tau_\infty$ is positive, and this implies the delay of hyperfast growth for small β perturbation.

Double shock waves

Finally, we compute the case of a dS with a double shock wave. As shown in Figure 22, we insert double shock waves and consider the critical time at which the future

boundary of the WdW patch extended from a certain time on the stretched horizon reach infinity, *i.e.*, $r_f = \infty$ of the point C.

As usual, the following is satisfied,

$$-e^{-\frac{t_w}{\ell}} e^{-\frac{t_L+r^*(r_{st})}{\ell}} = -e^{-\frac{2r^*(r_s)}{\ell}} \quad (\text{point A}) \quad (7.51)$$

$$-e^{-\frac{\tilde{L}t_w}{\ell^2}} \tilde{V} = -e^{-\frac{2\tilde{L}\tilde{r}^*(r_s)}{\ell^2}} \quad (\text{point B}) \quad (7.52)$$

$$\tilde{U}\tilde{V} = e^{-\frac{2\tilde{L}\tilde{r}^*(r_f)}{\ell^2}} \quad (\text{point C}) \quad (7.53)$$

$$-e^{-\frac{\tilde{L}t_w}{\ell^2}} \tilde{U} = -e^{-\frac{2\tilde{L}\tilde{r}^*(r_s)}{\ell^2}} \quad (\text{point D}) \quad (7.54)$$

$$-e^{-\frac{t_w}{\ell}} e^{\frac{t_R-r^*(r_{st})}{\ell}} = -e^{-\frac{2r^*(r_s)}{\ell}} \quad (\text{point E}) \quad (7.55)$$

where \tilde{V} is the coordinate value on the null line between point B and C, and \tilde{U} is the one between C and D. Just as a single shock wave case, in the double scaling limit (6.58), the effect of shock waves is simply the coordinate shift in U and V by β . Again setting $-t_L = t_R$, and from the left-right symmetry of the Penrose diagram, $\tilde{U} = \tilde{V}$, (7.51) and (7.55), and (7.52) and (7.54) are the same. From eq. (7.51) - (7.53), we obtain

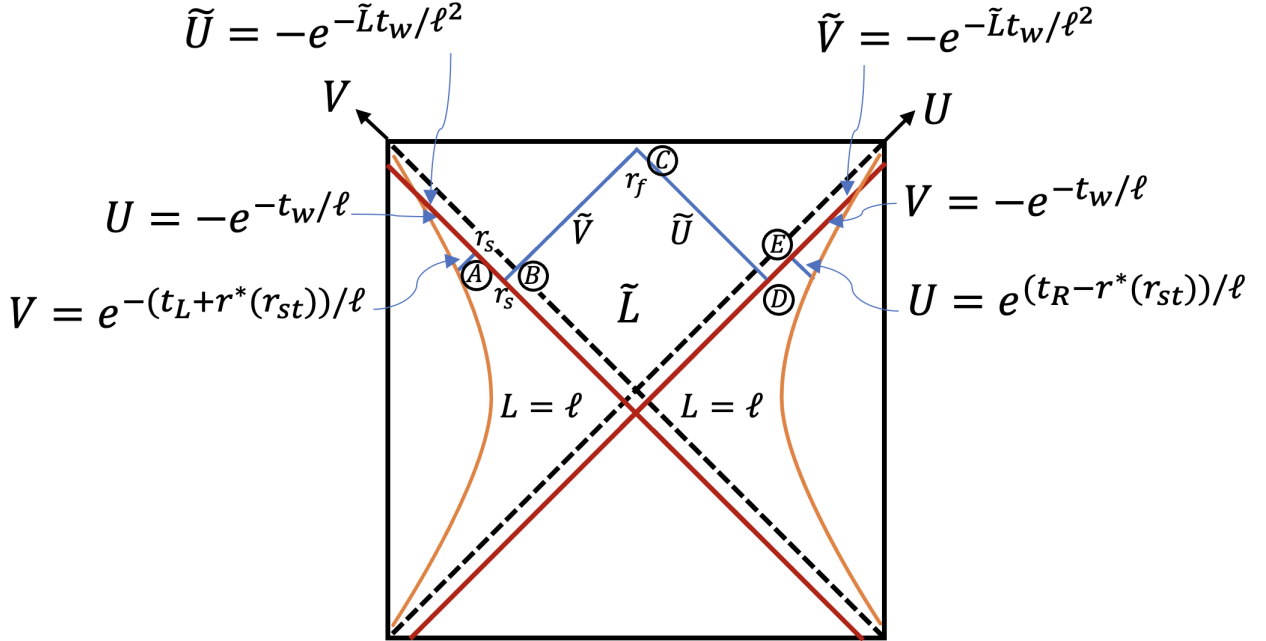


Figure 22: Future boundary of WdW patch in the case of a double shock wave in dS. The black hole mass of the below part is determined by the DTR condition.

$$t_L + t_w = 2r^*(r_s) - r^*(r_{st}) \quad (7.56)$$

$$t_w = 2\tilde{r}^*(r_s) - \tilde{r}^*(r_f) \quad (7.57)$$

Setting $-t_L = t_R \equiv \ell\tau$ and using $\tilde{r}^*(r_f) \rightarrow 0$ as $r_f \rightarrow \infty$,

$$\Delta\tau_\infty = \tau_\infty - \frac{r^*(r_{st})}{\ell} = \frac{2}{\ell} (\tilde{r}^*(r_s) - r^*(r_s)) \quad (7.58)$$

$$\rightarrow \beta + O(\beta^2) > 0. \quad (7.59)$$

Thus, as in the case of AdS, the change in critical time is twice as large as a single shock wave case. Here, we used the fact that the double shock wave solution is satisfied in the limit where β is small.

Let us understand this result in terms of constant shift of the metric in eq. (6.49) as BTZ case. By using formula (7.53), at $r = r_f \rightarrow \infty$ we have

$$\tilde{U}\tilde{V} \rightarrow 1, \quad (7.60)$$

From (6.59) (or equivalently (7.42)),

$$\tilde{V} = V - \beta \quad (7.61)$$

Using the left-right symmetry of the Penrose diagram, we obtain $\tilde{U} = \tilde{V}$ and

$$V = e^{-\frac{t_L + r^*(r_{st})}{\ell}} \rightarrow 1 + \beta \quad \Rightarrow \quad -\frac{t_L}{\ell} \rightarrow \frac{r^*(r_{st})}{\ell} + \log(1 + \beta). \quad (7.62)$$

Setting $-t_L = t_R = \ell\tau$, we obtain the critical time τ_∞ as the right hand side of (7.62) and therefore,

$$\Delta\tau_\infty = \tau_\infty - \frac{r^*(r_{st})}{\ell} = \log(1 + \beta) = \beta + O(\beta^2) > 0 \quad (7.63)$$

This is the same quantity as in (7.58).

7.3 CV calculation

Finally, let us derive the above critical time delay based on CV calculation as well. For that purpose, we need to calculate the volume of the extremal geodesic anchored to a time slice on the stretched horizon. The following discussion is based on geodesic surface prescriptions between different patches, as is worked out in [106, 107]. We are interested in three dimensions. However, we will proceed a little in the general dimension and finally discuss the three-dimensional case.

In the Eddington-Finkelstein coordinate, the metric for the left (right) static patch and the future patch is written in terms of v_L (u_R) as

$$ds^2 = -f(r)dv_L^2 + 2dv_L dr + r^2 d\Omega_{d-1}^2 \quad (= -f(r)du_R^2 - 2du_R dr + r^2 d\Omega_{d-1}^2). \quad (7.64)$$

Then the volume of the geodesic is given by

$$V = \Omega_{d-1} \int ds r^{d-1} \sqrt{-f\dot{v}_L^2 + 2\dot{v}_L \dot{r}} \quad \left(= \Omega_{d-1} \int ds r^{d-1} \sqrt{-f\dot{u}_R^2 - 2\dot{u}_R \dot{r}} \right) \quad (7.65)$$

where the dot is derivative with respect to geodesic parameter s . Ω_{d-1} is the volume of a unit $(d-1)$ -dimensional sphere. To simplify the notation, we sometimes omit L and R in v_L and u_R .

The shock wave separates spacetime into several patches, as a result, different $f(r)$ is assigned for each spacetime patch. However, there is a conserved quantity in each patch. If we regard (7.65) as the action, its Lagrangian is independent of v (or u). Therefore the following P is conserved with respect to s ;

$$P \equiv \frac{1}{\Omega_{d-1}} \frac{\delta V}{\delta \dot{v}} = \frac{(\dot{r} - f\dot{v})r^{d-1}}{\sqrt{-f\dot{v}^2 + 2\dot{v}\dot{r}}}, \quad \left(P \equiv \frac{1}{\Omega_{d-1}} \frac{\delta V}{\delta \dot{u}} = \frac{(-\dot{r} - f\dot{u})r^{d-1}}{\sqrt{-f\dot{u}^2 - 2\dot{u}\dot{r}}} \right). \quad (7.66)$$

Since (7.65) is invariant under the reparametrization for parameter s , we can always choose a parameterization gauge such that

$$\sqrt{-f\dot{v}^2 + 2\dot{v}\dot{r}} = r^{d-1}, \quad \left(\sqrt{-f\dot{u}^2 - 2\dot{u}\dot{r}} = r^{d-1} \right). \quad (7.67)$$

Then we have

$$P = \dot{r} - f\dot{v}, \quad (P = -\dot{r} - f\dot{u}). \quad (7.68)$$

Consider a geodesic line extending from the left stretched horizon to the right stretched horizon. r extends from the left stretched horizon to a point called the turning point $r = r_{turn}$. After that, r decreases to the right boundary. r is a continuous parameter on the shock wave due to the C^0 nature of the metric and we set $r = r_s$ at the point where the geodesic line crosses the shock wave as before.

As we have mentioned, P is conserved only within each patch. Therefore we denote P in the patch where the cosmological horizon is L , and \tilde{P} for \tilde{L} . Similarly we put $\tilde{\cdot}$, for the quantity in \tilde{L} , such as $\tilde{f}(r)$, \tilde{u} , \tilde{v} , etc. See figure 23.

Eq. (7.67) and (7.68) give

$$\dot{r} = +\sqrt{P^2 + r^{2d-2}f(r)}, \quad \left(\dot{r} = -\sqrt{P^2 + r^{2d-2}f(r)} \right), \quad (7.69)$$

$$\dot{v} = \frac{1}{f(r)} \left(-P + \sqrt{P^2 + r^{2d-2}f(r)} \right), \quad \left(\dot{u} = \frac{1}{f(r)} \left(-P + \sqrt{P^2 + r^{2d-2}f(r)} \right) \right), \quad (7.70)$$

where we choose the convention that s increase starting from left stretched horizon toward r_{turn} . With this, the volume is given by

$$\begin{aligned} \mathcal{C}_V &= \Omega_{d-1} \int ds r^{2(d-1)} \\ &= 2\Omega_{d-1} \left(\int_{r_{st}}^{r_s} \frac{r^{2(d-1)}}{\sqrt{P^2 + f(r)r^{2(d-1)}}} dr + \int_{r_s}^{r_{turn}} \frac{r^{2(d-1)}}{\sqrt{\tilde{P}^2 + \tilde{f}(r)r^{2(d-1)}}} dr \right). \end{aligned} \quad (7.71)$$

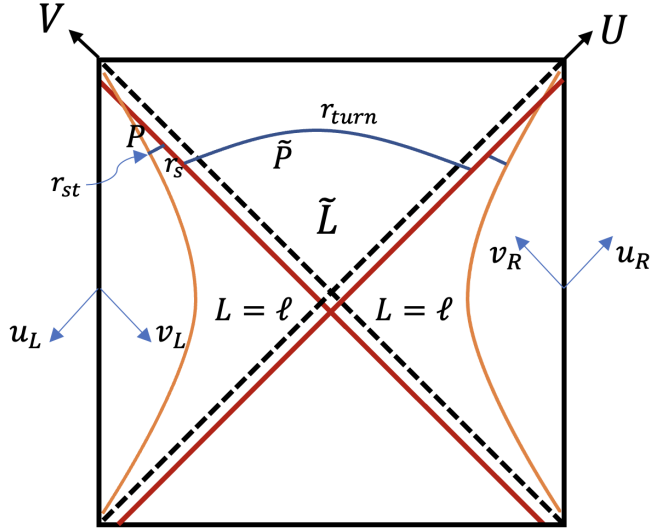


Figure 23: Figure of a geodesic line. The turning point is assumed to be in the interior of pure dS. The momentum of pure dS is assumed to be P , and that of the SdS patch is assumed to be \tilde{P} .

Turning point is defined as the point where the \dot{r} is zero,

$$\left(1 - \frac{r_{turn}^2}{\tilde{L}^2}\right) r_{turn}^{2(d-1)} + \tilde{P}^2 = 0 \quad (7.72)$$

As is clearly seen from this equation, the turning point $r_{turn} \rightarrow \infty$ as $\tilde{P} \rightarrow \infty$. Therefore, we will investigate $\tilde{P} \rightarrow \infty$ limit. In fact, in this limit, $P \rightarrow \infty$ as well because the effect of the shock wave in the double scaling limit (6.58) is simply a coordinate shift¹².

Using (7.69) and (7.70), the variation of u and v along the geodesic can be calculated by the following integral

$$\Delta v = \int \frac{\dot{v}}{\dot{r}} dr = \int T(P, r) dr, \quad \left(\Delta u = \int \frac{\dot{u}}{\dot{r}} dr = - \int T(P, r) dr \right), \quad (7.73)$$

where $T(P, r)$ is

$$T(P, r) = \frac{1}{f(r)} - \frac{P}{f(r) \sqrt{P^2 + f(r) r^{2(d-1)}}}. \quad (7.74)$$

¹²Under the coordinate shift, if momentum diverges in one patch, it also diverges in another patch as well. More formally, one can obtain the relation between \tilde{P} and P as follows. 1) Deriving the equation of motion for $r(s)$ from (7.65) as $\ddot{r} = \frac{\dot{v}^2}{2} \partial_v f + \frac{1}{2} \partial_r (r^{2d-2} f)$. 2) By integrating out this equation with respect to s between $r = r_s - \epsilon$ to $r_s + \epsilon$ with $\epsilon \rightarrow 0$, we obtain how \dot{r} jumps by crossing the shock wave. 3) By furthermore using this with (7.68), (7.69) and (7.70), we obtain the relation between \tilde{P} and P . By taking $\tilde{P} \rightarrow \infty$, one can see in fact that $P \rightarrow \infty$ as well.

Consider a geodesic that leaves the left-stretched horizon and reaches the right-stretched horizon. From the left stretched horizon to r_{turn} , we use v_L and \tilde{v}_L , and from r_{turn} to the right stretched horizon, we use u_R and u_R , as

$$v_L(r_s) - v_L(r_{st}) = + \int_{r_{st}}^{r_s} T(P, r) dr, \quad (7.75)$$

$$\tilde{v}_L(r_{turn}) - \tilde{v}_L(r_s) = + \int_{r_s}^{r_{turn}} T(\tilde{P}, r) dr, \quad (7.76)$$

$$\tilde{u}_R(r_{turn}) - \tilde{u}_R(r_s) = - \int_{r_s}^{r_{turn}} T(\tilde{P}, r) dr, \quad (7.77)$$

$$u_R(r_s) - u_R(r_{st}) = - \int_{r_{st}}^{r_s} T(P, r) dr, \quad (7.78)$$

Note that $v_L(r_s) \neq \tilde{v}_L(r_s)$ since v_L jump at the shock wave¹³. In fact, from the definitions of u and v in eq. (6.45), we have

$$\begin{aligned} \Delta v(r_s) &\equiv \tilde{v}_L(r_s) - v_L(r_s) = (\tilde{u}_L(r_s) + 2\tilde{r}^*(r_s)) - (u_L(r_s) + 2r^*(r_s)) \\ &= 2(\tilde{r}^*(r_s) - r^*(r_s)). \end{aligned} \quad (7.79)$$

Here we use the continuity of u_L on the $u = \text{constant}$ shock wave (= shock wave propagating V direction). Similarly $u_R(r_s) \neq \tilde{u}_R(r_s)$ and

$$\begin{aligned} \tilde{u}_R(r_s) - u_R(r_s) &= (\tilde{v}_R(r_s) - 2\tilde{r}^*(r_s)) - (v_R(r_s) - 2r^*(r_s)) \\ &= -2(\tilde{r}^*(r_s) - r^*(r_s)) = -\Delta v(r_s). \end{aligned} \quad (7.80)$$

due to the continuity of v_R on the $v = \text{constant}$ shock wave (= shock wave propagating U direction).

Adding (7.75) with (7.76), and (7.78) with (7.77), we have

$$\tilde{v}_L(r_{turn}) - v_L(r_{st}) - \Delta v(r_s) = \int_{r_{st}}^{r_s} T(P, r) dr + \int_{r_s}^{r_{turn}} T(\tilde{P}, r) dr, \quad (7.81)$$

$$\tilde{u}_R(r_{turn}) - u_R(r_{st}) + \Delta v(r_s) = - \int_{r_{st}}^{r_s} T(P, r) dr - \int_{r_s}^{r_{turn}} T(\tilde{P}, r) dr, \quad (7.82)$$

Using the definitions of u and v , we have

$$u_R(r_{st}) - \tilde{u}_R(r_{turn}) + \tilde{v}_L(r_{turn}) - v_L(r_{st}) = t_R - t_L - 2r^*(r_{st}) + 2\tilde{r}^*(r_{turn}) \quad (7.83)$$

Thus, by subtracting (7.82) from (7.81), we have

$$t_R - t_L - 2r^*(r_{st}) + 2\tilde{r}^*(r_{turn}) - 2\Delta v(r_s) = 2 \int_{r_{st}}^{r_s} T(P, r) dr + 2 \int_{r_s}^{r_{turn}} T(\tilde{P}, r) dr. \quad (7.84)$$

¹³In (6.51), we use u_L which covers left and past patch, where u_L does not jump but v_L jumps at the shock wave.

As we have mentioned, in the limit where the turning point $r_{turn} \rightarrow \infty$, both P and \tilde{P} goes to infinity, then the right hand side of eq. (7.84) vanishes. This is because $T(P, r)$ given (7.74) vanishes as

$$T(\tilde{P}, r) = O\left(\frac{r^{2d-2}}{\tilde{P}^2}\right) \rightarrow 0 \quad (\text{at } \tilde{P} \rightarrow \infty), \quad (7.85)$$

and from (7.72),

$$\tilde{P}^2 = O\left((r_{turn})^{2d}\right) \rightarrow \infty \quad (\text{at } r_{turn} \rightarrow \infty), \quad (7.86)$$

therefore

$$\int^{r_{turn}} T(\tilde{P}, r) dr = O\left(\frac{1}{r_{turn}}\right) \rightarrow 0 \quad (\text{at } r_{turn} \rightarrow \infty). \quad (7.87)$$

Finally setting $t_R = -t_L = \ell\tau$ and using $\tilde{r}^*(r_{turn}) \rightarrow 0$ at $r_{turn} \rightarrow \infty$, we have

$$\ell\tau_\infty = r^*(r_{st}) + \Delta v(r_s) = r^*(r_{st}) + 2(\tilde{r}^*(r_s) - r^*(r_s)) \quad (7.88)$$

Thus we have

$$\ell\tau_\infty^{(0)} = r^*(r_{st}), \quad (7.89)$$

$$\Delta\tau_\infty = \tau_\infty - \tau_\infty^{(0)} = \frac{2}{\ell}(\tilde{r}^*(r_s) - r^*(r_s)) \quad (7.90)$$

which is exactly the same as eq. (7.35) and (7.58). Therefore, in three dimensions, as (7.59),

$$\Delta\tau_\infty > 0 \quad (7.91)$$

In this way, even with the CV argument¹⁴, exactly the same conclusions can be derived as WdW patch argument for CA/CV2.0.

8 Summary

In this doctoral thesis, two main points were discussed.

First: we have confirmed that action complexity in dS₂ JT gravity, with the effect of the dilaton properly taken into account, diverges at the finite time $\tau = \tau_\infty$ given in eq. (4.36). Instead, volume complexity reaches an $\mathcal{O}(1)$ critical value, although

¹⁴In fact one can also show $\tilde{r}^*(r_s) > r^*(r_s)$ and thus $\Delta\tau_\infty > 0$ in higher dimensions as well. For example, in 3+1 dimensions, blackening factor becomes $f(r) = 1 - \frac{r^2}{\ell^2} - \frac{2G_N E}{r} \sim 1 - \frac{r^2}{\ell^2} - \frac{2G_N E}{\ell}$ since $r_s \rightarrow \ell$. Compared with the blackening factor in 2+1 dimension, this is just a formal replacement $8G_N E \rightarrow 2G_N E/\ell$, therefore inequality (7.47) holds as well.

with a diverging rate as the critical time $\tau = \tau_\infty$ is approached. We point out that for larger times τ , when geodesics anchored at the stretched horizon meet the future infinity of dS_2 , the definition of volume complexity requires particular care. An analysis has been done in [47], where extremal curves are replaced by piecewise geodesics including a cutoff portion nearby the future infinity. With this prescription, volume is divergent too, but at the edge of the two regimes, there is an infinite jump. On the other hand, action complexity is well-defined even after the critical time τ_∞ , when the WDW patch is cut off by the future infinity. The crucial difference between volume and action complexity in two dimensions is due to the dilaton. Since the solution of JT gravity is characterized by both the metric and the dilaton, the effect of the latter is crucial. The dilaton naturally arises by dimensional reduction of three-dimensional dS spacetime, which provides the “right action” in eq. (4.28). This is because the dimensional reduction of dS_3 yields dS_2 with a linear dilaton, which is the solution of JT gravity. Consistently, by evaluating the on-shell action in eq. (4.28), we obtain the same action complexity as for dS_3 [47], see eq. (4.48). Note that all contributions in eq. (4.28) are boundary terms. This is expected since the bulk JT gravity action vanishes on-shell. We also stress that in dS spacetime the dilaton diverges at the future infinity. This behaviour of the dilaton is crucial for action complexity in JT gravity to show the hyperfast growth predicted in [3].

We have observed that the CV conjecture suffers a Weyl field-redefinition issue. A field-redefinition should not affect the physics, but volume complexity is manifestly modified by Weyl field-redefinition. In higher dimensions, there is a preferred frame, the Einstein frame. However, in two dimensions, since $\sqrt{g}R$ is invariant under Weyl transformation, there is no such preferred frame and this leads to an ambiguity in the definition of the CV conjecture. On the contrary, the CA conjecture is free from this problem, because the on-shell action is invariant under field-redefinition. As a way out, we have proposed a particular gauge choice in dS_2 JT gravity under which the so-called refined volume behaves qualitatively as action complexity.

Second: we systematically study shock wave geometries and see how the shock waves affect the WdW patch for CA/CV2.0 complexity. We study on both BTZ and dS background, and see that the effects of shock waves are exactly opposite signs between BTZ and dS. Especially we see that the hyperfast nature of the dS complexity is always delayed, *i.e.*, the critical time at which complexity diverges, becomes always greater by shock wave perturbation which satisfies ANEC.

Our result is consistent with Gao and Wald’s theorem [65] and also the analysis in [69]. If we compute the geodesic distance between the north and south pole with shock wave insertion, then unlike the BTZ case where the wormhole becomes longer, the distance becomes lesser. This reflects the point that the two-point function between the north pole and south pole grows instead of decay before the scrambling time $\ell \log S$ [69]. This is due to the fact that de Sitter’s Penrose diagram has shrunk

horizontally and the geodesic length has shortened.

The point that the shock waves delay the hyperfast nature might not be so surprising. dS is the spacetime where the cosmological constant dominates. Once we perturb the spacetime by the shock wave insertion in the far past, then cosmological constant dominance can be destroyed due to the shock waves. However, considering this to be a characteristic of dual field theory, our results suggest something very nontrivial. This is because complexity becomes generically greater under the perturbation. Therefore, the results obtained here provide a restriction to the structure of the state of field theories for holographic dual to dS, which could be a double-scaled limit of SYK, $DSSYK_\infty$ proposed by Susskind. Thus, a dual state like TFD in de Sitter must have its complexity, such that the critical time at which the complexity diverges is delayed for perturbations that correspond to shock waves in bulk spacetime.

We wish our analysis of complexity is useful as one of these criteria and will help us understand more about dS dual in the future.

Acknowledgments

First of all, I would like to express my sincere gratitude to my supervisor Norihiro Iizuka for teaching me so much, from basic knowledge to how to carry out research and his spirit, and for giving me advice not only on research but also on my career and life. I would also like to appreciate all the wonderful physicists with whom I collaborated during my PhD course. In particular, I give a huge thank to Sunil Kumar Sake and Nicolás Zenoni for advancing together and discussing the research on which this thesis is based. I would also thank the members of Osaka Univ. Particle Physics Theory Group for their support, especially the secretary. Finally, I would like to thank my father and mother for their psychological and physical support.

References

- [1] T. Anegawa, N. Iizuka, S. K. Sake, and N. Zenoni, “Is Action Complexity better for de Sitter space in Jackiw-Teitelboim gravity?,” [arXiv:2303.05025 \[hep-th\]](#).
- [2] T. Anegawa and N. Iizuka, “Shock waves and delay of hyperfast growth in de Sitter complexity,” *JHEP* **08** (2023) 115, [arXiv:2304.14620 \[hep-th\]](#).
- [3] L. Susskind, “Entanglement and Chaos in De Sitter Space Holography: An SYK Example,” *JHAP* **1** no. 1, (2021) 1–22, [arXiv:2109.14104 \[hep-th\]](#).
- [4] J. M. Maldacena, “The Large N limit of superconformal field theories and supergravity,” *Adv. Theor. Math. Phys.* **2** (1998) 231–252, [arXiv:hep-th/9711200](#).

- [5] G. 't Hooft, “Dimensional reduction in quantum gravity,” *Conf. Proc. C* **930308** (1993) 284–296, [arXiv:gr-qc/9310026](#).
- [6] L. Susskind, “The World as a hologram,” *J. Math. Phys.* **36** (1995) 6377–6396, [arXiv:hep-th/9409089](#).
- [7] A. Strominger, “The dS / CFT correspondence,” *JHEP* **10** (2001) 034, [arXiv:hep-th/0106113](#).
- [8] R. Bousso, A. Maloney, and A. Strominger, “Conformal vacua and entropy in de Sitter space,” *Phys. Rev. D* **65** (2002) 104039, [arXiv:hep-th/0112218](#).
- [9] V. Balasubramanian, J. de Boer, and D. Minic, “Notes on de Sitter space and holography,” *Class. Quant. Grav.* **19** (2002) 5655–5700, [arXiv:hep-th/0207245](#).
- [10] S. Sachdev and J. Ye, “Gapless spin fluid ground state in a random, quantum Heisenberg magnet,” *Phys. Rev. Lett.* **70** (1993) 3339, [arXiv:cond-mat/9212030 \[cond-mat\]](#).
- [11] A. Kitaev, “A simple model of quantum holography,” *Talks at KITP* (2015) .
- [12] L. Susskind, “De Sitter Holography: Fluctuations, Anomalous Symmetry, and Wormholes,” *Universe* **7** no. 12, (2021) 464, [arXiv:2106.03964 \[hep-th\]](#).
- [13] L. Susskind, “Scrambling in Double-Scaled SYK and De Sitter Space,” [arXiv:2205.00315 \[hep-th\]](#).
- [14] B. Bhattacharjee, P. Nandy, and T. Pathak, “Krylov complexity in large q and double-scaled SYK model,” *JHEP* **08** (2023) 099, [arXiv:2210.02474 \[hep-th\]](#).
- [15] H. Lin and L. Susskind, “Infinite Temperature’s Not So Hot,” [arXiv:2206.01083 \[hep-th\]](#).
- [16] L. Susskind, “De Sitter Space, Double-Scaled SYK, and the Separation of Scales in the Semiclassical Limit,” [arXiv:2209.09999 \[hep-th\]](#).
- [17] A. A. Rahman, “dS JT Gravity and Double-Scaled SYK,” [arXiv:2209.09997 \[hep-th\]](#).
- [18] S. H. Shenker and D. Stanford, “Black holes and the butterfly effect,” *JHEP* **03** (2014) 067, [arXiv:1306.0622 \[hep-th\]](#).
- [19] Y. Sekino and L. Susskind, “Fast Scramblers,” *JHEP* **10** (2008) 065, [arXiv:0808.2096 \[hep-th\]](#).
- [20] J. Maldacena, S. H. Shenker, and D. Stanford, “A bound on chaos,” *JHEP* **08** (2016) 106, [arXiv:1503.01409 \[hep-th\]](#).
- [21] J. Maldacena and D. Stanford, “Remarks on the Sachdev-Ye-Kitaev model,” *Phys. Rev. D* **94** no. 10, (2016) 106002, [arXiv:1604.07818 \[hep-th\]](#).
- [22] J. Polchinski and V. Rosenhaus, “The Spectrum in the Sachdev-Ye-Kitaev Model,” *JHEP* **04** (2016) 001, [arXiv:1601.06768 \[hep-th\]](#).

- [23] J. Haferkamp, P. Faist, N. B. T. Kothakonda, J. Eisert, and N. Y. Halpern, “Linear growth of quantum circuit complexity,” *Nature Phys.* **18** no. 5, (2022) 528–532, [arXiv:2106.05305 \[quant-ph\]](#).
- [24] M. A. Nielsen, “A geometric approach to quantum circuit lower bounds,” 2005. <https://arxiv.org/abs/quant-ph/0502070>.
- [25] L. Susskind, “Computational Complexity and Black Hole Horizons,” *Fortsch. Phys.* **64** (2016) 24–43, [arXiv:1403.5695 \[hep-th\]](#). [Addendum: *Fortsch.Phys.* **64**, 44–48 (2016)].
- [26] L. Susskind, “Entanglement is not enough,” *Fortsch. Phys.* **64** (2016) 49–71, [arXiv:1411.0690 \[hep-th\]](#).
- [27] A. R. Brown, D. A. Roberts, L. Susskind, B. Swingle, and Y. Zhao, “Holographic Complexity Equals Bulk Action?,” *Phys. Rev. Lett.* **116** no. 19, (2016) 191301, [arXiv:1509.07876 \[hep-th\]](#).
- [28] A. R. Brown, D. A. Roberts, L. Susskind, B. Swingle, and Y. Zhao, “Complexity, action, and black holes,” *Phys. Rev. D* **93** no. 8, (2016) 086006, [arXiv:1512.04993 \[hep-th\]](#).
- [29] J. Couch, W. Fischler, and P. H. Nguyen, “Noether charge, black hole volume, and complexity,” *JHEP* **03** (2017) 119, [arXiv:1610.02038 \[hep-th\]](#).
- [30] D. Stanford and L. Susskind, “Complexity and Shock Wave Geometries,” *Phys. Rev. D* **90** no. 12, (2014) 126007, [arXiv:1406.2678 \[hep-th\]](#).
- [31] R. Jackiw, “Lower Dimensional Gravity,” *Nucl. Phys. B* **252** (1985) 343–356.
- [32] C. Teitelboim, “Gravitation and Hamiltonian Structure in Two Space-Time Dimensions,” *Phys. Lett. B* **126** (1983) 41–45.
- [33] A. R. Brown, H. Gharibyan, H. W. Lin, L. Susskind, L. Thorlacius, and Y. Zhao, “Complexity of Jackiw-Teitelboim gravity,” *Phys. Rev. D* **99** no. 4, (2019) 046016, [arXiv:1810.08741 \[hep-th\]](#).
- [34] K. Goto, H. Marrochio, R. C. Myers, L. Queimada, and B. Yoshida, “Holographic Complexity Equals Which Action?,” *JHEP* **02** (2019) 160, [arXiv:1901.00014 \[hep-th\]](#).
- [35] M. Alishahiha, “On complexity of Jackiw–Teitelboim gravity,” *Eur. Phys. J. C* **79** no. 4, (2019) 365, [arXiv:1811.09028 \[hep-th\]](#).
- [36] S.-K. Jian, B. Swingle, and Z.-Y. Xian, “Complexity growth of operators in the SYK model and in JT gravity,” *JHEP* **03** (2021) 014, [arXiv:2008.12274 \[hep-th\]](#).
- [37] R.-G. Cai, S. He, S.-J. Wang, and Y.-X. Zhang, “Revisit on holographic complexity in two-dimensional gravity,” *JHEP* **08** (2020) 102, [arXiv:2001.11626 \[hep-th\]](#).
- [38] Y.-S. An and R.-H. Peng, “Effect of the dilaton on holographic complexity growth,” *Phys. Rev. D* **97** no. 6, (2018) 066022, [arXiv:1801.03638 \[hep-th\]](#).

- [39] S. Chapman, D. A. Galante, and E. D. Kramer, “Holographic complexity and de Sitter space,” *JHEP* **02** (2022) 198, [arXiv:2110.05522 \[hep-th\]](#).
- [40] A. Belin, R. C. Myers, S.-M. Ruan, G. Sárosi, and A. J. Speranza, “Does Complexity Equal Anything?,” *Phys. Rev. Lett.* **128** no. 8, (2022) 081602, [arXiv:2111.02429 \[hep-th\]](#).
- [41] A. Belin, R. C. Myers, S.-M. Ruan, G. Sárosi, and A. J. Speranza, “Complexity equals anything II,” *JHEP* **01** (2023) 154, [arXiv:2210.09647 \[hep-th\]](#).
- [42] A. Akhavan, M. Alishahiha, A. Naseh, and H. Zolfi, “Complexity and Behind the Horizon Cut Off,” *JHEP* **12** (2018) 090, [arXiv:1810.12015 \[hep-th\]](#).
- [43] L. V. Iliesiu, M. Mezei, and G. Sárosi, “The volume of the black hole interior at late times,” *JHEP* **07** (2022) 073, [arXiv:2107.06286 \[hep-th\]](#).
- [44] M. Alishahiha, S. Banerjee, and J. Kames-King, “Complexity via replica trick,” *JHEP* **08** (2022) 181, [arXiv:2205.01150 \[hep-th\]](#).
- [45] M. Alishahiha and S. Banerjee, “On the saturation of late-time growth of complexity in supersymmetric JT gravity,” *JHEP* **01** (2023) 134, [arXiv:2209.02441 \[hep-th\]](#).
- [46] R. Auzzi, G. Nardelli, G. P. Ungureanu, and N. Zenoni, “Volume complexity of dS bubbles,” [arXiv:2302.03584 \[hep-th\]](#).
- [47] E. Jørstad, R. C. Myers, and S.-M. Ruan, “Holographic complexity in dS_{d+1} ,” *JHEP* **05** (2022) 119, [arXiv:2202.10684 \[hep-th\]](#).
- [48] L. Susskind, “Three Lectures on Complexity and Black Holes,” SpringerBriefs in Physics. Springer, 10, 2018. [arXiv:1810.11563 \[hep-th\]](#).
- [49] S. Chapman and G. Policastro, “Quantum computational complexity from quantum information to black holes and back,” *Eur. Phys. J. C* **82** no. 2, (2022) 128, [arXiv:2110.14672 \[hep-th\]](#).
- [50] R. Jefferson and R. C. Myers, “Circuit complexity in quantum field theory,” *JHEP* **10** (2017) 107, [arXiv:1707.08570 \[hep-th\]](#).
- [51] S. Chapman, M. P. Heller, H. Marrochio, and F. Pastawski, “Toward a Definition of Complexity for Quantum Field Theory States,” *Phys. Rev. Lett.* **120** no. 12, (2018) 121602, [arXiv:1707.08582 \[hep-th\]](#).
- [52] L. Hackl and R. C. Myers, “Circuit complexity for free fermions,” *JHEP* **07** (2018) 139, [arXiv:1803.10638 \[hep-th\]](#).
- [53] R. Khan, C. Krishnan, and S. Sharma, “Circuit Complexity in Fermionic Field Theory,” *Phys. Rev. D* **98** no. 12, (2018) 126001, [arXiv:1801.07620 \[hep-th\]](#).
- [54] P. Caputa, N. Kundu, M. Miyaji, T. Takayanagi, and K. Watanabe, “Anti-de Sitter Space from Optimization of Path Integrals in Conformal Field Theories,” *Phys. Rev. Lett.* **119** no. 7, (2017) 071602, [arXiv:1703.00456 \[hep-th\]](#).

- [55] P. Caputa and J. M. Magan, “Quantum Computation as Gravity,” *Phys. Rev. Lett.* **122** no. 23, (2019) 231302, [arXiv:1807.04422 \[hep-th\]](#).
- [56] A. Belin, A. Lewkowycz, and G. Sárosi, “Complexity and the bulk volume, a new York time story,” *JHEP* **03** (2019) 044, [arXiv:1811.03097 \[hep-th\]](#).
- [57] J. Erdmenger, M. Gerbershagen, and A.-L. Weigel, “Complexity measures from geometric actions on Virasoro and Kac-Moody orbits,” *JHEP* **11** (2020) 003, [arXiv:2004.03619 \[hep-th\]](#).
- [58] M. Flory and M. P. Heller, “Geometry of Complexity in Conformal Field Theory,” *Phys. Rev. Res.* **2** no. 4, (2020) 043438, [arXiv:2005.02415 \[hep-th\]](#).
- [59] M. Flory and M. P. Heller, “Conformal field theory complexity from Euler-Arnold equations,” *JHEP* **12** (2020) 091, [arXiv:2007.11555 \[hep-th\]](#).
- [60] N. Chagnet, S. Chapman, J. de Boer, and C. Zukowski, “Complexity for Conformal Field Theories in General Dimensions,” *Phys. Rev. Lett.* **128** no. 5, (2022) 051601, [arXiv:2103.06920 \[hep-th\]](#).
- [61] J. Erdmenger, M. Flory, M. Gerbershagen, M. P. Heller, and A.-L. Weigel, “Exact Gravity Duals for Simple Quantum Circuits,” *SciPost Phys.* **13** no. 3, (2022) 061, [arXiv:2112.12158 \[hep-th\]](#).
- [62] G. Sárosi, “AdS₂ holography and the SYK model,” *PoS Modave2017* (2018) 001, [arXiv:1711.08482 \[hep-th\]](#).
- [63] G. J. Turiaci, M. Usatyuk, and W. W. Weng, “2D dilaton-gravity, deformations of the minimal string, and matrix models,” *Class. Quant. Grav.* **38** no. 20, (2021) 204001, [arXiv:2011.06038 \[hep-th\]](#).
- [64] S. Baiguera, R. Berman, S. Chapman, and R. C. Myers, “The cosmological switchback effect,” *JHEP* **07** (2023) 162, [arXiv:2304.15008 \[hep-th\]](#).
- [65] S. Gao and R. M. Wald, “Theorems on gravitational time delay and related issues,” *Class. Quant. Grav.* **17** (2000) 4999–5008, [arXiv:gr-qc/0007021](#).
- [66] S. H. Shenker and D. Stanford, “Multiple Shocks,” *JHEP* **12** (2014) 046, [arXiv:1312.3296 \[hep-th\]](#).
- [67] D. A. Roberts, D. Stanford, and L. Susskind, “Localized shocks,” *JHEP* **03** (2015) 051, [arXiv:1409.8180 \[hep-th\]](#).
- [68] S. H. Shenker and D. Stanford, “Stringy effects in scrambling,” *JHEP* **05** (2015) 132, [arXiv:1412.6087 \[hep-th\]](#).
- [69] L. Aalsma and G. Shiu, “Chaos and complementarity in de Sitter space,” *JHEP* **05** (2020) 152, [arXiv:2002.01326 \[hep-th\]](#).
- [70] L. Aalsma, A. Cole, E. Morvan, J. P. van der Schaar, and G. Shiu, “Shocks and information exchange in de Sitter space,” *JHEP* **10** (2021) 104, [arXiv:2105.12737 \[hep-th\]](#).

- [71] L. Aalsma, S. E. Aguilar-Gutierrez, and W. Sybesma, “An outsider’s perspective on information recovery in de Sitter space,” *JHEP* **01** (2023) 129, [arXiv:2210.12176 \[hep-th\]](#).
- [72] M. Berkooz, M. Isachenkov, V. Narovlansky, and G. Torrents, “Towards a full solution of the large N double-scaled SYK model,” *JHEP* **03** (2019) 079, [arXiv:1811.02584 \[hep-th\]](#).
- [73] H. W. Lin, “The bulk Hilbert space of double scaled SYK,” *JHEP* **11** (2022) 060, [arXiv:2208.07032 \[hep-th\]](#).
- [74] E. Shaghoulian and L. Susskind, “Entanglement in De Sitter space,” *JHEP* **08** (2022) 198, [arXiv:2201.03603 \[hep-th\]](#).
- [75] L. Susskind, “De Sitter Space has no Chords. Almost Everything is Confined,” [arXiv:2303.00792 \[hep-th\]](#).
- [76] L. Susskind, “A Paradox and its Resolution Illustrate Principles of de Sitter Holography,” [arXiv:2304.00589 \[hep-th\]](#).
- [77] O. Aharony, S. S. Gubser, J. M. Maldacena, H. Ooguri, and Y. Oz, “Large N field theories, string theory and gravity,” *Phys. Rept.* **323** (2000) 183–386, [arXiv:hep-th/9905111](#).
- [78] T. Nishioka, S. Ryu, and T. Takayanagi, “Holographic Entanglement Entropy: An Overview,” *J. Phys. A* **42** (2009) 504008, [arXiv:0905.0932 \[hep-th\]](#).
- [79] M. Natsuume, *AdS/CFT Duality User Guide*, vol. 903. 2015. [arXiv:1409.3575 \[hep-th\]](#).
- [80] V. E. Hubeny, “The AdS/CFT Correspondence,” *Class. Quant. Grav.* **32** no. 12, (2015) 124010, [arXiv:1501.00007 \[gr-qc\]](#).
- [81] D. Harlow, “Jerusalem Lectures on Black Holes and Quantum Information,” *Rev. Mod. Phys.* **88** (2016) 015002, [arXiv:1409.1231 \[hep-th\]](#).
- [82] T. Hartman, “Quantum Gravity and Black Holes: Lecture notes,” Lecture in Cornell University (2015) .
- [83] N. Iizuka, “Introduction to AdS/CFT,” Talks at 2nd Ex Universe school (2022) .
- [84] G. T. Horowitz and A. Strominger, “Black strings and P-branes,” *Nucl. Phys. B* **360** (1991) 197–209.
- [85] S. S. Gubser, I. R. Klebanov, and A. M. Polyakov, “Gauge theory correlators from noncritical string theory,” *Phys. Lett. B* **428** (1998) 105–114, [arXiv:hep-th/9802109](#).
- [86] E. Witten, “Anti-de Sitter space and holography,” *Adv. Theor. Math. Phys.* **2** (1998) 253–291, [arXiv:hep-th/9802150](#).
- [87] C. Csaki, H. Ooguri, Y. Oz, and J. Terning, “Glueball mass spectrum from supergravity,” *JHEP* **01** (1999) 017, [arXiv:hep-th/9806021](#).

- [88] R. de Mello Koch, A. Jevicki, M. Mihailescu, and J. P. Nunes, “Evaluation of glueball masses from supergravity,” *Phys. Rev. D* **58** (1998) 105009, [arXiv:hep-th/9806125](#).
- [89] R. C. Brower, S. D. Mathur, and C.-I. Tan, “Discrete spectrum of the graviton in the AdS(5) black hole background,” *Nucl. Phys. B* **574** (2000) 219–244, [arXiv:hep-th/9908196](#).
- [90] R. C. Brower, S. D. Mathur, and C.-I. Tan, “Glueball spectrum for QCD from AdS supergravity duality,” *Nucl. Phys. B* **587** (2000) 249–276, [arXiv:hep-th/0003115](#).
- [91] J. Maldacena and L. Susskind, “Cool horizons for entangled black holes,” *Fortsch. Phys.* **61** (2013) 781–811, [arXiv:1306.0533 \[hep-th\]](#).
- [92] T. Hartman and J. Maldacena, “Time Evolution of Entanglement Entropy from Black Hole Interiors,” *JHEP* **05** (2013) 014, [arXiv:1303.1080 \[hep-th\]](#).
- [93] R. Bousso, “A Covariant entropy conjecture,” *JHEP* **07** (1999) 004, [arXiv:hep-th/9905177](#).
- [94] E. Shaghoulian, “The central dogma and cosmological horizons,” *JHEP* **01** (2022) 132, [arXiv:2110.13210 \[hep-th\]](#).
- [95] P. Hayden and J. Preskill, “Black holes as mirrors: Quantum information in random subsystems,” *JHEP* **09** (2007) 120, [arXiv:0708.4025 \[hep-th\]](#).
- [96] N. Lashkari, D. Stanford, M. Hastings, T. Osborne, and P. Hayden, “Towards the Fast Scrambling Conjecture,” *JHEP* **04** (2013) 022, [arXiv:1111.6580 \[hep-th\]](#).
- [97] V. Chandrasekaran, G. Penington, and E. Witten, “Large N algebras and generalized entropy,” [arXiv:2209.10454 \[hep-th\]](#).
- [98] V. Narovlansky and H. Verlinde, “Double-scaled SYK and de Sitter Holography,” [arXiv:2310.16994 \[hep-th\]](#).
- [99] A. A. Rahman and L. Susskind, “Comments on a Paper by Narovlansky and Verlinde,” [arXiv:2312.04097 \[hep-th\]](#).
- [100] V. Chandrasekaran, R. Longo, G. Penington, and E. Witten, “An algebra of observables for de Sitter space,” *JHEP* **02** (2023) 082, [arXiv:2206.10780 \[hep-th\]](#).
- [101] S. Ryu and T. Takayanagi, “Holographic derivation of entanglement entropy from AdS/CFT,” *Phys. Rev. Lett.* **96** (2006) 181602, [arXiv:hep-th/0603001](#).
- [102] S. Ryu and T. Takayanagi, “Aspects of Holographic Entanglement Entropy,” *JHEP* **08** (2006) 045, [arXiv:hep-th/0605073](#).
- [103] V. E. Hubeny, M. Rangamani, and T. Takayanagi, “A Covariant holographic entanglement entropy proposal,” *JHEP* **07** (2007) 062, [arXiv:0705.0016 \[hep-th\]](#).
- [104] M. R. Dowling and M. A. Nielsen, “The geometry of quantum computation,” *Quant. Inf. Comput.* **8** no. 10, (2008) 0861–0899, [arXiv:quant-ph/0701004](#).

- [105] L. Susskind and Y. Zhao, “Switchbacks and the Bridge to Nowhere,” [arXiv:1408.2823 \[hep-th\]](#).
- [106] S. Chapman, H. Marrochio, and R. C. Myers, “Holographic complexity in Vaidya spacetimes. Part I,” *JHEP* **06** (2018) 046, [arXiv:1804.07410 \[hep-th\]](#).
- [107] S. Chapman, H. Marrochio, and R. C. Myers, “Holographic complexity in Vaidya spacetimes. Part II,” *JHEP* **06** (2018) 114, [arXiv:1805.07262 \[hep-th\]](#).
- [108] J. W. York, Jr., “Role of conformal three geometry in the dynamics of gravitation,” *Phys. Rev. Lett.* **28** (1972) 1082–1085.
- [109] G. W. Gibbons and S. W. Hawking, “Action Integrals and Partition Functions in Quantum Gravity,” *Phys. Rev. D* **15** (1977) 2752–2756.
- [110] A. Svesko, E. Verheijden, E. P. Verlinde, and M. R. Visser, “Quasi-local energy and microcanonical entropy in two-dimensional nearly de Sitter gravity,” *JHEP* **08** (2022) 075, [arXiv:2203.00700 \[hep-th\]](#).
- [111] H. Nariai, “On a new cosmological solution of einstein’s field equations of gravitation,” *Sci. Rep. Tohoku Univ. Ser. 1* **34** (1950) 62.
- [112] P. H. Ginsparg and M. J. Perry, “Semiclassical Perdurance of de Sitter Space,” *Nucl. Phys. B* **222** (1983) 245–268.
- [113] D. Anninos, “De Sitter Musings,” *Int. J. Mod. Phys. A* **27** (2012) 1230013, [arXiv:1205.3855 \[hep-th\]](#).
- [114] J. Maldacena, G. J. Turiaci, and Z. Yang, “Two dimensional Nearly de Sitter gravity,” *JHEP* **01** (2021) 139, [arXiv:1904.01911 \[hep-th\]](#).
- [115] L. Lehner, R. C. Myers, E. Poisson, and R. D. Sorkin, “Gravitational action with null boundaries,” *Phys. Rev. D* **94** no. 8, (2016) 084046, [arXiv:1609.00207 \[hep-th\]](#).
- [116] K. Parattu, S. Chakraborty, B. R. Majhi, and T. Padmanabhan, “A Boundary Term for the Gravitational Action with Null Boundaries,” *Gen. Rel. Grav.* **48** no. 7, (2016) 94, [arXiv:1501.01053 \[gr-qc\]](#).
- [117] G. Hayward, “Gravitational action for space-times with nonsmooth boundaries,” *Phys. Rev. D* **47** (1993) 3275–3280.
- [118] D. Carmi, R. C. Myers, and P. Rath, “Comments on Holographic Complexity,” *JHEP* **03** (2017) 118, [arXiv:1612.00433 \[hep-th\]](#).
- [119] S. Chapman, H. Marrochio, and R. C. Myers, “Complexity of Formation in Holography,” *JHEP* **01** (2017) 062, [arXiv:1610.08063 \[hep-th\]](#).
- [120] D. Carmi, S. Chapman, H. Marrochio, R. C. Myers, and S. Sugishita, “On the Time Dependence of Holographic Complexity,” *JHEP* **11** (2017) 188, [arXiv:1709.10184 \[hep-th\]](#).
- [121] M. Alishahiha, “Holographic Complexity,” *Phys. Rev. D* **92** no. 12, (2015) 126009, [arXiv:1509.06614 \[hep-th\]](#).

- [122] P. Bueno, V. S. Min, A. J. Speranza, and M. R. Visser, “Entanglement equilibrium for higher order gravity,” *Phys. Rev. D* **95** no. 4, (2017) 046003, [arXiv:1612.04374 \[hep-th\]](#).
- [123] M. Alishahiha, A. Faraji Astaneh, A. Naseh, and M. H. Vahidinia, “On complexity for F(R) and critical gravity,” *JHEP* **05** (2017) 009, [arXiv:1702.06796 \[hep-th\]](#).
- [124] J. Hernandez, R. C. Myers, and S.-M. Ruan, “Quantum extremal islands made easy. Part III. Complexity on the brane,” *JHEP* **02** (2021) 173, [arXiv:2010.16398 \[hep-th\]](#).
- [125] T. Dray and G. ’t Hooft, “The Effect of Spherical Shells of Matter on the Schwarzschild Black Hole,” *Commun. Math. Phys.* **99** (1985) 613–625.
- [126] I. H. Redmount, “Blue-Sheet Instability of Schwarzschild Wormholes,” *Prog. Theor. Phys.* **73** (1985) 1401.
- [127] E. Poisson and W. Israel, “Internal structure of black holes,” *Phys. Rev. D* **41** (1990) 1796–1809.
- [128] S. Deser and R. Jackiw, “Three-Dimensional Cosmological Gravity: Dynamics of Constant Curvature,” *Annals Phys.* **153** (1984) 405–416.
- [129] M. Spradlin, A. Strominger, and A. Volovich, “Les Houches lectures on de Sitter space,” in *Les Houches Summer School: Session 76: Euro Summer School on Unity of Fundamental Physics: Gravity, Gauge Theory and Strings*, pp. 423–453. 10, 2001. [arXiv:hep-th/0110007](#).
- [130] M. Hotta and M. Tanaka, “Shock wave geometry with nonvanishing cosmological constant,” *Class. Quant. Grav.* **10** (1993) 307–314.
- [131] M. Hotta and M. Tanaka, “Gravitational shock waves and quantum fields in de sitter space,” *Phys. Rev. D* **47** (Apr, 1993) 3323–3329. <https://link.aps.org/doi/10.1103/PhysRevD.47.3323>.
- [132] K. Sfetsos, “On gravitational shock waves in curved space-times,” *Nucl. Phys. B* **436** (1995) 721–745, [arXiv:hep-th/9408169](#).